DuctAPE Theory

Author: Judd Mehr
Last Updated: June 26, 2024

1.1 Introduction

In the preliminary and conceptual stages of design, it is often helpful to have tools that make some sacrifices in fidelity in favor of computational efficiency. It may also be desirable to sacrifice some flexibility to further decrease computation time costs in the beginning stages of design. To this end, a low-fidelity tool for the evaluation of ducted propulsors, catered specifically to electric ducted fans, is described in this chapter. One of the major limitations in flexibility is that we require that:

Assumption 1.1

The system is modeled axisymmetrically.

Limitations: There are two major limitations to the axisymmetric assumption: the first is that we can no longer model non-symmetric inflow conditions. The second is that the internal flow, specifically aft of the rotor(s) is assumed to be uniform in the tangential direction (axisymmetric), removing any modeling of unsteady wake conditions. An additional limitation comes in modeling flow near the center line, where we will see that division by numbers approaching zero can cause numerical issues.

Justification: By making the axisymmetric assumption, we are able to utilize much faster computation methods, or at least faster versions of already relatively fast methods. Specifically in our case, we can use axisymmetric panel methods employing far less elements than would be required for a three-dimensional method. Although our operational cases are limited to axial inflow, there are still many uses in that limited design space.

Therefore, we call our tool Ducted Axisymmetric Propulsor Evaluation, or DuctAPE for short. As alluded to, the overall goal of DuctAPE is to provide a computationally inexpensive tool to be used in a multidisciplinary design and optimization setting for preliminary and conceptual design.

In this chapter we cover the methodology derivation required for DuctAPE as well as some implementation details and various verification and validation along the way. The solver is comprised of two major components, which will be first presented in isolation before the full coupling is considered. The first that will be covered is the analysis of the duct and center body (see section 1.2), and the second is the analysis of the rotor and wake (see section 1.3).

1.2   No-rotor Solution: Axisymmetric Panel Method

One of the major pieces of the DuctAPE solver is an axisymmetric panel method. The implementation for an axisymmetric panel method is similar to the implementation of typical planar panel methods, but there are a few differences. We include here details for the axisymmetric panel method used.

1.2.1   Potential Flow Theory

Potential flow theory deals with the analysis of flow fields that can be modeled as the gradient of scalar functions. In our case, we are specifically interested in the scalar function called the velocity potential[a], ϕ, and its gradient: velocity, $V = \nabla \phi$. Potential flows conform to assumption 1.2 by definition[b].

[a] Thus the name potential flow theory

[b] Due to the vector identity that for any vector, ϕ, the curl of the gradient of the vector is zero: $\nabla \times \nabla \phi = 0$

Assumption 1.2

The velocity field is irrotational, such that

$$\omega = \nabla \times V = 0$$

everywhere in the field except for the axes of free vortices.

Limitations: We cannot directly model viscous effects in the flow, and later (in our wake model) we lose some fidelity by forcing an irrotational interpretation of inherently rotational phenomena.

Justification: We will see shortly that this allows us to greatly simplify the analysis to a linear system of equations, greatly reducing the computational expense. At high enough Reynolds numbers, the flow appears to be inviscid for large portions of the flow field as well.

For our application, we also assume

Assumption 1.3

The velocity field is incompressible, such that

$$\nabla \cdot V = 0.$$

Limitations: We cannot model highly compressible flows.

> **Justification:** For our application, we should not need to model highly compressible flows, but we can later apply some compressibility corrections (assuming that the flow is reasonably close to incompressible).

From assumption 1.3 we see that

$$\nabla \cdot \nabla \phi = \nabla^2 \phi = 0, \tag{1.1}$$

which is the Laplace equation. Along with the implication of assumption 1.2 that our flow is inviscid[c], the fact that the Laplace equation is a linear operator is a major key to the reduction in required computational expense for potential flow methods. Because the Laplace equation is a linear operator, we can model relatively complicated flow features (such as a duct and center body) using a superposition of elementary flows, each satisfying the Laplace equation (for example point sources and free vortices). The superposition of any number of elementary flows of unknown strength can be assimilated into a single linear system of equations and solved directly. In our application, we are mostly concerned with determining the strengths of elementary flows distributed along imaginary boundaries we define based on useful shapes (such as the surfaces of ducts and center bodies) that induce a potential flow field that matches what we would see for an actual solid body in reality.[d] We call problems dealing with values on boundaries: boundary value problems (for obvious reasons). A common way to approach the solution of boundary value problem is with a boundary integral equation.

[c] An irrotational flow is always inviscid, but an inviscid flow is not necessarily irrotational

[d] In reality, flow is neither irrotational, nor incompressible, but we find that in many cases it is close enough that potential flow theory provides a good approximation.

Boundary Integral Equation

For a given aerodynamic body, representable by a simply connected contour (for example, $\mathcal{S}$ as shown in figure 1.1) we want to be able to find the velocity (and thereby pressure) distribution on that body surface as well as its influence on the remainder of the flow field. One way to find the surface velocity distribution is to leverage potential flow theory. Using potential flow theory, we can construct a boundary integral equation describing the influence of distributions of elementary flow distributions along a give boundary. We can then use this boundary integral equation to solve the boundary value problem for the unknown surface velocity distribution. Fortunately, Erik Ivar Fredholm developed a set of integral equations for application to boundary value problems[1]. For our application, we will use a Fredholm integral equation of the second kind:

[1] Fredholm, "Sur une classe d'équations fonctionnelles," 1903.

$$f(t) = \vartheta(t) + \oint_{\mathcal{S}} K(s,t)\varphi(s)\mathrm{d}s. \tag{1.2}$$

To understand what each term in equation (1.2) represents, we really need to start with an understanding of the problem we are trying to solve. As mentioned, we would like to solve for the strengths associated with elementary flow field distributions that induce a potential flow field
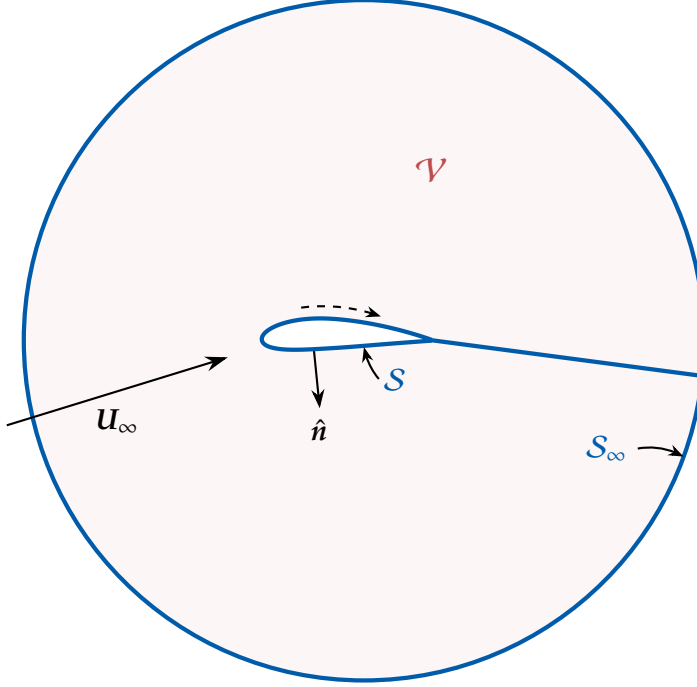
Figure 1.1: An example of a simply connected contour, $\mathcal{S}$, representing, in this case, an airfoil. The dashed arrow represent the direction about which the contour is traversed, with $\hat{n}$ being the unit surface normal associated with the direction of travel.

which matches our chosen geometry for a set of external flow conditions. There are several ways to go about setting up a boundary value problem, and we are going to choose to apply what is often termed the no flow through condition. In other words, we are going to apply the boundary condition that the velocity normal[e] to the body is zero. Because we are applying a boundary condition on velocity, which is the gradient of the velocity potential, we are applying what is called the Neumann boundary condition.[f] We are now ready to start defining the terms in equation (1.2).

Starting with the integral term, which represents the influence of a distribution of elementary flows along the boundary, we have the kernel K which in our case will be the expression for the unit induced velocities of the surface segment, $\mathrm{d}s$, acting normal to the surface at point t. Mathematically, we can state this as

[e] Using the normal directed out of the body, or into the space $\mathcal{V}$ as depicted in figure 1.1.

[f] As opposed to a Dirichlet boundary condition, which is typically applied directly to the value of the potential on the boundary.

$$
\begin{aligned}
K(s,t) &= \frac{\partial \hat{\phi}(s,t)}{\partial \hat{n}_t} \\
&= \nabla \hat{\phi}(s,t) \cdot \hat{n}(t) \\
&= \hat{V}(s,t) \cdot \hat{n}(t).
\end{aligned}
\tag{1.3}
$$

where $\hat{\phi}$ is the unit velocity potential, $\hat{V}$ is the unit velocity, and $\hat{n}$ is the unit normal to the surface. The other term in the integrand, $\varphi(s)$ is the distribution of strengths of elementary flows along the boundary. We will choose to use free vortices as our elementary flows and we represent their strengths with the symbol γ.

The other term on the right hand side, $\vartheta(t)$ represents the jump in velocity across the boundary. It can be shown that the jump in tangential velocity associated with a vortex distribution along the boundary is $\vartheta(t) = -\gamma/2$.[2–4] And for the orthogonal case of the normal velocity (which we are concerned with at this point), the jump term is zero.

Lastly, the term on the left hand side, $f(t)$ represents any externally induced velocity in the negative normal direction[g] on the boundary at point t. The typical externally induced velocity is due to (but not limited to) a uniform free stream.[h] Mathematically we state the externally induced velocity as

$$
\begin{aligned}
\varphi(t) &= \frac{\partial \phi_\infty}{\partial \hat{n}_t} \\
&= \nabla \phi_\infty \cdot \hat{n}(t) \\
&= V_\infty \cdot \hat{n}(t).
\end{aligned}
\tag{1.4}
$$

2 Lewis, *Vortex Element Methods for Fluid Dynamic Analysis of Engineering Systems*, 1991.

3 Martensen, "Die Berechnung der Druckverteilung an dicken Gitterprofilen mit Hilfe von Fredholmschen Integralgleichungen zweiter Art," 1959.

4 Courant *et al.*, *Methods of Mathematical Physics*, 1962.

[g] Remember that we want the total normal velocity at the boundary to be zero, so adding this term to both sides should give us zero.

[h] Note that a uniform flow is another of the elementary flows satisfying the Laplace equation.

All together our Fredholm integral equation of the second kind, applied to the Neumann problem for an unknown distribution of free vortices along a chosen boundary is

$$
\oint_S \gamma(s) \frac{\partial \hat{\phi}(s,t)}{\partial \hat{n}} \mathrm{d}s = -\frac{\partial \phi_\infty}{\partial \hat{n}}
\tag{1.5a}
$$

$$
- \text{ or } -
$$

$$
\oint_S \gamma(s) \hat{V}(s,t) \cdot \hat{n} \mathrm{d}s = -V_\infty \cdot \hat{n}.
\tag{1.5b}
$$

We now have a boundary integral equation that we want to use to solve for the unknown distribution of vortex strengths, $\gamma(s)$. As we will see, we will apply this equation at various points, t, along the boundary simultaneously to form a system of equations for which to solve for $\gamma(s)$.

1.2.2 The Panel Method: A Numerical Approach to Solving Boundary Integral Equations

Solving the boundary integral equation over an entire boundary all at once is not, in general, a tractable approach. Instead, we approximate the boundary as a series of segments and sum the integrals over those individual segments. We often approximate the boundary as a polygon, discretizing the boundary using flat segments over which the surface integral is simplified. For two- and general three-dimensional geometries, these flat segments are often referred to as panels, thus the name "panel method."

In panel methods, we also do not apply the no through flow condition everywhere in the boundary, but rather at a set of control points along the boundary. We choose to place one control point at the center of each panel. We can therefore assemble a system of integral equations for each of the control points, summing the integral of the influence of all the panels on each control point and use that system of equations to solve

for the unknown vortex strength distribution required to match the flow field to our prescribed geometry. In order to set up a system of equations, we first need to discretize the boundary into panels.

Discretizing bodies into panels

> **Assumption 1.4**
>
> *Smooth bodies can be reasonably represented by a discrete number of flat panels.*
>
> **Limitations:** By approximating the geometry as a polygon, rather than a single continuous curve, we lose some accuracy in our computation.
>
> **Justification:** As mentioned, it is much easier to solve the problem through the sum of individual components of the boundary, and especially if we simplify those sections into pieces over which the integral is simpler to solve. In addition, with a sufficient number of panels, we obtain a close approximation of the body curvature and therefore the solution of the continuous integral over the entire boundary.

The bodies which we would like to model in our application are axisymmetric bodies of revolution (such as the center body) and annular airfoils (such as the duct comprised of a casing and nacelle) of an electric ducted fan. According to assumptions 1.1 and 1.4 we can model the geometry as axisymmetric bands, as shown in figure 1.2(a). Furthermore, as shown in section 1.2.4, we may reduce the geometry for analysis to two dimensions without loss of generality after applying axisymmetry, modeling the geometry with representative cross sections in the r-z plane in cylindrical coordinates.The discretized boundary in our implementation then takes the form of 2D panels (representing the axisymmetric bands). Figure 1.2(a) shows what is intended by a flat, axisymmetric band, and figure 1.2(b) shows the panel representation of said band.
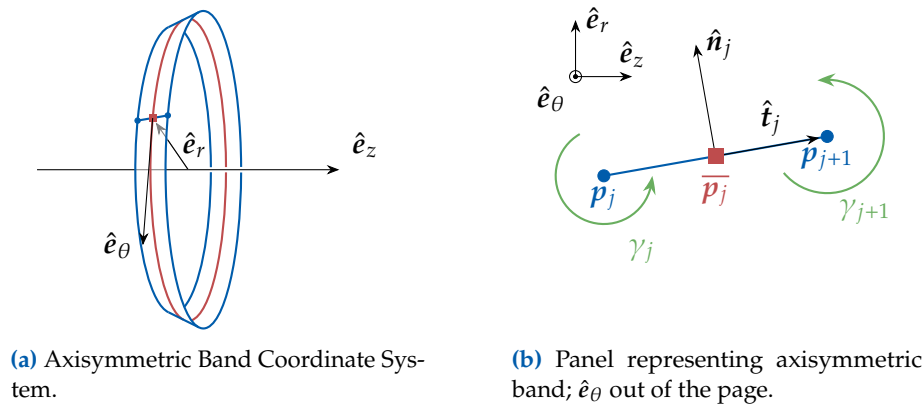

(a) Axisymmetric Band Coordinate System.

(b) Panel representing axisymmetric band; $\hat{e}_\theta$ out of the page.

Figure 1.2: Axisymmetric band and panel geometry definitions.

One of the convenient traits of a panel method is that we simply need to know the geometry and relative position of each of the panels to calculate the unit induced velocities presented in section 1.2.4. As an overview of the panel geometry we need to know, we refer to figure 1.2 in which we see a panel defined from the point, p_j, to the point, p_{j+1}. We take the midpoint of the panel to be $\overline{p}_j = (p_j + p_{j+1})/2$; and we define the unit normal, $\hat{n}_j$, as shown in figure 1.2(b), such that $\hat{n}_j = \hat{e}_\theta \times \hat{t}_j$, where $\hat{e}_\theta$ is the unit vector tangent to the vortex band in the positive θ-direction according to the right hand rule, and $\hat{t}_j$ is the unit tangent to the panel from p_j to p_{j+1} such that $\hat{t}_j = (p_{j+1} - p_j)/\|p_{j+1} - p_j\|$. In other words, we will assume that the discretized panels are defined such that increasing panel indices lead to the curve being traversed in a clockwise direction.

Applying boundary conditions

As discussed in section 1.2.1, we are trying to solve the boundary value problem using the Neumann boundary conditions. As mentioned, we will apply this boundary condition at the control points placed at the center of each panel ($\overline{p}$ in figure 1.2(b)). Since the boundary condition states that the normal velocity, due to all contributions, is zero at the control points, we also need to include the freestream contribution to our boundary condition. Putting the surface influence and freestream influences together, we can, for the ith control point, state our approximate boundary integral equation as

$$\sum_{j=1}^{N} \left[K_{ij} \cdot \hat{n}_i \right] + V_\infty \cdot \hat{n}_i = 0, \tag{1.6}$$

Though we often put the freestream component on the right hand side for convenience, leaving us with

$$\boxed{\sum_{j=1}^{N} K_{ij} \cdot \hat{n}_i = -V_\infty \cdot \hat{n}_i} \tag{1.7}$$

where K is comprised of what the induced velocity on the ith control point[i] due to the jth segment of the surface (the jth panel in our case), calculated from the integral term found in our boundary integral equation, equation (1.5). It is the set of equation (1.7) for each of the control points that will comprise the bulk of our system of equations.

[i] Note that the ith control point here is synonymous with the point represented by the variable t in equation (1.5).

Calculating Panel Induced Velocities

In order to calculate the panel induced velocities, we want to discretize the vortex distribution along the boundary in a similar fashion to our discretization of the geometry above. In fact, as mentioned, we will split the integral of our boundary integral equation into segments—integrating over each panel. Along each panel then, we need to define a distribution of vortex strengths. There are several options for how

we might choose to discretize the vortex distributions along each panel. For example, we may choose to not distribute the strengths and simply use discrete ring vortices along the boundary. Alternatively, we may select the strength of the distribution to be constant along each panel. We may instead select the strength of the distribution to vary linearly along each panel. We could even choose a higher order distribution. For our use case, we will select a linear distribution scheme along each panel, with the panel end points acting as "nodes" between which we will integrate. Discretizing the vorticity distribution along the surface into linear segments then gives us an unknown vorticity magnitude, γ_j, at each panel endpoint (node).

We choose a linear distribution along each panel primarily because discrete distributions and constant distributions have or introduce issues[j] that are solved by moving to a linear distribution[5]. An added benefit is that a linear distribution allows a more accurate solution for a coarser discretization of the geometry than constant strength panels do. We choose not to utilize a higher order method mainly due to the difficulty of integrating our axisymmetric kernel (presented in **??**).

Because the surface integrals of velocities induced by axisymmetric vortex rings are exceptionally difficult to solve analytically, we will take a numerical approach. Specifically, we will utilize Gauss-Kronrod quadrature via the QuadGK.jl[k] package in the Julia[6] language. In general, quadrature is the process of approximating an integral of a function using a sum of weighted samples of the function:

$$\int_a^b f(x)\mathrm{d}x \approx \sum_k^N w_k f(x_k), \tag{1.8}$$

where the main task of the setup is to decide where along the integration interval to place the sample points, x_k, and what weights, w_k, to apply to those samples. Gauss-Kronrod quadrature is based on Gauss-Legendre quadrature, which uses orthogonal polynomial theory to select sample points and weights that allow for exact integration of polynomials up to degree $2N - 1$ (where N is the number of sample points), and other sufficiently smooth functions remarkably well. Despite being based on Gauss-Legendre quadrature, however, Gauss-Kronrod quadrature is not quite as accurate as pure Gauss-Legendre quadrature in a one-to-one comparison. Gauss-Kronrod quadrature can exactly integrate polynomials up to $3N + 1$ for $2N + 1$ sample points. The decrease in accuracy for the same conditions is the trade off required to be able to both calculate the integral approximation and the error in the integral approximation. The ability to quickly estimate error directly leads to capabilities for h-adaptive quadrature, which is an adaptive method that refines the integration range along portions that require further refinement for accuracy (such as sharp peaks, or perhaps discontinuities). So although not as accurate out of the box, obtaining more accurate integrals over domains that would be difficult for pure Gauss-Legendre quadrature becomes relatively simple, and a worthwhile trade.

[j] Specifically, as mentioned by Katz and Plotkin, discrete distributions are "inadequate near the stagnation points of a thick airfoil," and in practice are used for zero thickness airfoils rather than for closed surfaces. Additionally, constant vortex distributions introduce several issues also discussed by Katz and Plotkin that are solved by moving to a linear distribution scheme.

[5] Katz *et al.*, *Low speed aerodynamics*, 2001.

[k] https://juliamath.github.io/QuadGK.jl/stable/gauss-kronrod/

[6] Bezanson *et al.*, "Julia: A fresh approach to numerical computing," 2017.

In the nominal case when a panel induces velocity on the surface, but not on itself, we set things up as follows for a given panel and surface point, t: We start with the portion of the surface integral associated with the jth panel

$$\int_{p_j}^{p_{j+1}} \gamma(s) \frac{\partial \hat{\phi}(s,t)}{\partial \hat{n}_t} ds. \tag{1.9}$$

Because the unit normal applies at t, it is a constant in this integral. As such, we can express the integral in terms of the integration of velocities only, which are then multiplied by the components of the normal vector after integration.

$$
\begin{aligned}
v_{tj} &= \int_{p_j}^{p_{j+1}} \gamma(s) \frac{\partial \hat{\phi}(s,t)}{\partial \hat{n}_t} ds \\
&= \left(\int_{p_j}^{p_{j+1}} \gamma(s) \nabla \hat{\phi}(s,t) ds \right) \cdot \hat{n}_t \\
&= \left(\int_{p_j}^{p_{j+1}} \gamma(s) \hat{V}(s,t) ds \right) \cdot \hat{n}_t.
\end{aligned}
\tag{1.10}
$$

To get the integral in terms of components of velocity, we can split up the integral into its components

$$v_{z_{tj}} = \left(\int_{p_j}^{p_{j+1}} \gamma(s) v_z(s,t) ds \right) n_{i_z}, \tag{1.11a}$$

$$v_{r_{tj}} = \left(\int_{p_j}^{p_{j+1}} \gamma(s) v_r(s,t) ds \right) n_{i_r}. \tag{1.11b}$$

Since we are working toward assembling a system of equations, and we have introduced the unknown vortex magnitudes, γ_j, which define the vorticity distribution along the boundary, we need to obtain the integrals over the panels in terms of each of the panel node strengths (γ_j). As we perform our numerical integration, the quadrature procedure selects sample points along the range of integration as already mentioned. To make things easier to implement, we will transform our integrals such that the integrator will integrate on the range (0,1) and we will introduce the transformed variable ζ as the variable of integration.

$$v_{z_{tj}} = \left(\Delta s \int_0^1 \gamma(s(\zeta)) v_z(s(\zeta),t) d\zeta \right) n_{i_z}, \tag{1.12a}$$

$$v_{r_{tj}} = \left(\Delta s \int_0^1 \gamma(s(\zeta)) v_r(s(\zeta),t) d\zeta \right) n_{i_r}. \tag{1.12b}$$

where Δs is the length of the range of integration, or panel length. Referencing figure 1.3, we see that the quadrature function samples

[l] This is made possible due to the linear vortex distribution along a flat panel.

can be split into the influences of each of the panel nodes by a simple geometric weighting:[l]

$$f_j(x_k) = w_k f(s(\zeta_k), t) \qquad (1 - \zeta_k) \qquad \text{due to } \gamma_j \qquad \text{(1.13a)}$$
$$f_{j+1}(x_k) = w_k f(s(\zeta_k), t) \qquad \zeta_k \qquad \text{due to } \gamma_{j+1}. \qquad \text{(1.13b)}$$

In other words, we return a piece of the integral weighted according to the sample point location along the range of integration. Because we transformed the range of integration to $(0, 1)$, we can simply take these geometrically proportional weights to be $1 - \zeta$ and ζ where $\zeta \in (0, 1)$ for the jth and $(j + 1)$th nodes, respectively. Note that the γ_j values are also constant relative to ζ and are therefore not included in the integrand expressions of equation (1.13). This allows us to pull out all of the γ_j terms which are the unknowns for which we want to solve using the system of equations we are assembling. All together, the unit velocities normal to the ith panel, induced by the jth panel (defined by the jth and $(j + 1)$th nodes), or what we term the influence coefficients, IC, are
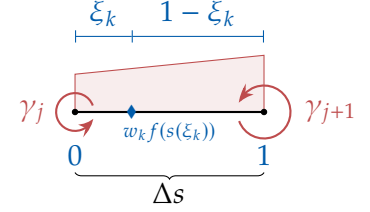
Figure 1.3: Visual representation of splitting the integral into the portions for each panel node.

$$IC_{ij} = \left(\Delta s_j \sum_k^N w_k v_z(s(\zeta_k), t)(1 - \zeta_k) \right) n_{i_z} + \left(\Delta s_j \sum_k^N w_k v_r(s(\zeta_k), t)(1 - \zeta_k) \right) n_{i_r}$$

$$IC_{i(j+1)} = \left(\Delta s_j \sum_k^N w_k v_z(s(\zeta_k), t)\zeta_k \right) n_{i_z} + \left(\Delta s_j \sum_k^N w_k v_r(s(\zeta_k), t)\zeta_k \right) n_{i_r},$$

$$\text{(1.14)}$$

for the jth and $(j + 1)$th nodes, respectively.

In the singular case, where the panel induces velocity on itself, more consideration is required. We first need to remember that we chose the midpoint of each panel to be the control point. Because the expression for induced velocity is singular when the distance between the point of influence and the point being influenced is zero, there is a singularity at the panel midpoint of a panel inducing velocity on its own control point. Knowing beforehand exactly where the singularity lies makes things somewhat easier to approach, but we still need to address the singularity. We will take a separation of singularity approach to calculate the self-induced case. The separation of singularity method is, in brief, to subtract out the singular piece of the integral while solving the integral, then afterward adding back in the singular piece solved analytically to avoid the computational issues associated with the computer attempting to divide by zero. Basically, as the integral tends to positive and negative infinity on either side of the singular point, we cancel out the non-convergent values on either side of the singular point and replace them with an analytic approximation. Mathematically we have the integral

$$v_{jj} = \int_{p_j}^{p_{j+1}} \gamma(s)I(s)ds, \qquad \text{(1.15)}$$

where

$$I(s) = \frac{\partial \hat{\phi}(s, \overline{p}_j)}{\partial \hat{n}_j}$$

We need to subtract off the singular part, S, (inside the integral), and then add back an analytical expression, A, for the integral of subtracted singular part (outside the integral). The other thing we need to do is to tell the quadrature package where the singular point is so that it can avoid placing sample points right on the singularity. Under the hood, the quadrature package actually splits the integral into two, integrating from the start of the integration range to the singular point, then from the singular point to the end of the integration range.[m]

$$v_{jj} = \int_{p_j}^{p_{j+1}} \gamma(\zeta)\Big(\big(I(s(\zeta), \overline{p}_j) - S(s(\zeta), \overline{p}_j)\big)\Big)\,d\zeta + \gamma A(\overline{p}_j). \qquad (1.16)$$

After these modifications to account for the singularity, the procedure for applying the quadrature is the same as before giving us the influence coefficients for the panel on itself to be

$$
\begin{aligned}
IC_{ii} =&\,\Delta s_i \left(\sum_k^N w_k \left[\big(v_z(s(\zeta_k), \overline{p}_i)\big)(1 - \zeta_k) - \frac{1}{2}S_z(s(\zeta_k), \overline{p}_i) \right] + \frac{1}{2}A_z(\overline{p}_i) \right) n_{i_z} \\
&+ \Delta s_i \left(\sum_k^N w_k \left[\big(v_r(s(\zeta_k), \overline{p}_i)\big)(1 - \zeta_k) - \frac{1}{2}S_r(s(\zeta_k), \overline{p}_i) \right] + \frac{1}{2}A_r(\overline{p}_i) \right) n_{i_r} \\
IC_{i(i+1)} =&\,\Delta s_i \left(\sum_k^N w_k \left[\big(v_z(s(\zeta_k), \overline{p}_i)\big)\zeta - \frac{1}{2}S_z(s(\zeta_k), \overline{p}_i) \right] + \frac{1}{2}A_z(\overline{p}_i) \right) n_{i_z} \\
&+ \Delta s_i \left(\sum_k^N w_k \left[\big(v_r(s(\zeta_k), \overline{p}_i)\big)\zeta - \frac{1}{2}S_r(s(\zeta_k), \overline{p}_i) \right] + \frac{1}{2}A_r(\overline{p}_i) \right) n_{i_r}
\end{aligned}
$$

$$(1.17)$$

where [n]

$$
\begin{aligned}
S_z(p_o, p) =&\, \frac{r_o - r}{2\pi \left[(z - z_o)^2 + (r - r_o)^2\right]} - \frac{1}{8\pi r_o}\left[\ln\left(\frac{(z - z_o)^2 + (r - r_o)^2}{64 r_o^2}\right)\right] \\
S_r(p_o, p) =&\, \frac{z - z_o}{2\pi \left[(z - z_o)^2 + (r - r_o)^2\right]},
\end{aligned}
$$

$$(1.18)$$

and

$$A_z(p) = \frac{1}{4\pi r}\left(1 + \ln\frac{8r}{\Delta s}\right)$$

$$A_r(p) = 0;$$

$$(1.19)$$

and the multiplication by 1/2 on the singular and analytic terms is due to the fact that the singular point is half way between the nodes, so each node is responsible for exactly half of the influence.

Assembling the linear system

To find the strengths of each vortex node that result in a vortex distribution inducing a flow field matching our prescribed body geometry, we need to assemble a system composed of equation (1.7) for each panel. Note, however, that currently our expression for K is indexed according to panel, and contains information about more than one panel node, which we need to remedy in order to get expressions for the individual strengths at each node. This is precisely why we separated out the node influences in the previous subsection. Thus each node has a component of influences associated with each panel to which it is an edge point. For the jth node then, we can add the contributions due to the $(j-1)$th and jth panels for which it is an edge point. This allows us to assemble the influence coefficient matrix based on a node-control point scheme rather than a panel-control point scheme:

$$G_{ij} = \begin{cases} IC_{ij} & \text{for } j = 1, N+1 \\ IC_{ij} + IC_{i(j-1)} & \text{for } 2 \leq j \leq N \end{cases} \quad (1.20)$$

where G is the $N \times N + 1$ matrix whose elements, G_{ij}, are the influence coefficients of the jth node ($N + 1$ total) on the ith control point (N total); and the influence components, IC, are defined in equations (1.14) and (1.17) for the nominal and self-induced cases, respectively. Since G is not square, as it has one more unknown than boundary conditions, we cannot solve the system directly as is. Fortunately, we also require an additional condition to make things work.

The Kutta Condition

One of the shortcomings of using potential flow theory is that by itself, it lacks inherent mechanisms for ensuring the flow leaves the surface of lifting bodies at the correct location and in the correct direction. One solution to this problem is known as the Kutta condition, which can be stated in several equivalent ways. However it is be stated, the Kutta condition requires the flow over a lifting body with a sharp trailing edge to leave the body at the trailing edge in a manner roughly tangent to the trailing edge. Therefore we can artificially enforce conditions that are observed in real, viscous flows at relatively low angles of attack. Just as there are several equivalent ways to state the Kutta condition, there are several ways that the Kutta condition may be implemented. One method is to require zero circulation at the trailing edge. We can enforce this by setting the strengths of the first and last panel nodes to be equal[o] and opposite such that

[o] Note that for a sharp trailing edge, where the nodes are coincident, they really should be equal anyway since they occupy the same point in space.

$$\gamma_1 + \gamma_N = 0. \quad (1.21)$$

In order to make our system square, we simply add the Kutta condition as the $N + 1$th equation.

By itself, this version of the Kutta condition can lead to spurious spikes in surface velocity near the trailing edge. In order increase the numerical robustness of the panel method, we apply an additional, indirect Kutta condition by placing an additional control point just inside the interior of the duct trailing edge and define an associated unit normal oriented such that the unit normal is effectively in the direction of the bisection angle of the trailing edge panels. We also place an additional control point inside the center body if it has a blunt trailing edge.[p]

[p] We will discuss shortly the case where the center body has a sharp trailing edge.

We apply the same boundary condition on these control point as the other control points in that we set the normal velocity induced by the freestream to be equal and opposite to the tangential velocity induced by the body boundaries on the control point.

$$\sum_{j=1}^{N+1} \gamma_j G_{kj}^{\circ\!-} = -V_\infty \cdot \hat{n}_k. \tag{1.22}$$

where the elements of $G^{\circ\!-}$ are the expressions defined in equation (1.14).

Upon the addition of this equation, however, we find ourselves with insufficient unknowns (one for each body being modeled). To remedy this insufficiency, we simply apply a dummy strength, τ_k, for the kth body and set all of its associated influence coefficients, $\mathcal{T}$, to 1 for the panels of the body it is applied to and zero elsewhere (including itself).

$$\mathcal{T}_{ik} = \begin{cases} 1 & \text{if } i = k \\ 0 & \text{otherwise} \end{cases} \tag{1.23}$$

We mentioned placing the additional control point just inside the trailing edge. This is done (rather than right at the middle of the trailing edge gap between the trailing edge nodes) to avoid numerical issues if the trailing edge is indeed sharp. We specifically place the node along the line bisecting the trailing edge angle and passing through the point halfway between the trailing edge nodes. The position is calculated as follows

$$z_{cp} = \overline{z}_{TE} - \epsilon \overline{\Delta s}_{TE} \frac{z_{\text{diff}}}{s_{\text{diff}}} \tag{1.24a}$$

$$r_{cp} = \overline{r}_{TE} - \epsilon \overline{\Delta s}_{TE} \frac{r_{\text{diff}}}{s_{\text{diff}}} \tag{1.24b}$$

$$\hat{n}_{z_{cp}} = \frac{z_{\text{diff}}}{s_{\text{diff}}} \tag{1.24c}$$

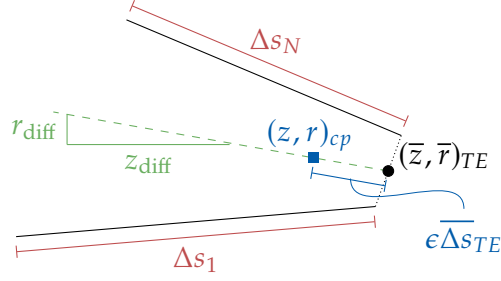$$\hat{n}_{r_{cp}} = \frac{r_{\text{diff}}}{s_{\text{diff}}} \tag{1.24d}$$

where

Figure 1.4: Geometric explanation of internal control point placement.

$$\epsilon = 0.05 \tag{1.25}$$

$$\bar{z}_{TE} = \frac{z_1 + z_{N+1}}{2} \tag{1.26}$$

$$\bar{r}_{TE} = \frac{r_1 + r_{N+1}}{2} \tag{1.27}$$

$$\overline{\Delta s}_{TE} = \frac{\Delta s_1 + \Delta s_N}{2} \tag{1.28}$$

$$z_{\text{diff}} = \Delta z_N - \Delta z_1 \tag{1.29}$$

$$r_{\text{diff}} = \Delta r_N - \Delta r_1 \tag{1.30}$$

$$s_{\text{diff}} = \left[z_{\text{diff}}^2 + r_{\text{diff}}^2 \right]^{1/2} \tag{1.31}$$

where the $\Delta(\cdot)$ lengths are calculated in the clockwise direction as before, and ϵ is chosen for generally good numerical behavior.

Additional Considerations for Open Bodies

The Kutta condition we have applied assumes that the trailing edge is both sharp and thin. This approximation tends to be relatively good for a large variety of geometries, and is well behaved numerically, but eventually breaks down. Specifically in the case of blunt trailing edges, when the trailing edge panel nodes are not coincident, the flow field can tend to flow into the inside of the body through the open trailing edge. To prevent this, we will add a trailing edge panel with distribution strengths determined from the adjacent panels, similar to the method used by XFOIL[7,8] for blunt trailing edges.

For any trailing edge panel, we will set a vortex and source distribution along the panel based on its orientation to the adjacent panels and the distribution strengths at the shared node locations:

7 Drela, "XFOIL: An Analysis and Design System for Low Reynolds Number Airfoils," 1989.

8 Fidkowski, "A Coupled Inviscid–Viscous Airfoil Analysis Solver, Revisited," 2022.

$$\gamma_{TE_j} = \left(\hat{\boldsymbol{n}}_{TE_j} \cdot \hat{\boldsymbol{n}}_{\text{adj}_j} \right) \gamma_{\text{adj}_j} \tag{1.32}$$

$$\sigma_{TE_j} = - \left| \hat{\boldsymbol{n}}_{TE_j} \times \hat{\boldsymbol{n}}_{\text{adj}_j} \right| \gamma_{\text{adj}_j}. \tag{1.33}$$

where the "adj" subscript indicates the adjacent panel. Based on these definitions of strength distributions across the trailing edge panels, we

can take the unit strengths (relative to the unknown distribution strengths on the shared nodes) to be

$$\hat{\gamma}_{TE_j} = \hat{\boldsymbol{n}}_{TE_j} \cdot \hat{\boldsymbol{n}}_{\text{adj}_j} \tag{1.34}$$

$$\hat{\sigma}_{TE_j} = -\left| \hat{\boldsymbol{n}}_{TE_j} \times \hat{\boldsymbol{n}}_{\text{adj}_j} \right|. \tag{1.35}$$

For trailing edge panels which have a node on the axis of rotation, for example, in the case of a center body with a blunt trailing edge, we set the strength (γ_{TE_j}) and derivative ($\partial \gamma_{TE_j} / \partial \gamma$) of the vortex distribution at the axis to zero. Since we do not have an adjacent panel on the axis side of such a trailing edge panel, we will simply use the same adjacent panel to calculate values for both source nodes of the trailing edge panel.[q]

To add the trailing edge panels to the linear system we do not want to add any more equations, because we have defined the trailing edge panel strengths according to unknowns we already have in the system. As such, we simply need to augment the influence coefficients for the panels adjacent to the trailing edge panels, since all the trailing edge panel information comes directly from those adjacent panels. For each panel with a node bordering a trailing edge panel, we add the following to the unit induced velocity on every control point

$$\hat{\boldsymbol{V}}^{\gamma}_{iTE_j} \overset{\pm}{=} \hat{\boldsymbol{V}}^{\gamma}_{iTE_j} \hat{\gamma}_{TE_j} + \hat{\boldsymbol{V}}^{\sigma}_{iTE_j} \hat{\sigma}_{TE_j}. \tag{1.36}$$

In other words, we add the unit induced velocity associated with the trailing edge node to the panel sharing that node scaled by how aligned the trailing edge and adjacent panel are. As an example, if the duct had a blunt trailing edge, we would define a trailing edge panel spanning the gap from the first to the last node in the airfoil geoemetry. We would then define the strengths and changes in strength relative to the first and last panels of the geometry (those at the trailing edge). Finally, we would augment the unit induced velocity due to the first and last nodes by the above expressions for the trailing edge gap panel we defined. We can apply this to the velocity directly, or we can simply add the velocities dotted with the control point normal vectors to the influence coefficient matrix after the fact.

$$G_{ij} \overset{\pm}{=} \left[\hat{\boldsymbol{V}}^{\gamma}_{iTE_j} \hat{\gamma}_{TE_j} + \hat{\boldsymbol{V}}^{\sigma}_{iTE_j} \hat{\sigma}_{TE_j} \right] \cdot \hat{\boldsymbol{n}}_i, \tag{1.37}$$

where the jth components of unit induced velocity, $\hat{V}$, are calculated from equation (1.14).[r]

Additional Considerations for Nodes on the Axis of Revolution

As we have already discussed, annular airfoils with non-zero cambered cross-sections require the addition of a Kutta condition. Bodies of revolution do not require such a condition in an axisymmetric scheme, but rather have other unique features to consider. Specifically, bodies

[q] We are effectively defining a constant strength source panel in this case.

[r] Exchanging the vortex ring induced unit velocities for those induced by source rings for the source terms in equation (1.37).

of revolution will have a panel node on the axis of revolution (at the leading edge). As we will see in the definition of unit induced velocity (equation (1.88)), if an influence point lies on the axis, that is if $r_o = 0$, then the induced velocity becomes infinite. In reality, the induced velocity from such a point is zero. Therefore in our system, we will need to prescribe the strengths of panel nodes on the axis of rotation to be zero strength. In order to achieve this, we take an approach similar to applying the Kutta condition: we simply add the equation

$$\gamma_{LE}^{cb} = 0 \tag{1.38}$$

to the system, where γ_{LE}^{cb} is the prescribed node strength for the center body leading edge. This additional equation also solves the issue of the matrix not being square due to there still being $N + 1$ nodes and only N panels for a body of revolution. If the center body trailing edge is sharp, then we have an additional node on the axis of rotation and also need to prescribe its strength to zero. As it turns out, we do not actually need the additional internal control point for bodies of revolution, but it doesn't hurt us to have it implemented. In the case of a closed trailing edge, we will effectively remove the internal control point and substitute its equation with an equation prescribing the trailing edge node strength to be zero like the leading edge node:

$$\gamma_{TE}^{cb} = 0. \tag{1.39}$$

Since we still have an additional equation, we will keep the dummy variable in place simply to keep the system square.

Solving the linear system

To avoid confusion, we will let G^* represent the influence matrix augmented by the Kutta condition, additional trailing edge control point equations, and any prescribed node equations. Because the overall coupled solver in DuctAPE will need to solve the linear system for the panel method many times, it is advantageous to do as much precomputation as possible for the panel method. The first thing that we will note is that the body geometry will not change throughout the coupled solve. This means that the influence matrix G^* can be fully precomputed and stored. Due to this fact, we can also speed up the multiple linear solves by performing a Lower-Upper (LU) decomposition of G^* such that

$$G^* = LU \tag{1.40}$$

where L and U are the lower and upper triangular matrices of the LU decomposition. By precomputing the LU decomposition, we can speed up the solution process of the linear system, which can now be expressed as

$$LU\gamma = b \tag{1.41}$$

where $b = (-V_\infty \cdot \hat{n})$. We can solve this system through the forward and backward substitution in two steps:

1. Solve $Ly = b$ for y.

2. Solve $U\gamma = y$ for γ.

Although this is a two-step process, it ends up being numerically more efficient than a more direct system solve method, and again has the benefit of being able to be precomputed and used repeatedly.

1.2.3   Obtaining Body-induced Velocities

Velocity Tangent to the Body Surface

After we have solved for the node strengths, γ, that coincide with our selected body geometry, we desire to use those strengths to find the velocity somewhere in the field. We are especially interested in finding the surface velocity on the body and using it to determine the pressure distribution on the body surface. In order to obtain the surface velocity, we need to find the velocity induced tangent to the panels. We can do so by applying the same kind of Fredholm integral expression, but this time taking the tangential derivative, and remembering that the jump term across the boundary for the tangential velocity is $-\gamma/2$ outward and $\gamma/2$ inward[3]:

3 Martensen, "Die Berechnung der Druckverteilung an dicken Gitterprofilen mit Hilfe von Fredholmschen Integralgleichungen zweiter Art," 1959.

$$v_{\tan}(t) = \pm\frac{\gamma(t)}{2} + \oint_S \gamma(s)\frac{\partial\hat{\phi}(s,t)}{\partial\hat{t}_t}ds + \frac{\partial\phi_\infty}{\partial\hat{t}_t} \tag{1.42a}$$

$$- \text{ or } -$$

$$v_{\tan}(t) = \pm\frac{\gamma(t)}{2} + \oint_S \gamma(s)\hat{V}(s,t) \cdot \hat{t}(t)ds + V_\infty \cdot \hat{t}(t). \tag{1.42b}$$

We can therefore use the same discretization scheme and induced velocity expressions as we did to create our linear system. To simplify things further, we can also simply take the sum of the full induced velocities on the control points and the magnitude will be the surface velocity. This is due to the fact that we solved for the vortex strengths based on the boundary condition of zero flow normal to the control points; therefore when all the velocity components are summed, all that is left is the velocity tangent to the surface.[s]

s Remember that the jump term is a jump in tangential velocity and the linear system solution only gave us a magnitude, so before adding the jump term in, we need to make sure to separate it into components tangent to the panel.

$$v_{\tan_i} = \left| \pm\frac{\overline{\gamma}_i}{2}\hat{t}_i + \sum_{j=1}^{N+1}\left[\gamma_j M_{ij}\right] + V_\infty \right|, \tag{1.43}$$

where

$$\overline{\gamma}_i = \frac{\gamma_i + \gamma_{i+1}}{2}, \tag{1.44}$$

and

$$M_{ij} = \begin{cases} IC_{ij}^t & \text{for } j = 1, N+1 \\ IC_{ij}^t + IC_{i(j-1)}^t & \text{for } 2 \le j \le N, \end{cases} \tag{1.45}$$

where for the nominal case, the components of the influence coefficients are defined identically to equation (1.14), but we keep them in vector format for simplicity:

$$IC_{ij}^t = \left(\Delta s_j \sum_k^N w_k v_z(s(\zeta_k), t)(1 - \zeta_k) \right) + \left(\Delta s_j \sum_k^N w_k v_r(s(\zeta_k), t)(1 - \zeta_k) \right)$$

$$IC_{i(j+1)}^t = \left(\Delta s_j \sum_k^N w_k v_z(s(\zeta_k), t)\zeta_k \right) \quad + \left(\Delta s_j \sum_k^N w_k v_r(s(\zeta_k), t)\zeta_k \right). \tag{1.46}$$

For the self-induced case, again, the expressions are identical to equation (1.17), but again we keep things in vector format rather than dotting with the normal:

$$IC_{ii}^t = \left(\Delta s_i \sum_k^N w_k \left[v_z(s(\zeta_k), \overline{p}_i) - S_z(s(\zeta_k), \overline{p}_i) + \frac{A_z(\overline{p}_i)}{\Delta s_i} \right] (1 - \zeta_k) \right)$$

$$+ \left(\Delta s_i \sum_k^N w_k \left[v_r(s(\zeta_k), \overline{p}_i) - S_r(s(\zeta_k), \overline{p}_i) + \frac{A_r(\overline{p}_i)}{\Delta s_i} \right] (1 - \zeta_k) \right)$$

$$IC_{i(i+1)}^t = \left(\Delta s_i \sum_k^N w_k \left[v_z(s(\zeta_k), \overline{p}_i) - S_z(s(\zeta_k), \overline{p}_i) + \frac{A_z(\overline{p}_i)}{\Delta s_i} \right] \zeta_k \right)$$

$$+ \left(\Delta s_i \sum_k^N w_k \left[v_r(s(\zeta_k), \overline{p}_i) - S_r(s(\zeta_k), \overline{p}_i) + \frac{A_r(\overline{p}_i)}{\Delta s_i} \right] \zeta_k \right). \tag{1.47}$$

Note that the coefficients, M, along with the system influence coefficients, G^*, can be precomputed and stored, although there is really no need for an LU-decomposition for M as there is no linear solve, but rather a direct matrix-vector multiplication to calculate the tangential velocity. In addition, the procedure in the presence of a trailing edge gap panel is identical to that presented for the normal induced velocities, with the exception already discussed here: that no dot product need be taken.

Velocity at Arbitrary Points in Space

For arbitrary points in space, the procedure for obtaining velocities is nearly identical, with the exceptions that there will be no self-induced or jump terms off the body surface, and we need not dot the components with any unit vector, as we typically want to know the velocity components in the global reference frame.

$$V_{\text{field}}(q) = \oint_S \gamma(s) \nabla \phi(s, q) \mathrm{d}s + \nabla \phi_\infty \tag{1.48a}$$

$$- \text{ or } -$$

$$V_{\text{field}}(q) = \oint_S \gamma(s) V(s, q) \mathrm{d}s + V_\infty. \tag{1.48b}$$

We can still use the same discretization scheme and induced velocity expressions as we did to create our linear system, and body surface velocity calculations, but this time, instead of dotting the velocity vector with some vector, we will keep things in a vector format. In other words, we will keep the axial and radial components of induced velocity separate:

$$V_{\text{field}}(q) = M\gamma + V_\infty. \tag{1.49}$$

where

$$M_j = \begin{cases} IC_j^f & \text{for } j = 1, N+1 \\ IC_j^f + IC_{j-1}^f & \text{for } 2 \leq j \leq N, \end{cases} \tag{1.50}$$

where

$$IC_j^f = \left[\Delta s_j \sum_k^N w_k v_z(s(\zeta_k), q)(1 - \zeta_k), \Delta s_j \sum_k^N w_k v_r(s(\zeta_k), q)(1 - \zeta_k) \right]$$

$$IC_{j+1}^f = \left[\Delta s_j \sum_k^N w_k v_z(s(\zeta_k), q)\zeta_k, \Delta s_j \sum_k^N w_k v_r(s(\zeta_k), q)\zeta_k \right]. \tag{1.51}$$

1.2.4 Ring Vortex Induced Velocities

We still have not defined the expression for the unit induced velocity due to a free vortex, $\hat{V}(s, t)$. This section covers the derivation of the induced velocity due to ring vortices, or in other words, axisymmetric free vortices. To derive an expression for the unit induced velocity due to a ring vortex, let us begin by defining some vector potential, ψ, such that[t]

[t] remembering the vector identity $\nabla \cdot \nabla \times \psi = 0$.

$$V = \nabla \times \psi, \tag{1.52}$$

and

$$\nabla \cdot \psi = 0, \tag{1.53}$$

or in other words, ψ is a divergence free vector field.[u]

[u] Therefore automatically satisfying continuity.

Next we take the definition of vorticity (vorticity is the curl of the velocity) and plug in our expression for ψ:

$$\omega = \nabla \times V$$
$$= \nabla \times (\nabla \times \psi) \tag{1.54}$$
$$= \nabla (\nabla \cdot \psi) - \nabla^2 \psi \quad \text{(vector identity)}.$$

Since we defined ψ to be divergence free, our expression for vorticity simplifies to the Poisson equation

$$\omega = -\nabla^2 \psi. \tag{1.55}$$

We can apply a Green's function in order to solve for ψ in three dimensions, where the known Green's function[v] takes the form of

$$G = \frac{-1}{4\pi |r|}, \tag{1.56}$$

where $|r|$ is the Euclidean distance from the point of influence and the point of interest. Applying this Green's function to the solution of ψ yields

$$\psi = \frac{1}{4\pi} \int_V \frac{\omega(q)}{|r|} d^3 s. \tag{1.57}$$

Now that we have a fundamental expression for ψ, let us look at the case for a vortex ring. We begin with some assumptions about the vortex ring that follow from assumption 1.1.

> **Assumption 1.5**
>
> *The vortex ring is circular, such that the ring radius is constant.*
>
> $$r_o = constant$$

> **Assumption 1.6**
>
> *The vortex ring circulation is constant and in the tangential direction*
>
> $$\mathbf{\Gamma} = \gamma \hat{e}_\theta$$

These assumptions formalize our axisymmetric assumption somewhat, and from them we can conclude that the vortex ring has no influence in the tangential direction, $\hat{e}_\theta$.

In figure 1.5 we see the coordinate system we will be using going forward. Without loss of generality, we will set the field point, p, to be on the $\theta = 0$ plane.

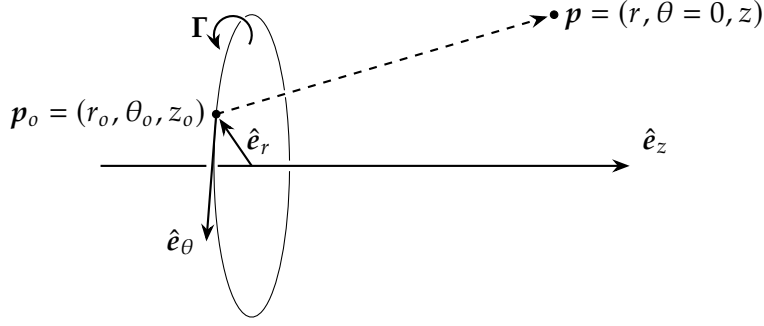Putting the solution to Poisson's equation in terms of our coordinate system gives

[v] See nearly any math text covering partial differential equation solution methods.

Figure 1.5: Coordinate system for vortex ring induced velocity.

$$\psi = \frac{1}{4\pi} \int_{\mathcal{V}} \frac{\omega(x')}{|p - p'|} r_o d\theta' dr' dz'. \tag{1.58}$$

For a vortex ring, which is infinitesimally thin in the $\hat{e}_r$ and $\hat{e}_z$ directions, we can define the vorticity of the ring to be

$$\omega(p) = \gamma \delta(z - z_o) \delta(r - r_o) \hat{e}_\theta. \tag{1.59}$$

where δ is the Dirac delta function. Plugging this expression in for vorticity, gives

$$\psi = \frac{1}{4\pi} \int_{\mathcal{V}} \frac{\gamma \delta(z - z_o) \delta(r - r_o) \hat{e}_\theta(\theta')}{|p - p'|} r_o d\theta' dr' dz'$$

$$\psi = \frac{1}{4\pi} \int_{-\pi}^{\pi} \frac{\gamma \hat{e}_\theta(\theta')}{|p - p'|} r_o d\theta', \tag{1.60}$$

which we can simplify by taking the constants out of the integral:

$$\psi = \frac{\gamma r_o}{4\pi} \int_{-\pi}^{\pi} \frac{\hat{e}_\theta(\theta')}{|p - p'|} d\theta'. \tag{1.61}$$

Next, let us tackle the denominator of the integrand, which is the Euclidean distance between a point on the vortex ring and a point we have chosen to be on the $\theta = 0$ plane. We apply the distance formula, for which we need to find the individual differences in each coordinate position. To obtain the Euclidean distance, it may be easier to momentarily think in terms of Cartesian coordinates, keeping the z-direction the same. Thus the length in the z-direction is simply the difference in the z-coordinates, $z - z_o$. To get the x and y distances, we require slightly more consideration. If we let the y-direction be normal to the $x - z$ plane (the $\theta = 0$ plane) on which the field point is defined, then we let the y component of the field point be $y = 0$, which means the distance in the y-direction is simply the position of the point on the ring, y_o. At a given θ_o, the distance in the y-direction will be $y_o = r_o \sin \theta_o$; θ being right hand positive taken about the z-axis. In the x-direction, we see that at the field point, the x-position is simply r, since the point lies on the $x - z$ plane. For the point on the vortex ring, we see that similar to the y-direction, the

x-position is $x_o = r_o \cos \theta_o$. Before putting everything together, let us apply a normalization that will prove to be convenient in our notation later. We will normalize the positions of the points by the vortex ring radius. We do this by multiplying by $r_o/r_o = 1$ giving the points in Cartesian coordinates as

$$p = r_o \left[\frac{z}{r_o} \hat{e}_z, \; 0\hat{e}_y, \; \frac{r}{r_o} \hat{e}_x \right] \tag{1.62}$$

$$p_o = r_o \left[\frac{z_o}{r_o} \hat{e}_z, \; \sin \theta_o \hat{e}_y, \; \cos \theta_o \hat{e}_x \right] \tag{1.63}$$

Putting all of these together we have

$$|p - p_o| = r_o \left[\left(\frac{z - z_o}{r_o} \right)^2 + (\sin \theta_o)^2 + \left(\frac{r}{r_o} - \cos \theta_o \right)^2 \right]^{1/2}. \tag{1.64}$$

To help clean up the notation, we will introduce the following normalized variables.

$$\xi = \frac{z - z_o}{r_o} \tag{1.65}$$

$$\rho = \frac{r}{r_o}. \tag{1.66}$$

In addition, we can simplify the radicand of our Euclidean distance expression by expanding the last term and applying the trigonometric identity $\sin^2 \theta + \cos^2 \theta = 1$:

$$\begin{aligned} &\xi^2 + \sin^2 \theta_o + \left(\rho - \cos \theta_o \right)^2 \\ &\xi^2 + \sin^2 \theta_o + \rho^2 + \cos^2 \theta_o - 2\rho \cos \theta_o \\ &\xi^2 + \left(\sin^2 \theta_o + \cos^2 \theta_o \right) + \rho^2 - 2\rho \cos \theta_o \quad \text{(trig identity)} \\ &\xi^2 + \rho^2 + 1 - 2\rho \cos \theta_o \end{aligned} \tag{1.67}$$

With this simplified radicand, equation (1.64) becomes

$$|p - p_o| = r_o \left[\xi^2 + \rho^2 + 1 - 2\rho \cos \theta_o \right]^{1/2}, \tag{1.68}$$

which if we plug back in to our full expression for ψ (equation (1.61)) we have

$$\psi = \frac{\gamma}{4\pi} \int_{-\pi}^{\pi} \frac{\hat{e}_\theta(\theta')}{\left[\xi^2 + \rho^2 + 1 - 2\rho \cos \theta' \right]^{1/2}} \mathrm{d}\theta'. \tag{1.69}$$

We now will apply one more advantage of our axisymmetric assumption, which is that both the potential and velocity fields are axisymmetric.

Because the field point is set, without loss of generality, on the $x - z$ (or $\theta = 0$) plane, we can take the radially induced velocity at the field point to be only in the x-direction, and the tangential component to be only in the y-direction. Therefore we make take $\hat{e}_\theta$ to be its y component: $\cos\theta\hat{e}_y$. Likewise, $\hat{e}_r$ can be replaced with its x-component: $\cos\theta\hat{e}_x$. Conveniently, this allows us to perform one integration over θ as the single variable rather than having to perform a double integration of x and y thereby reducing our expression for ψ to only the tangential component, ψ_θ. Therefore we replace the $\hat{e}_\theta(\theta')$ in the numerator of equation (1.69) with $\cos(\theta')$ to arrive at the expression for the tangential component of ψ,

$$\psi_\theta(x, x_o) = \frac{\gamma}{4\pi} \int_{-\pi}^{\pi} \frac{\cos(\theta')}{\left[\xi^2 + \rho^2 + 1 - 2\rho\cos\theta'\right]^{1/2}} d\theta'. \tag{1.70}$$

We are now left with a simplified expression for ψ, but that is still a relatively difficult integral to implement numerically, and perhaps more difficult to approach analytically. To make our lives easier, we are going to get our expression in terms of elliptic integrals, which are far simpler to implement numerically. We can make this transformation by first making a slight change to the bounds of integration, taking advantage of the fact that the integrand is an even function.

$$\psi_\theta(x, x_o) = \frac{\gamma}{2\pi} \int_{0}^{\pi} \frac{\cos(\theta')}{\left[\xi^2 + \rho^2 + 1 - 2\rho\cos\theta'\right]^{1/2}} d\theta'. \tag{1.71}$$

Next, we will apply the substitution

$$\theta' = 2\varphi \tag{1.72}$$
$$d\theta' = 2d\varphi, \tag{1.73}$$

noting the bounds of integration need to be divided by 2 as well, and changed to $[0, \pi/2]$. Applying equation (1.72) and the trigonometric identity $\cos(2\varphi) = 2\cos^2(\varphi) - 1$ gives

$$\begin{aligned}\psi_\theta(x, x_o) &= \frac{\gamma}{\pi} \int_{0}^{\frac{\pi}{2}} \frac{2\cos^2(\varphi) - 1}{\left[\xi^2 + \rho^2 + 1 - 4\rho\cos^2\varphi + 2\rho\right]^{1/2}} d\varphi \\ &= \frac{\gamma}{\pi} \int_{0}^{\frac{\pi}{2}} \frac{2\cos^2(\varphi) - 1}{\left[\xi^2 + (\rho + 1)^2 - 4\rho\cos^2\varphi\right]^{1/2}} d\varphi.\end{aligned} \tag{1.74}$$

We will immediately apply another substitution

$$\cos\varphi = t \tag{1.75}$$

$$d\varphi = \frac{dt}{-\sin\varphi}$$

$$= -\frac{dt}{\sqrt{1-\cos^2\varphi}} \tag{1.76}$$

$$= -\frac{dt}{\sqrt{1-t^2}},$$

where $\cos(\pi/2) = 0$ and $\cos(0) = 1$ so we will flip the bounds and cancel out the negative in equation (1.76):

$$\psi_\theta(\boldsymbol{p}, \boldsymbol{p_o}) = \frac{\gamma}{\pi} \int_0^1 \frac{2t^2 - 1}{\left[\xi^2 + (\rho + 1)^2 - 4\rho t^2\right]^{1/2} \left[1 - t^2\right]^{1/2}} dt. \tag{1.77}$$

Next we multiply by the top and bottom of the integrand by $\left[(\rho + 1)^2 + \xi^2\right]^{-1/2}$, noting that this term is constant relative to the integral and can therefore be brought outside.

$$\psi_\theta(\boldsymbol{p}, \boldsymbol{p_o}) = \frac{\gamma}{\pi \left[(\rho + 1)^2 + \xi^2\right]^{1/2}} \int_0^1 \frac{2t^2 - 1}{\left[1 - \frac{4\rho t^2}{(\rho+1)^2+\xi^2}\right]^{1/2} \left[1 - t^2\right]^{1/2}} dt. \tag{1.78}$$

we now let

$$m = \frac{4\rho}{(\rho + 1)^2 + \xi^2} \tag{1.79}$$

which cleans things up to be

$$\psi_\theta(\boldsymbol{p}, \boldsymbol{p_o}) = \frac{\gamma}{\pi \left[(\rho + 1)^2 + \xi^2\right]^{1/2}} \int_0^1 \frac{2t^2 - 1}{\left[1 - mt^2\right]^{1/2} \left[1 - t^2\right]^{1/2}} dt. \tag{1.80}$$

Our integrand is now almost matching to elliptic integrals. We just need to apply some algebraic manipulations to the numerator to match elliptic integral expressions of the form

$$\mathcal{K}(m) = \int_0^1 \frac{dt}{\sqrt{(1-t^2)(1-mt^2)}} \tag{1.81}$$

$$\mathcal{E}(m) = \int_0^1 \frac{\sqrt{1-mt^2}}{\sqrt{(1-t^2)}} dt \tag{1.82}$$

where $\mathcal{K}(m)$ and $\mathcal{E}(m)$ are elliptic integrals of the first and second kind, respectively. Making the required algebraic manipulations yields

$$\psi_\theta(\boldsymbol{p}, \boldsymbol{p}_o) = -\frac{\gamma}{\pi \left[(\rho+1)^2 + \xi^2\right]^{1/2}} \int_0^1 \frac{1 - \frac{2}{m} + \frac{2}{m}(1 - mt^2)}{[1 - mt^2]^{1/2}[1 - t^2]^{1/2}} dt. \quad (1.83)$$

Splitting the integrand up we have

$$\psi_\theta(\boldsymbol{p}, \boldsymbol{p}_o) = -\frac{\gamma}{\pi \left[(\rho+1)^2 + \xi^2\right]^{1/2}} \left[\left(1 - \frac{2}{m}\right) \int_0^1 \frac{dt}{[1 - mt^2]^{1/2}[1 - t^2]^{1/2}} \right.$$
$$\left. + \frac{2}{m} \int_0^1 \frac{[1 - mt^2]^{1/2}}{[1 - t^2]^{1/2}} dt \right].$$
$$(1.84)$$

Each of the integrals is now in the form of an elliptic integral. Making the substitution for elliptic integrals gives

$$\psi_\theta(\boldsymbol{p}, \boldsymbol{p}_o) = -\frac{\gamma}{\pi \left[(\rho+1)^2 + \xi^2\right]^{1/2}} \left[\frac{2}{m}\mathcal{E}(m) - \left(\frac{2}{m} - 1\right)\mathcal{K}(m) \right]. \quad (1.85)$$

General Form of Induced Velocities

The next step is to obtain the induced velocity from the vector potential, $\psi_\theta(\boldsymbol{p}, \boldsymbol{p}_o)$. Remember that $\boldsymbol{V} = \nabla \times \boldsymbol{\psi}$, which expands in cylindrical coordinates to

$$\begin{aligned} \boldsymbol{V} = &\left(\frac{1}{r}\frac{\partial \psi_z}{\partial \theta} - \frac{\partial \psi_\theta}{\partial z}\right) \hat{e}_r \\ &+ \left(\frac{\partial \psi_r}{\partial z} - \frac{\partial \psi_z}{\partial r}\right) \hat{e}_\theta \\ &+ \frac{1}{r}\left(\frac{\partial (r\psi_\theta)}{\partial r} - \frac{\psi_r}{\theta}\right) \hat{e}_z. \end{aligned} \quad (1.86)$$

Since our axisymmetric assumption allowed us to eliminate all but the tangential component of the vector potential, all but the ψ_θ components in equation (1.86) disappear, leaving us with the following induced velocities in the r- and z-directions.

$$v_z = \frac{1}{r}\frac{\partial (r\psi_\theta)}{\partial r}, \quad (1.87a)$$

$$v_r = -\frac{\partial \psi_\theta}{\partial z}. \quad (1.87b)$$

After some tedious algebra (see section 1.A), we arrive at the following expressions for the unit[w] induced velocity due to a vortex ring.

[w] In other words, we have set $\gamma = 1$

$$v_z^\gamma = \frac{1}{2\pi r_o} \frac{1}{D_1} \left[\mathcal{K}(m) - \left(1 + \frac{2(\rho - 1)}{D_2} \right) \mathcal{E}(m) \right] \tag{1.88a}$$

$$v_r^\gamma = -\frac{1}{2\pi r_o} \frac{\xi/\rho}{D_1} \left[\mathcal{K}(m) - \left(1 + \frac{2\rho}{D_2} \right) \mathcal{E}(m) \right] \tag{1.88b}$$

where the superscript, γ, indicates a unit vortex induced velocity. In addition, $\mathcal{K}(m)$ and $\mathcal{E}(m)$ are complete elliptic integrals of the first and second kind, respectively, and

$$m = \left(\frac{4\rho}{\xi^2 + (\rho + 1)^2} \right) \tag{1.89}$$

$$\xi = \frac{z - z_o}{r_o} \tag{1.90}$$

$$\rho = \frac{r}{r_o} \tag{1.91}$$

$$D_1 = \left[\xi^2 + (\rho + 1)^2 \right]^{1/2} \tag{1.92}$$

$$D_2 = \xi^2 + (\rho - 1)^2. \tag{1.93}$$

1.2.5   Ring Source Induced Velocities

Although our method for modeling the body aerodynamics primarily uses vortex ring distributions, we will find later that we will want to know the expressions for source ring induced velocities as well. We include those expressions here for easy reference. Note that a similar process to the derivation of the vortex ring induced velocities can be used to develop expressions for the induced velocity due to a ring source. Here we simply state the expressions from Ryall and Collins[9], noting that the expressions for vortex induced velocity we have derived here also match the expressions they give.

9 Ryall *et al.*, "Design and Test of a Series of Annular Aerofoils," 1967.

$$v_z^\sigma = \frac{1}{2\pi r_o} \frac{\xi}{D_1} \left(\frac{2}{D_2} \mathcal{E}(m) \right) \tag{1.94a}$$

$$v_r^\sigma = \frac{1}{2\pi r_o} \frac{1/\rho}{D_1} \left[\mathcal{K}(m) - \left(1 - \frac{2\rho(\rho - 1)}{D_2} \right) \mathcal{E}(m) \right], \tag{1.94b}$$

where the superscript, σ, indicates a unit source induced velocity. The other variables in equation (1.94) are as defined for the vortex ring expressions.

1.2.6   Validation of Isolated Body Aerodynamics

Isolated Duct

For the isolated duct, we compare with data provided by Lewis for an annular airfoil using the NACA 66_2-015 geometry and with a length to

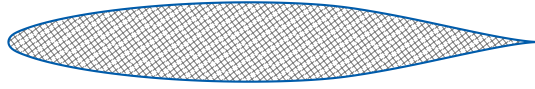2 Lewis, *Vortex Element Methods for Fluid Dynamic Analysis of Engineering Systems*, 1991.

Figure 1.6: Isolated annular airfoil cross section used for validation for a duct with length/diameter of 0.5988.

diameter ratio of 0.5988[2]. We generated smooth NACA 66-015 geometry using the airfoil tools within Open Vehicle Sketch Pad (OpenVSP)[10], and for the geometry producing figure 1.7, we interpolated the OpenVSP coordinates using a cosine spacing resulting in a total of 161 coordinate points, and thus 160 panels. See figure 1.6 for the cross sectional geometry we used. Figure 1.7 shows a comparison of the experimental data provided by Lewis and the computation output from DuctAPE. Observing figure 1.7, we see very good agreement with the experimental data, with minor discrepancies on the aft portion of the duct, due to viscous effects being ignored in the present methodology.
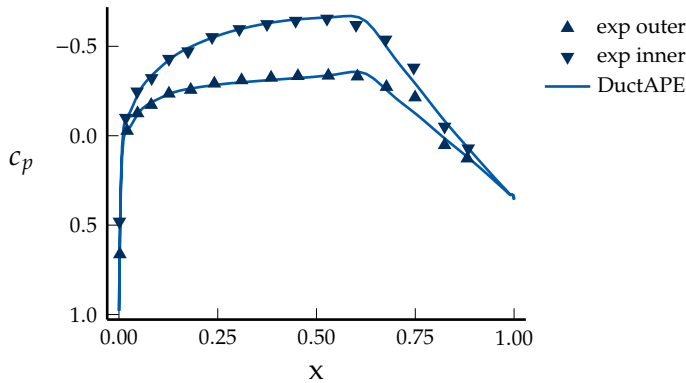
Figure 1.7: Comparison of experimental data with DuctAPE for an isolated duct shows very good agreement despite the inviscid approximation in DuctAPE's development.

Figure 1.8 shows a refinement convergence for the aforementioned geometry. We start with a very coarse refinement of 20 panels, and increase by 100 panels until reaching 700.[x] Comparing the value of the sum of the local surface pressure coefficients multiplied by the associated panel length, we see that for 160 panels, a typical number in general use cases, we have only a 0.93% difference from the value computed with 700 panels.

[x] Note that after 700 panels, the numerical integration scheme had trouble converging due to the proximity of the singularities for extremely small panels.

Isolated Center Body

For the isolated center body, we again compare with data provided by Lewis as shown in figure 1.9. Figure 1.7 shows a comparison of the experimental data provided by Lewis and the computation output from DuctAPE. We used the coordinates provided by Lewis to obtain the leading edge circular radius, the length of the flat portion, and the total length of the cross section to generate our own smooth geometry manually For the geometry producing figure 1.10, we interpolated the coordinates using a cosine spacing resulting in a total of 81 coordinate
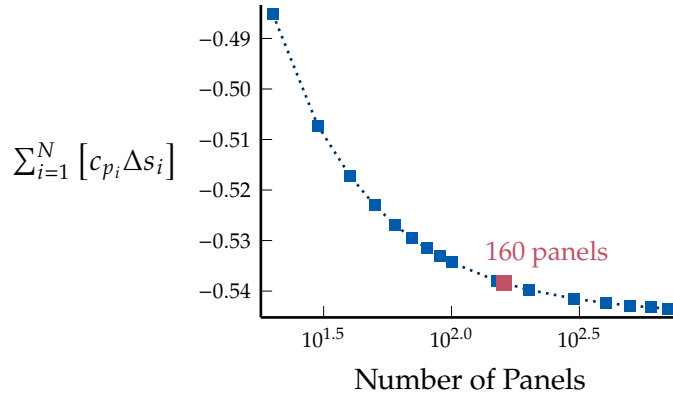
Figure 1.8: Between 100 and 200 panels is generally a sufficient refinement for our use case.

points, and thus 80 panels. Observing figure 1.10, we see good agreement with the experimental data, with discrepancies near the trailing edge which are, again, a result of the inviscid assumption in DuctAPE, as well as the small radial dimensions at the trailing edge, as discussed in section 1.2.2.

Figure 1.11 shows a refinement convergence for the aforementioned geometry. We start with a very coarse refinement of 20 panels, increasing by 10s until reaching 100 panels, after which we increase by 100 panels until reaching 350 (half of what was used in the duct validation). Comparing the value of the sum of the local surface pressure coefficients multiplied by the associated panel length, we see that for 80 panels, a typical number in general use cases, we have 14.7% difference from the value computed with 350 panels; though the absolute magnitudes are very small in the first place.

Multi-body System Verification

If we now combine these two geometries together, we can check that a multi-body system analysis works as expected. Unfortunately, we do not have any experimental data at the time for an isolated duct and center body, but we can compare with Ducted Fan Design Code, from which we have developed most of our methodology, for verification. Figure 1.14 shows the geometry of the duct and center body we have been using thus far for reference. We now place both in a single system in order to verify that multi-body systems work properly.

As can be seen in figure 1.13, the surface velocity on the hub and pressure on the duct match very well to DFDC, lending confidence in DuctAPE's ability to model both a duct and hub together.
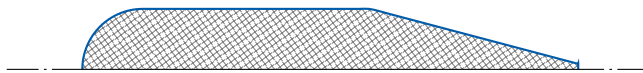

Figure 1.9: Isolated center body geometry used for validation; note the trailing edge does not extend all the way to zero radius.
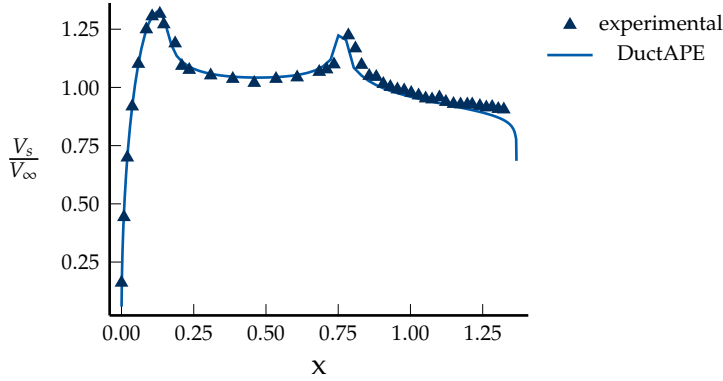
Figure 1.10: Comparison of experimental data with DuctAPE for an isolated hub shows good agreement despite the inviscid approximation in DuctAPE's development.

As a second check, we use geometry provided in the DFDC example files that contain blunt trailing edges on the duct and center body. In this case, we need to apply the augmentations to the system for trailing edge gap panels. We see in figure 1.15 that DuctAPE also matches well with DFDC in this case.
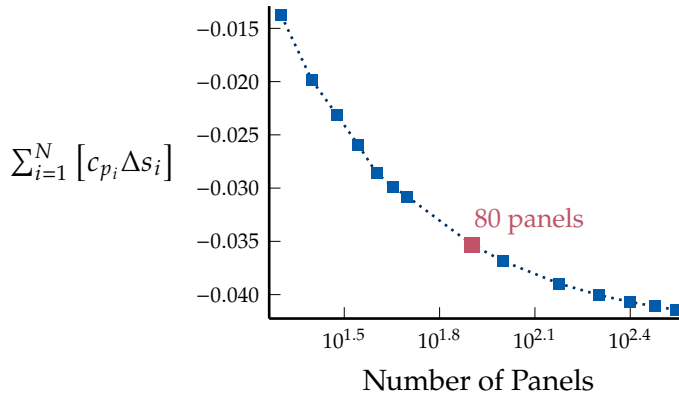

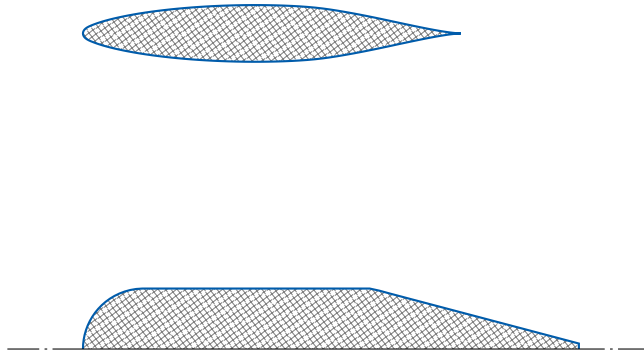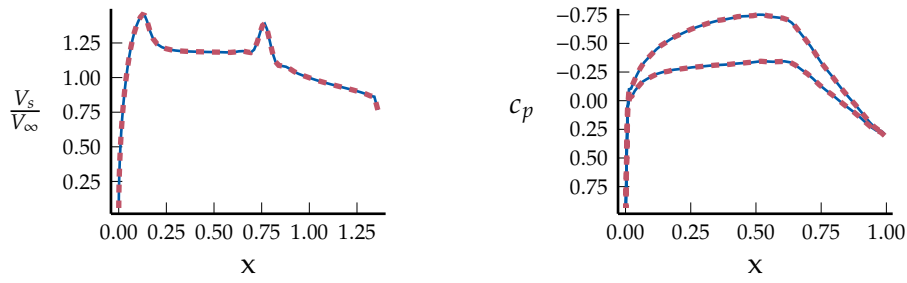**Figure 1.11:** Between 70 and 100 panels is generally a sufficient refinement for our use case.

Figure 1.12: Isolated duct and center body geometry together.

(a) Comparison of the surface velocity on the center body with sharp trailing edge calculated by DFDC and calculated by DuctAPE.

(b) Comparison of the surface pressure on the duct with sharp trailing edge calculated by DFDC and calculated by DuctAPE.

Figure 1.13: DuctAPE (blue) matches very well to DFDC (red dash) for the multi-body, no rotor case, with sharp trailing edges.

Figure 1.14: Duct and center body geometry provided in DFDC examples.

(a) Comparison of the surface velocity on the center body with blunt trailing edge calculated by DFDC and calculated by DuctAPE.

(b) Comparison of the surface pressure on the duct with blunt trailing edge calculated by DFDC and calculated by DuctAPE.

Figure 1.15: DuctAPE (blue) matches very well to DFDC (red dash) for the multi-body, no rotor case with blunt trailing edges.
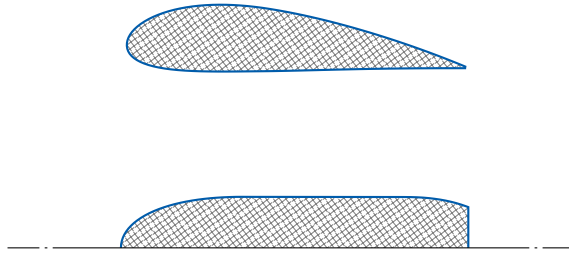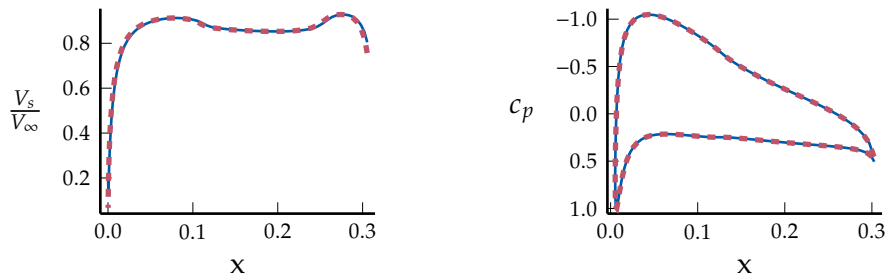
1.3 No Duct Solution: Rotor-Wake Lifting Line Model

1.3.1 Reference Frames

To begin, we need to start with an explanation of the various reference frames and velocity decompositions used in the rotor and wake models. We introduce multiple reference frames, because we would like to perform our analysis in steady frames. The first frame we will use is the absolute reference frame, which is the reference frame of an observer stationed at a static location on the duct wall. Since the aerodynamics of a rotor are inherently unsteady, we can't actually perfectly model things as steady. If we, however, change our reference frame to be relative to a blade as we pass across the blade, we can reasonably approximate the flow across the blade section as steady. In this blade relative, or simply relative, reference frame, the observer is stationed on a blade such that to the observer the blade is stationary.

Absolute Frame

Along with the absolute reference frame, we introduce the absolute coordinate system in figure 1.16. As can be seen, the duct is defined in a right-handed cylindrical coordinate system. We define the z axis to be along the axis of symmetry (also the center line/axis of rotation for the rotor(s)), positive in the downstream direction. The r axis is positive from the center line outward. Finally, θ is positive about the z-axis according to the right-handed system. We choose the origin to be located on the z axis, aligned with the duct leading edge, or in other words, the inlet plane.
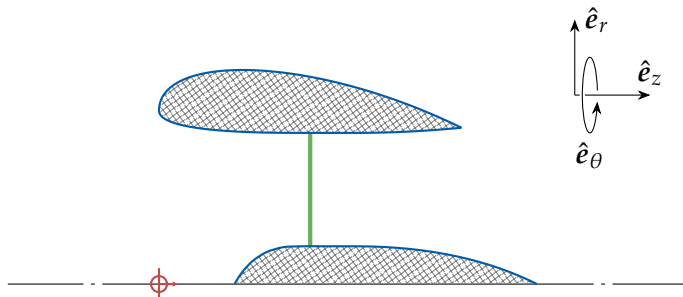
Figure 1.16: Meridional view showing the absolute reference frame. Example duct and center body geometry is shown in blue, the origin location is shown in red, and an example blade lifting line location is shown in green.

Relative Frame

It may be helpful to initially think of the blade element reference frame as orthogonal to the slice of the absolute frame shown in figure 1.16. Imagine standing on the blade looking from the direction of the duct wall toward the rotor hub (in the negative r direction). If you happen to be familiar with turbo-machinery conventions, the z-r slice of figure 1.16 is the meridional view, and the m-θ slice of figure 1.17 is the cascade view. We can use this cascade view to understand the various velocity

decompositions through which we can relate the absolute and relative reference frames. The blade rotates in the positive θ direction, and the m axis (where $dm^2 = dz^2 + dr^2$) is along a streamline passing through the lifting line representing the blade. That is to say, the m axis is the meridional axis, which may or may not be orthogonal to r for a given blade element.
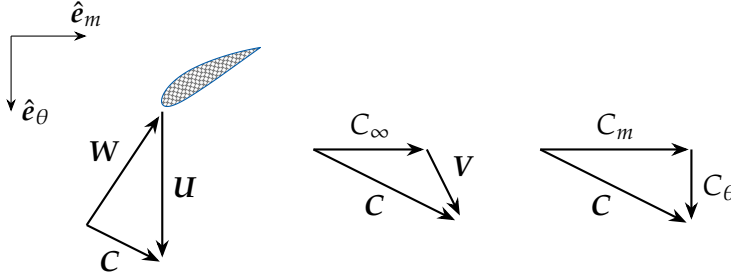

Figure 1.17: Cascade view showing the blade element relative frame with velocity decompositions.

Velocity Decomposition and Definition

The velocity triangles in figure 1.17 show how the various velocity components are combined into useful quantities. The components that give us the absolute local velocity, C, include: the freestream velocity, C_∞,[y] and the velocity induced by the rotors and duct, V. Together, we have

[y] We will assume according to assumption 1.1 that $C_\infty = ||C_\infty||\hat{z}$.

$$C = C_\infty \hat{z} + V \tag{1.95}$$

The relative velocity, W, is comprised of the absolute velocity, C, plus the rotational velocity at the respective radial station along the blade, $U = \Omega r \hat{\theta}$.

$$W = C - U$$
$$= C - \Omega r \hat{\theta} \tag{1.96}$$

It will be useful to put both C and W in terms of m and r. We get the velocities in terms of m and r by first separating out the various velocity components in the absolute reference frame and applying the definition of the meridional axis. The velocity in the absolute frame is broken down into its various components as

$$\begin{aligned} C_z &= V_z + C_\infty \\ C_r &= V_r \\ C_\theta &= V_\theta. \end{aligned} \tag{1.97}$$

Similarly, the relative velocity is broken down as[z]

[z] Note that we will use gray boxes to highlight expressions that are not used immediately, but will be vital in later sections of our development.

$$\begin{aligned} W_z &= V_z + C_\infty \\ W_r &= V_r \\ W_\theta &= V_\theta - \Omega r. \end{aligned} \tag{1.98}$$

These decompositions immediately yield the θ components of the velocities. To obtain the meridional component, we can use the definition of the meridional coordinate, that is, the direction tangent to the mean streamline in the $z - r$ (meridional) plane, to see that

$$C_m = W_m = C_z\hat{z} + C_r\hat{r}. \tag{1.99}$$

Now we have all the pieces to express the relative velocities in terms of the blade element frame (see the right-most velocity triangle in figure 1.17):

$$C = ||C_m||\hat{m} + C_\theta\hat{\theta} \tag{1.100}$$

$$W = ||C_m||\hat{m} + (C_\theta - \Omega r)\hat{\theta} \tag{1.101}$$

1.3.2 Rotor Blade Model

For the rotor blades, themselves, we model the blade element circulation and profile drag in the following subsections.

Blade Circulation

> **Assumption 1.7**
>
> *The rotor can reasonably be modeled as a lifting line such that local blade circulation can be expressed according to the Kutta-Joukowski theorem, which states:*
>
> $$F = \rho W \times \Gamma$$
>
> **Limitations:** We require the blade to be modeled as a single line, and we may not fully capture high solidity effects depending on how the force is obtained.
>
> **Justification:** This simplification allows for a more straightforward approach to the rotor-wake modeling, again reducing the computational complexity.

Modeling the rotor blades as lifting lines, if we take the velocity to be the local inflow velocity magnitude, $W = \left[W_z^2 + W_\theta^2\right]^{1/2}$ at the radial point of interest, we can take the perpendicular component of the force to be lift also at the radial point of interest. We can then rearrange the expression for the Kutta-Joukowski theorem in assumption 1.7 for the local circulation magnitude, $\Gamma(r)$, along the blade as

$$\Gamma(r) = \frac{L'}{\rho W}. \tag{1.102}$$

For each blade section, we will prescribe an airfoil polar such that the lift coefficient is known for a given angle of attack. If we then take the expression for the two-dimensional coefficient of lift—

$$c_\ell = \frac{2L'}{\rho W^2 c}, \tag{1.103}$$

where c is the blade element chord length, and c_ℓ is the local blade element lift coefficient— and substitute into our expression for circulation (again using the local meridional velocity), we arrive at

$$\Gamma(r) = \frac{1}{2} W c c_\ell, \tag{1.104}$$

where W, c, and c_ℓ are all functions of the radial position, r, along the rotor.

We use a blade element method approach to model the rotor aerodynamics, in that we use a lookup table to find the lift and drag coefficients based on the local blade element geometry and flow as shown in figure 1.18. In the case of a low-solidity rotor, we can simply use airfoil data based on the aerodynamic angle of attack, α, which is the inflow angle, β_1 minus the local blade element stagger angle, γ_{be}:

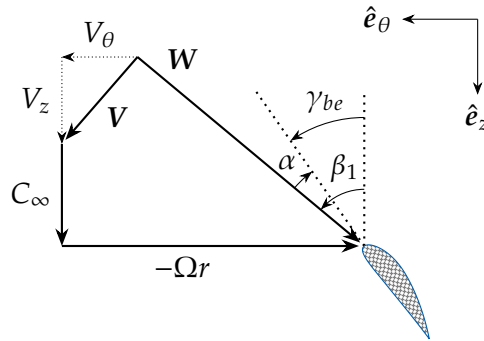**Figure 1.18:** Velocity decomposition with angles in the blade element frame.

$$\alpha = \beta_1 - \gamma_{be}, \tag{1.105}$$

where the inflow angle is defined as

$$\beta_1 = \arctan \frac{-W_\theta}{W_z} = \arctan \frac{\Omega r - V_\theta}{C_\infty + V_z}, \tag{1.106}$$

or in other words, the angle from the axis of rotation to the local inflow velocity vector, W, as seen in figure 1.18.

For higher solidity rotors, when cascade data is available, we look up the lift and drag coefficients based on the inflow and stagger angles directly. In addition, the section lift and drag coefficients may depend not only on the local angle of attack (or stagger and inflow angles), but may also be a function of the local Reynolds, Re_{be}, and Mach, M_{be}, numbers which we define in the typical manner:

$$Re_{be} = \frac{\rho_\infty W c}{\mu_\infty},$$
(1.107)

and

$$M_{be} = \frac{W}{a_{s_\infty}},$$
(1.108)

where ρ_∞, μ_∞, and a_{s_∞} are the freestream density, dynamic viscosity, and speed of sound, respectively. Here again, W and c are the local (at a given radial station) inflow magnitude and blade element chord length.

Rotor Profile Drag

> **Assumption 1.8**
>
> *The rotor blade section profile drag can be approximated by the addition of source elements along the rotor blade.*
>
> **Limitations:** We aren't fully modeling viscous effects in the wake.
>
> **Justification:** This allows us to model the wake inviscidly (which allows us to simplify the wake model later), while still approximating the viscous effects of the rotor on the wake velocities.

We define the rotor blade section profile drag per unit length in terms of a local airfoil polar drag coefficient using similar logic to how we defined the circulation due to lift. Though we are actually attempting to approximate a viscous effect inviscidly, so we are effectively equating the vorticity that would be introduced into the wake due to viscous profile drag with an approximate inviscid source distribution on the blade. Figure 1.19 shows visually this concept. The inviscid approximation of the profile drag per unit length then takes a similar form to the local circulation:

$$\Sigma = \frac{1}{2} W c c_d$$
(1.109)

where c_d is the blade element drag coefficient at the angle of attack described in section 1.3.2, and again, each of the terms on the right hand side are functions of the radial position along the blade. To get the total source sheet strength per unit length, we smear the total source strength per unit span of all the blades, B, around the circumference, 2π:

$$\sigma = \frac{B\Sigma}{2\pi}.$$
(1.110)
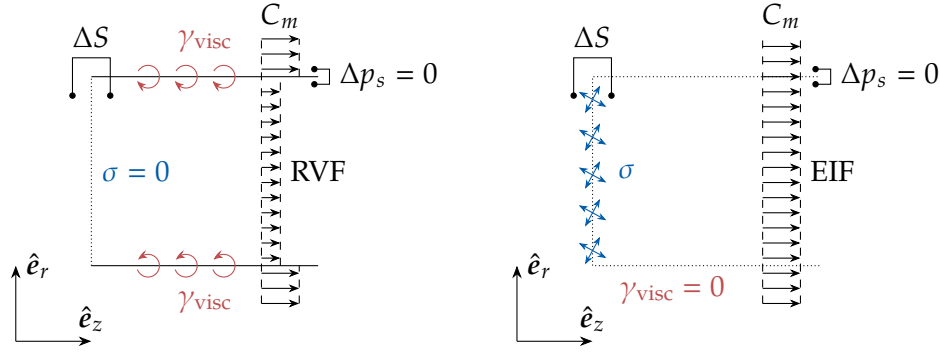
(a) The real, viscous formulation has no sources on the rotor blades, but rather sheds vorticity due to viscous effects.

(b) The equivalent inviscid formulation uses source distributions along the blade to approximate profile drag effects.

Figure 1.19: Visual comparison of real, viscous vs. equivalent inviscid formulations.

Therefore the expression for the smeared rotor source strength per unit length along the blade is

$$\sigma = \frac{B}{4\pi} W c c_d. \tag{1.111}$$

1.3.3 Wake Model

For a given position on a blade producing a circulation change, $\Delta\Gamma$, by conservation of circulation, a helical vortex filament of strength $-\Delta\Gamma$ is shed into the flow.

In order to represent 3D vortex filaments in our axisymmetric reference frames, we will also make the approximation that they can be smeared into equivalent axisymmetric vortex sheets in the m and θ directions.

> **Assumption 1.9**
>
> *Three-dimensional helical vortex filaments can be represented in a smeared axisymmetric model.*
>
> **Limitations:** We are not caputuring the full 3D and unsteady effects of the wake.
>
> **Justification:** We will see that we can develop a model that works very well with the panel method formulation of the solid body aerodynamics.

The smeared axisymmetric vortex sheets then have circulation to length ratios (densities) of γ_m and γ_θ in their respective directions. Because we are modeling the wake internal to the duct, we cannot guarantee a cylindrical wake, and therefore cannot simply model the wake with

straight vortex cylinders. Will will still use the concept of a wake cylinder, however to help us model discrete sections of the wake; so we continue with a description of how we smear a helical vortex filament into a cylindrical sheet.

We begin with a shed vortex sheet, the geometry of which we approximate by a left-handed helix such that the helical sheet is defined parametrically in terms of the variable $\bar{t}$ as

$$
\begin{aligned}
x(\bar{t}) &= r\cos(-\bar{t}) \\
y(\bar{t}) &= r\sin(-\bar{t}) \\
z(\bar{t}) &= \bar{t}\ell
\end{aligned}
\tag{1.112}
$$

in Cartesian coordinates, and

$$
\begin{aligned}
r(\bar{t}) &= r \\
\theta(\bar{t}) &= -\bar{t} \\
z(\bar{t}) &= \bar{t}\ell
\end{aligned}
\tag{1.113}
$$

in polar coordinates; where ℓ is the torsional parameter describing the distance traveled in the z direction relative to the angle traveled in θ:

$$
\ell = \frac{h}{2\pi} = \frac{\mathrm{d}z}{-\mathrm{d}\theta},
\tag{1.114}
$$

where h is the pitch of the helix, defined as the distance traveled in z for one rotation of the rotor blade, in other words, the distance traveled in z after traveling circumferentially $2\pi r$

$$
h = 2\pi r\frac{\ell}{r} = 2\pi r\frac{\mathrm{d}z}{-r\mathrm{d}\theta} = 2\pi\frac{\mathrm{d}z}{-\mathrm{d}\theta}.
\tag{1.115}
$$

Given the polar coordinates, we can define the pitch angle of the helix such that the tangent of that angle is the ratio of the distance traveled in z to the distance traveled circumferentially

$$
\tan\phi = \frac{\mathrm{d}z}{-r\mathrm{d}\theta} = \frac{\ell}{r}.
\tag{1.116}
$$

It may be good to mention here that typically we see ℓ defined in terms of h such that the torsional parameter is

$$
\ell = \frac{h}{2\pi}
\tag{1.117}
$$

From the pitch, we can obtain the apparent pitch, or the distance between the helix sheets created by consecutive blades by dividing the pitch by the number of blades, B,

$$
h_B = \frac{2\pi}{B}\frac{\mathrm{d}z}{-\mathrm{d}\theta}.
\tag{1.118}
$$

If we now assume that:

> **Assumption 1.10**
>
> *Vortex filaments are shed parallel to the relative inflow velocity, $\mathbf{W}$.*
>
> **Limitations:** This is a simplified modeling approach that ignores the some of the flow turning of the blade.
>
> **Justification:** By using this lifting line approach rather than some other approach, such as a lifting surface, we (like many of our other assumptions) simplify the model, allowing for simpler implementation and faster computation.

In other words, we assume that the local $\mathrm{d}z$ is in the direction of $\hat{e}_m$, and likewise $\mathrm{d}\theta$ in the direction of $\hat{e}_\theta$ as per figure 1.17, we obtain the non-dimensional length in the m direction for defining the γ_θ strength density

$$h_B \approx \frac{2\pi}{B}\left(\frac{W_m}{-W_\theta}\right).\tag{1.119}$$

(a) Wake Screw Geometry.
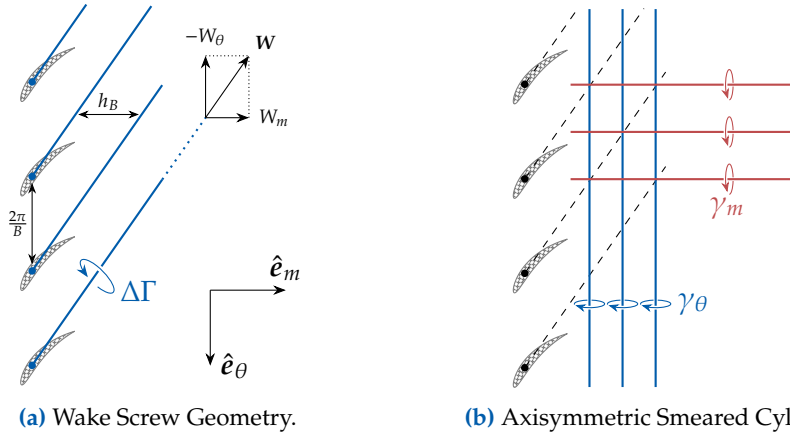

(b) Axisymmetric Smeared Cylinder.

Figure 1.20: 2D vortex sheets are generated from ratios of circulation to lengths between vortex sheets.

Figure 1.20 shows graphically the wake screw non-dimensional geometry and orientation of the smeared vorticity. To dimensionalize the lengths for a given smeared cylindrical surface, we multiply by the cylinder radius, r, to obtain the dimensional length. In addition, as we have defined our tangential vortices (see section 1.2) to be positive in the positive θ direction (the negative $\bar{t}$ direction), we need to apply an additional negative to ensure our vortices are oriented correctly. Thus

$$\boxed{\gamma_\theta = -\frac{-\Delta\Gamma}{h_B r} = -\Delta\Gamma\frac{B}{2\pi r}\left(\frac{W_\theta}{W_m}\right).}\tag{1.120}$$

To obtain an expression for γ_m we look at the distance between blades in the $\bar{t}$ direction, we know that the non-dimensional distance between

the blade sections is the distance about $\bar{t}$ divided by the number of blades (assuming even blade spacing), $2\pi/B$. For a given smeared cylinder of radius, r, we multiply by r to obtain the dimensional distance, $2\pi r/B$. To keep the vortices oriented positively in our reference frame, we need to apply an additional negative.Applying this additional negative the meridional vortex strength density (strength per unit length), γ_m, is

$$\gamma_m = \Delta\Gamma\frac{B}{2\pi r}. \tag{1.121}$$

Our expression for γ_m is generally applicable for steady state conditions if we use the local circulation jumps across the wake at any give point. Due to conservation of circulation, we know the circulation jumps anywhere downstream. On the other hand, γ_θ would only be generally applicable if we assumed that the Ωr component of W_θ (see equation (1.98)) was constant in the entire wake. In actuality, we only know Ωr right at the rotor lifting line, but not generally in the remainder of the wake. We therefore want to develop a more general expression for γ_θ based on requiring the wake to be force-free, or in other words, we demand static pressure continuity across the vortex sheets. The somewhat lengthy derivation for this more general expression for γ_θ comprises the rest of section 1.3.3.

Swirl/Circulation Relation

The swirl velocity induced by upstream rotor blades, V_θ, can be determined by applying Stokes' and Kelvin's theorems. If we define a control volume around a streamtube as shown in figure 1.21, where the first curve is taken about all upstream rotors along a streamline, and the second curve is taken about the axis of rotation, only in the r-θ plane with radius such that the edge of the contour lies on the same streamline upon which the first curve lies (see the dotted line in figure 1.21), we see by Kelvin's theorem (conservation of circulation), that the circulation due to the upstream rotors can be related to the tangential velocity downstream of the rotors through Stokes' theorem:

$$\widetilde{\Gamma} = \oint_0^{2\pi} \boldsymbol{V} \cdot r\mathrm{d}\boldsymbol{\theta}, \tag{1.122}$$

where $\widetilde{\Gamma}$ is the net circulation contribution of all the blades of the upstream rotors:

$$\widetilde{\Gamma} = \sum_{i=1}^N B_i\Gamma_i. \tag{1.123}$$

Performing the integration for a give radial position and rearranging for V_θ[aa] gives

[aa] Note that the θ component of V is the only component aligned with $\mathrm{d}\boldsymbol{\theta}$ and is circumferentially constant due to our smearing approxmation. In addition the contour is a circle, so the integral is determined immediately.
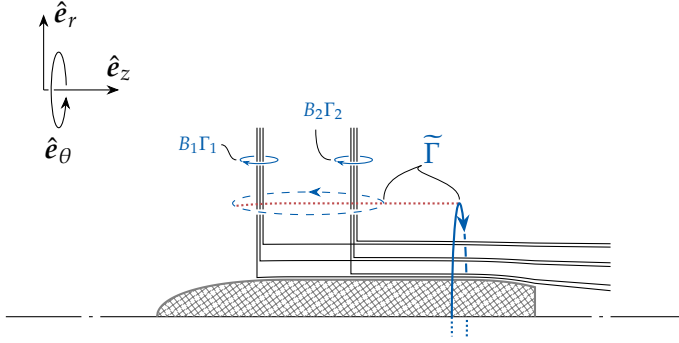
Figure 1.21: Circulation is conserved between the dashed and solid contours, noting the red dotted line indicating the streamline on which the $\widetilde{\Gamma}$ contours align. The integral over the contour about the axis of rotation yields V_θ in terms of $\widetilde{\Gamma}$.

$$V_\theta = C_\theta = \frac{\widetilde{\Gamma}}{2\pi r}, \tag{1.124}$$

where V_θ in our smeared, axisymmetric model is the circumferentially averaged swirl velocity induced by upstream rotors

For the self-induced case, the contour is placed at the rotor plane. This means that the rotor "sees" infinite trailing vortices from any upstream rotors, but only semi-infinite trailing vortices for itself. Thus the rotor experiences the full swirl induced by upstream rotors, but only half of its own swirl contribution:

$$(V_\theta)_{\text{self}} = \frac{1}{2\pi r}\left(\widetilde{\Gamma} + \frac{1}{2}B\Gamma\right), \tag{1.125}$$

where $B\Gamma$ here is the number of blades and circulation of the rotor itself.

Velocity Jumps
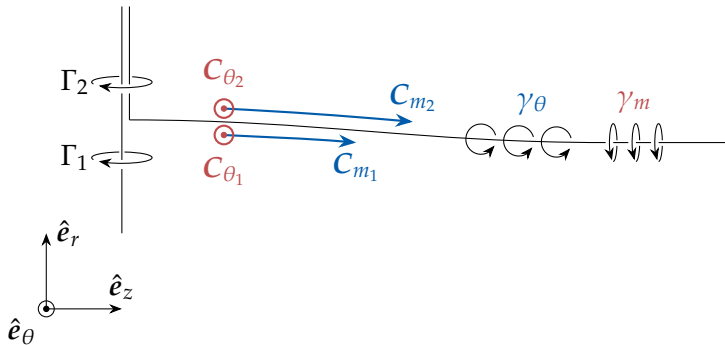
Figure 1.22: Circulation density can be related to velocity jump across axisymmetric vortex sheets.

The smeared sheet strengths of equations (1.120) and (1.121) can also be defined in terms of velocity jumps across the sheets.[ab] Starting with

[ab] Assuming here that the velocities in this subsubsection are the equivalent inviscid flow velocities, V_{inv}, implying that no additional vorticity is induced by blade profile drag. We also drop the "inv" subscript for simplicity.

equation (1.121), we can split the $\Delta\Gamma$ into $\Gamma_2 - \Gamma_1$ (taking $\widetilde{\Gamma} = B\Gamma$ for the single rotor) for a given vortex sheet

$$
\begin{aligned}
\gamma_m &= \frac{\Delta\widetilde{\Gamma}}{2\pi r} \\
&= \frac{B(\Gamma_2 - \Gamma_1)}{2\pi r}.
\end{aligned}
\tag{1.126}
$$

Then using equation (1.124)

$$
\begin{aligned}
V_{\theta_2} - V_{\theta_1} &= \frac{B\Gamma_2}{2\pi r} - \frac{B\Gamma_1}{2\pi r} \\
&= \frac{B(\Gamma_2 - \Gamma_1)}{2\pi r};
\end{aligned}
\tag{1.127}
$$

which we can then substitute in to get the sheet strength in terms of the velocity jump:

$$
\boxed{\gamma_m = \frac{B(\Gamma_2 - \Gamma_1)}{2\pi r} = C_{\theta_2} - C_{\theta_1}.}
\tag{1.128}
$$

As it so happens, in general for inviscid flows, the jump in tangential velocity across a vortex sheet is equal to the sheet vorticity per unit length (what we've previously called the circulation density). Therefore we can similarly equate equation (1.120) to a jump in the meridional velocities across the vortex sheet:

$$
\boxed{\gamma_\theta = -\frac{B(\Gamma_2 - \Gamma_1)}{2\pi r}\frac{W_{\theta_{\mathrm{avg}}}}{W_{m_{\mathrm{avg}}}} = C_{m_1} - C_{m_2}.}
\tag{1.129}
$$

where, to obtain the relative velocity components on the sheet, we combine the blade relative velocities just to either side of the sheet into averages, W_{avg}, as

$$
W_{\theta_{\mathrm{avg}}} \equiv \frac{1}{2}(W_{\theta_1} + W_{\theta_2}) = \frac{1}{2}(C_{\theta_1} + C_{\theta_2} - 2\Omega r)
\tag{1.130}
$$

$$
W_{m_{\mathrm{avg}}} \equiv \frac{1}{2}(W_{m_1} + W_{m_2}) = \frac{1}{2}(C_{m_1} + C_{m_2}).
\tag{1.131}
$$

If we divide equation (1.128) by equation (1.129), we get

$$
\begin{aligned}
\frac{\gamma_m}{\gamma_\theta} &= -\frac{W_{m_{\mathrm{avg}}}}{W_{\theta_{\mathrm{avg}}}} \\
\gamma_m W_{\theta_{\mathrm{avg}}} &= -\gamma_\theta W_{m_{\mathrm{avg}}} \\
W_{m_{\mathrm{avg}}}\gamma_\theta + W_{\theta_{\mathrm{avg}}}\gamma_m &= 0.
\end{aligned}
\tag{1.132}
$$

Substituting in the average velocities from equations (1.130) and (1.131) then gives

$$\frac{1}{2}(C_{m_1} + C_{m_2})\gamma_\theta + \frac{1}{2}(C_{\theta_1} + C_{\theta_2} - 2\Omega r)\gamma_m = 0. \qquad (1.133)$$

Then applying the definitions of the vortex strengths from equations (1.128) and (1.129) yields

$$\frac{1}{2}(C_{m_1} + C_{m_2})(C_{m_2} - C_{m_1}) + \frac{1}{2}(C_{\theta_1} + C_{\theta_2} - 2\Omega r)(C_{\theta_2} - C_{\theta_1}) = 0. \quad (1.134)$$

Simplifying

$$\frac{1}{2}(C_{m_1}^2 - C_{m_2}^2 + \cancel{C_{m_1}C_{m_2}} - \cancel{C_{m_1}C_{m_2}}) = -\frac{1}{2}(C_{\theta_2}^2 - C_{\theta_1}^2 + \cancel{C_{\theta_1}C_{\theta_2}} - \cancel{C_{\theta_1}C_{\theta_2}}) - \Omega r(C_{\theta_2} - C_{\theta_1})$$

$$\frac{1}{2}\left(C_{m_1}^2 - C_{m_2}^2 + C_{\theta_1}^2 - C_{\theta_2}^2\right) = -(C_{\theta_1} - C_{\theta_2})\Omega r$$

$$\frac{1}{2}\left((C_{m_1}^2 + C_{\theta_1}^2) - \left(C_{m_2}^2 + C_{\theta_2}^2\right)\right) = -(C_{\theta_1} - C_{\theta_2})\Omega r$$

$$\frac{1}{2}\left(C_1^2 - C_2^2\right) = -(C_{\theta_1} - C_{\theta_2})\Omega r$$

$$(1.135)$$

where $C^2 = C_m^2 + C_\theta^2$. Then applying the definition in equation (1.127) (and multiplying both sides by -1),

$$\boxed{\frac{1}{2}\left(C_2^2 - C_1^2\right) = -\frac{B(\Gamma_2 - \Gamma_1)}{2\pi}\Omega.} \qquad (1.136)$$

Thermodynamic Pressure Relationships

Total Pressure To determine the pressure relationships, we begin with the understanding that a rotor induces downstream changes in total enthalpy and entropy which are accompanied by changes in total pressure. We can relate these changes in pressure, enthalpy and entropy through the first and second laws of thermodynamics as follows. The first law of thermodynamics expressed in terms of enthalpy and in differential form is:

$$dq = dh - v dp_t \qquad (1.137)$$

where q is specific heat, h is specific entropy, v is specific volume and p_t is total pressure. The second law of thermodynamics, assuming an idealized (reversible) process, is expressed in differential form as:

$$T ds = dq \qquad (1.138)$$

where T is total temperature, and s is specific entropy. Plugging in the second law (equation (1.138)) into the first law (equation (1.137)) gives:

$$T ds = dh - v dp_t \qquad (1.139)$$

Which is a form of Gibb's equation in terms of enthalpy. We now have an expression relating pressure, enthalpy, and entropy. We will now use this differential expression (equation (1.139)) to arrive at a simpler and more useful expression for our application. First, we'll isolate entropy on the left hand side for convenience.

$$\mathrm{d}s = \frac{\mathrm{d}h}{T} - \frac{v\mathrm{d}p_t}{T}. \tag{1.140}$$

Moving away from using enthalpy briefly, we will assume:

> **Assumption 1.11**
>
> *The fluid is a calorically perfect gas.*
>
> **Limitations:** The specific heat capacity is constant.
>
> **Justification:** Our application is primarily at low Mach flows in electric ducted fans, for which air can reasonably be modeled as a calorically perfect gas. This allows us to obtain a simple relation between change in enthalpy, entropy and pressure.

In which case, we can relate enthalpy and temperature in both the following ways:

$$\mathrm{d}h = c_p\mathrm{d}T \tag{1.141}$$
$$h = c_pT, \tag{1.142}$$

where c_p here is the specific heat. Substituting equation (1.141)[ac] into equation (1.140), we have

[ac] note that since the rest of the terms are still in differential form, we cannot directly use equation (1.142) at this point.

$$\mathrm{d}s = \frac{c_p\mathrm{d}T}{T} - \frac{v\mathrm{d}p_t}{T}. \tag{1.143}$$

If we also apply the ideal gas law,

$$p_tv = RT$$
$$v = \frac{RT}{p_t} \tag{1.144}$$

to the last term, we have

$$\mathrm{d}s = \frac{c_p\mathrm{d}T}{T} - \frac{R\cancel{T}\mathrm{d}p_t}{\cancel{T}p_t}$$
$$\mathrm{d}s = c_p\frac{\mathrm{d}T}{T} - R\frac{\mathrm{d}p_t}{p_t}. \tag{1.145}$$

We now integrate equation (1.145) from the ambient to local conditions:

$$\int_{s_\infty}^{s} ds = c_p \int_{T_\infty}^{T} \frac{dT}{T} - R \int_{p_{t_\infty}}^{p_t} \frac{dp_t}{p_t}$$
$$s\Big|_{s_\infty}^{s} = c_p \ln(T)\Big|_{T_\infty}^{T} - R \ln(p_t)\Big|_{p_{t_\infty}}^{p_t}$$
$$s - s_\infty = c_p \left[\ln(T) - \ln(T_\infty)\right] - R \left[\ln(p_t) - \ln(p_{t_\infty})\right] \tag{1.146}$$
$$s - s_\infty = c_p \ln\left(\frac{T}{T_\infty}\right) - R \ln\left(\frac{p_t}{p_{t_\infty}}\right).$$

Next, we want to bring enthalpy back into the picture. To do so, we now utilize equation (1.142), multiplying the temperatures by c_p to get back into terms of specific enthalpy

$$s - s_\infty = c_p \ln\left(\frac{c_p T}{c_p T_\infty}\right) - R \ln\left(\frac{p_t}{p_{t_\infty}}\right)$$
$$s - s_\infty = c_p \ln\left(\frac{h}{h_\infty}\right) - R \ln\left(\frac{p_t}{p_{t_\infty}}\right). \tag{1.147}$$

If we now define changes relative to the (far upstream) freestream values (∞ subscripts) as:

$$\widetilde{p_t} = p_t - p_{t_\infty} \tag{1.148}$$
$$\widetilde{h} = h - h_\infty \tag{1.149}$$
$$\widetilde{s} = (s - s_\infty)/R, \tag{1.150}$$

then we can express equation (1.147) as[ad]

$$\widetilde{s} = \frac{c_p}{R} \ln\left(1 + \frac{\widetilde{h}}{h_\infty}\right) - \ln\left(1 + \frac{\widetilde{p_t}}{\widetilde{p_{t_\infty}}}\right). \tag{1.151}$$

[ad] Remembering that for x/y, subtracting and adding $1 = y/y$ gives $(x-y)/y+y/y = (x-y)/y + 1$

Now we will assume that

<div style="border:1px solid">

Assumption 1.12

The Mach number is sufficiently low such that

$$\frac{\widetilde{p_t}}{p_{t_\infty}} \ll 1 \tag{1.152}$$

$$\frac{\widetilde{h}}{h_\infty} \ll 1 \tag{1.153}$$

$$\widetilde{s} \ll 1, \tag{1.154}$$

Limitations: We are limited to low mach number regimes.

Justification: We can simplify the relationship between entropy, enthalpy, and pressure, again allowing for a simpler methodology

</div>

and faster computation.

With assumption 1.12 we can simplify equation (1.151) by noting that the Taylor series expansion for a logarithm is

$$\ln(x) = (x - 1) + \frac{1}{2}(x - 1)^2 + \text{higher order terms,} \tag{1.155}$$

if $x \approx 1$. Therefore, by assumption 1.12, we can simplify equation (1.151) using the first term in Taylor series approximations of each of the logarithm terms.

$$\widetilde{s} = \frac{c_p}{R} \ln \left(1 + \frac{\widetilde{h}}{h_\infty} \right) - \ln \left(1 + \frac{\widetilde{p}_t}{p_{t_\infty}} \right)$$

$$\widetilde{s} \simeq \frac{c_p}{R} \frac{\widetilde{h}}{h_\infty} - \frac{\widetilde{p}_t}{p_{t_\infty}}$$

$$\widetilde{s} \simeq \frac{\cancel{c_p}}{R} \frac{\widetilde{h}}{\cancel{c_p} T_\infty} - \frac{\widetilde{p}_t}{p_{t_\infty}} \qquad \text{apply equation (1.142)} \tag{1.156}$$

$$\widetilde{s} \simeq \frac{\rho_\infty}{p_{t_\infty}} \widetilde{h} - \frac{\widetilde{p}_t}{p_{t_\infty}} \qquad \text{apply ideal gas law}$$

$$p_{t_\infty} \widetilde{s} \simeq \rho_\infty \widetilde{h} - \widetilde{p}_t.$$

Rearranging leaves us with

$$\widetilde{p}_t \simeq \rho \left(\widetilde{h} - \widetilde{S} \right), \tag{1.157}$$

where

$$\widetilde{S} \equiv \frac{p_{t_\infty}}{\rho_\infty} \widetilde{s}, \tag{1.158}$$

where ρ is the air density, and for our steady, low Mach application, p_{t_∞}/ρ_∞ is nearly constant, so we can convect $\widetilde{S}$ downstream in place of $\widetilde{s}$. Therefore we end up seeing that the total pressure at any point in the rotor wake is the freestream total pressure plus any upstream work or losses:

$$p_t = p_{t_\infty} + \rho \left(\widetilde{h} - \widetilde{S} \right) \tag{1.159}$$

Static Pressure   The static pressure, p_s, is the total pressure minus the dynamic pressure:

$$p_s = p_t - \frac{1}{2} \rho V_{visc}^2. \tag{1.160}$$

Substituting in from equation (1.159) gives us

$$p_s = p_{t_\infty} - \frac{1}{2}\rho V_{visc}^2 + \rho\left(\widetilde{h} - \widetilde{S}\right), \tag{1.161}$$

where V_{visc} is the real viscous flow velocity. Rather than finding the full viscous flow field, which (among other things) would require more costly wake treatment, we can use the equivalent inviscid flow velocity, V_{inv}, through the addition of a source sheet at the drag elements in the flow (see assumption 1.8), removing the need for trailing vortex sheets for drag elements. See figure 1.19 for a visual representation of this concept. Using the equivalent inviscid flow simply eliminates entropy from equation (1.161)

$$p_s = p_{t_\infty} - \frac{1}{2}\rho V_{inv}^2 + \rho\widetilde{h}. \tag{1.162}$$

Disk Jumps

The specific work, w_c, done by a rotor is related to a jump in enthalpy across the rotor. As such, we can obtain $\widetilde{h}$ as the accumulation of changes in enthalpy across upstream disks.

$$\widetilde{h} = \sum_{i=1}^{N} \Delta h_{\text{disk}_m} \tag{1.163}$$

where the jump relation Δh_{disk} is defined according to the Euler turbine equation:

$$\Delta h_{\text{disk}} = w_c = \Omega\Delta(rC_\theta). \tag{1.164}$$

We can relate the jump in enthalpy to the circulation by applying our lifting line assumption (assumption 1.7), which means that there is no radial deviation in flow across the blade, as well as substituting in for C_θ from equation (1.124) (for a single disk).

$$\begin{aligned}
\Delta h_{\text{disk}} &= \Omega rC_\theta \\
&= \Omega \cancel{r}\frac{B\Gamma}{2\pi\cancel{r}} \\
&= \Omega\frac{B\Gamma}{2\pi}.
\end{aligned} \tag{1.165}$$

Pressure Jumps Using equation (1.162), we see the jump in static pressure across a vortex sheet is

$$p_{s_2} - p_{s_1} = -\frac{1}{2}\rho\left(V_{inv_2}^2 - V_{inv_1}^2\right) + \rho\left(\widetilde{h}_2 - \widetilde{h}_1\right). \tag{1.166}$$

If we substitute equation (1.165) in for the enthalpy terms, and equation (1.136) for the velocity terms in equation (1.166), we can simplify as follows

$$p_{s_2} - p_{s_1} = -\rho \frac{B(\Gamma_2 - \Gamma_1)}{2\pi}\Omega + \rho \frac{B(\Gamma_2 - \Gamma_1)}{2\pi}\Omega \tag{1.167}$$

$$p_{s_2} - p_{s_1} = 0 \tag{1.168}$$

which shows that there is no static pressure jump across the sheet, as would be expected in reality.

Tangential Vortex Sheet Strength

As promised at the beginning of section 1.3.3, we are finally posed to obtain a general expression for the tangential vortex sheet strength, γ_θ. Just as a reminder, we've needed all this preparation because the tangential sheet strength at an arbitrary downstream location is not generally equal to the value just behind the rotor disk. This is because we don't automatically know what the Ωr portion of the tangential velocity is anywhere except right at the rotor disk. Thus we have used the zero static pressure jump across the wake sheet as our condition for finding a general term for γ_θ. We'll begin with equation (1.166), setting the pressure jump to zero, as is physical, and divide out the density (assumed to be constant in our low Mach case) to obtain

$$\frac{1}{2}\left(C_2^2 - C_1^2\right) = \widetilde{h}_2 - \widetilde{h}_1. \tag{1.169}$$

Expanding out the left hand side gives

$$C_{m_2}^2 - C_{m_1}^2 + C_{\theta_2}^2 - C_{\theta_1}^2 = 2\left(\widetilde{h}_2 - \widetilde{h}_1\right). \tag{1.170}$$

Applying equation (1.124) for the C_θ terms:

$$C_{m_2}^2 - C_{m_1}^2 = -\left(\frac{1}{2\pi r}\right)^2\left(\widetilde{\Gamma}_2^2 - \widetilde{\Gamma}_1^2\right) + 2\left(\widetilde{h}_2 - \widetilde{h}_1\right). \tag{1.171}$$

To get the general expression for γ_θ, we have two options: if C_{m_2} is known, then using equation (1.129)

$$\gamma_\theta = C_{m_1} - C_{m_2}, \tag{1.129}$$

where from equation (1.171)

$$C_{m_1}^2 = C_{m_2}^2 + \left(\frac{1}{2\pi r}\right)^2\left(\widetilde{\Gamma}_2^2 - \widetilde{\Gamma}_1^2\right) - 2\left(\widetilde{h}_2 - \widetilde{h}_1\right), \tag{1.172}$$

gives us our general expression. We can march equation (1.172) radially inward, starting with $C_{m_2} = C_\infty$ just outside the outermost vortex sheet. On the other hand, if $C_{m_{\text{avg}}}$ is known instead, we can still use equation (1.171) to obtain γ_θ as follows:

$$C_{m_{\text{avg}}} = \frac{1}{2}\left(C_{m_1} + C_{m_2}\right) \tag{1.173}$$

$$C_{m_2}^2 - C_{m_1}^2 = \left(C_{m_1} + C_{m_2}\right)\left(C_{m_2} - C_{m_1}\right). \tag{1.174}$$

Substituting from equation (1.129)

$$C_{m_2}^2 - C_{m_1}^2 = -\left(C_{m_1} + C_{m_2}\right)\gamma_\theta. \tag{1.175}$$

Substituting from equation (1.173)

$$C_{m_2}^2 - C_{m_1}^2 = -2C_{m_{\text{avg}}}\gamma_\theta. \tag{1.176}$$

Rearranging for γ_θ and substituting from equation (1.171):

$$\gamma_\theta = -\frac{1}{2C_{m_{\text{avg}}}}\left(-\left(\frac{1}{2\pi r}\right)^2\left(\widetilde{\Gamma}_2^2 - \widetilde{\Gamma}_1^2\right) + 2\left(\widetilde{h}_2 - \widetilde{h}_1\right)\right). \tag{1.177}$$

1.3.4 Generating Rotor Wake Geometry

The question we must now ask ourselves is *where* is equation (1.177) applied? We may first think to model the rotor wake by integrating along streamlines, which could be done. An alternative method, however, is to define a "grid" defined by the solution of an elliptic partial differential system, using the solid bodies as the boundaries of the grid. By wisely choosing the partial differential equations to solve, we can generate a grid that is aligned with the streamlines for the inviscid isolated body system. Thompson, Thames, and Mastin[11] provide further insights into the benefits of this approach, which we will use for our application.

11 Thompson *et al.*, "Automatic numerical generation of body-fitted curvilinear coordinate system for field containing any number of arbitrary two-dimensional bodies," 1974.

Assumption 1.13

The wake streamlines can be reasonably approximated as lying on an elliptic grid.

Limitations: We are again ignoring viscous effects of the rotor/wake.

Justification: This is perhaps one of the greatest reducers of computational cost for the code, as it allows us to pre-compute the potentially large matrices for the induced velocities in the system.

By defining the wake geometry to lie on an elliptic grid, we can discretize the axisymmetric wake lines into axisymmetric vortex panels and apply the circulation density (vortex strength distribution) from equation (1.177) along the discretized wake panels. In order to define our wake geometry, our first task is to define the appropriate partial differential equation. As we are seeking to find the streamlines, we begin with the stream function.

Axisymmetric Stream Function

The z and r components of absolute velocity can be defined in terms of the axisymmetric stream function, $\psi(z, r)$, as

$$C_z = \frac{1}{\rho r}\frac{\partial \psi}{\partial r} \tag{1.178a}$$

$$C_r = \frac{-1}{\rho r}\frac{\partial \psi}{\partial z} \tag{1.178b}$$

where ρ is the air density. Additionally, the circumferential vorticity is defined as

$$\omega_\theta \equiv \frac{\partial C_z}{\partial r} - \frac{\partial C_r}{\partial z}. \tag{1.179}$$

If we plug equation (1.178) into equation (1.179), and apply the chain rule, we arrive at

$$\omega_\theta = \frac{1}{\rho r}\left(\frac{\partial^2 \psi}{\partial z^2} + \frac{\partial^2 \psi}{\partial r^2}\right) + \frac{\partial \psi}{\partial z}\frac{\partial}{\partial z}\left(\frac{1}{\rho r}\right) + \frac{\partial \psi}{\partial r}\frac{\partial}{\partial r}\left(\frac{1}{\rho r}\right). \tag{1.180}$$

which we can rearrange into a Poisson equation for ψ:

$$\omega_\theta = \frac{1}{\rho r}\left(\frac{\partial^2\psi}{\partial z^2}+\frac{\partial^2\psi}{\partial r^2}\right)+\frac{\partial\psi}{\partial z}\frac{\partial}{\partial z}\left(\frac{1}{\rho r}\right)+\frac{\partial\psi}{\partial r}\frac{\partial}{\partial r}\left(\frac{1}{\rho r}\right)$$

$$\omega_\theta = \frac{1}{\rho r}\left(\frac{\partial^2\psi}{\partial z^2}+\frac{\partial^2\psi}{\partial r^2}\right)$$

$$-\rho r C_r\frac{\partial}{\partial z}\left(\frac{1}{\rho r}\right)+\rho r C_z\frac{\partial}{\partial r}\left(\frac{1}{\rho r}\right) \qquad\text{(sub in equation (1.178))}$$

$$\rho r \omega_\theta = \frac{\partial^2\psi}{\partial z^2}+\frac{\partial^2\psi}{\partial r^2}$$

$$-\rho^2 r^2 C_r\frac{\partial}{\partial z}\left(\frac{1}{\rho r}\right)+\rho^2 r^2 C_z\frac{\partial}{\partial r}\left(\frac{1}{\rho r}\right) \qquad\text{(remove fraction)}$$

$$\rho r \omega_\theta = \frac{\partial^2\psi}{\partial z^2}+\frac{\partial^2\psi}{\partial r^2}$$

$$-\rho^2 r^2 C_r\left[\frac{1}{\rho}\frac{\partial}{\partial z}\cancel{\left(\frac{1}{r}\right)}^{0}+\frac{1}{r}\frac{\partial}{\partial z}\left(\frac{1}{\rho}\right)\right]$$

$$+\rho^2 r^2 C_z\left[\frac{1}{\rho}\frac{\partial}{\partial r}\left(\frac{1}{r}\right)+\frac{1}{r}\frac{\partial}{\partial r}\left(\frac{1}{\rho}\right)\right] \qquad\text{(product rule)}$$

$$\rho r \omega_\theta = \frac{\partial^2\psi}{\partial z^2}+\frac{\partial^2\psi}{\partial r^2}$$

$$-\rho^2 r^2 C_r\frac{-1}{\rho^2 r}\frac{\partial\rho_z}{\partial z}+\rho^2 r^2 C_z\left(\frac{-1}{\rho r^2}+\frac{-1}{\rho^2 r}\frac{\partial\rho_r}{\partial r}\right) \qquad\text{(take derivatives)}$$

$$\rho r \omega_\theta = \frac{\partial^2\psi}{\partial z^2}+\frac{\partial^2\psi}{\partial r^2}-rC_r\frac{\partial\rho_z}{\partial z}+rC_z\frac{\partial\rho_r}{\partial r}-\rho C_z \qquad\text{(simplify)}$$

$$\rho r \omega_\theta = \nabla^2\psi + r\left(\boldsymbol{C}_m\times\nabla\rho\right)\hat{\boldsymbol{e}}_\theta - \rho C_z \qquad\text{(condense)}$$

$$\rho r \omega_\theta = \nabla^2\psi + r\left(\boldsymbol{C}_m\times\nabla\rho\right)\hat{\boldsymbol{e}}_\theta - \frac{1}{r}\frac{\partial\psi}{\partial r} \qquad\text{(sub in equation (1.178))}$$

$$\nabla^2\psi = \frac{1}{r}\frac{\partial\psi}{\partial r} - r\left(\boldsymbol{C}_m\times\nabla\rho\right)\hat{\boldsymbol{e}}_\theta + \rho r\omega_\theta. \qquad\text{(rearrange)}$$

$$(1.181)$$

We do not know what the value is for ω_θ immediately, so we will find an expression for it using terms we do have. For an ideal, calorically perfect gas, the Crocco relation applied to our axisymmetric, steady flow in terms of total pressure is

$$\boldsymbol{C} \times \boldsymbol{\omega} = v \nabla \widetilde{p}_t$$

$$\boldsymbol{C} \times \boldsymbol{\omega} = \frac{1}{\rho} \nabla \widetilde{p}_t \qquad \text{(definition of specific volume)}$$

$$\boldsymbol{C} \times \boldsymbol{\omega} \simeq \frac{1}{\rho} \nabla \left[\rho \left(\widetilde{h} - \widetilde{S} \right) \right] \qquad \text{(apply equation (1.157))}$$

$$\boldsymbol{C} \times \boldsymbol{\omega} \simeq \nabla \left(\widetilde{h} - \widetilde{S} \right) \qquad \text{(incompressible)}$$

$$\boldsymbol{C} \times \boldsymbol{\omega} \simeq \nabla \widetilde{h} - \nabla \widetilde{S} \qquad \text{(distributive property)}$$

$$C_m \omega_\theta - C_\theta \omega_m \simeq \nabla \widetilde{h} - \nabla \widetilde{S} \qquad \text{(expand LHS)}$$

$$(1.182)$$

where we have defined C_θ in equation (1.124) as

$$C_\theta = \frac{\widetilde{\Gamma}}{2\pi r}; \qquad (1.124)$$

and the ω_m component of vorticity is defined as[ae]

$$\omega_m = -\frac{1}{r} \frac{\partial (r C_\theta)}{\partial n}$$

$$= -\frac{1}{2\pi r} \frac{\partial \widetilde{\Gamma}}{\partial n}. \qquad \text{(plug in equation (1.124))}$$

$$(1.183)$$

Thus[af]

$$C_\theta \omega_m \simeq -\frac{\widetilde{\Gamma}}{(2\pi r)^2} \frac{\partial \widetilde{\Gamma}}{\partial n}$$

$$\simeq -\frac{1}{2} \left(\frac{1}{2\pi r} \right)^2 \frac{\partial (\widetilde{\Gamma}^2)}{\partial n},$$

$$(1.184)$$

which we can substitute back into equation (1.182) to get an expression for ω_θ

$$\omega_\theta = \frac{-\frac{1}{2} \left(\frac{1}{2\pi r} \right)^2 \nabla \left(\widetilde{\Gamma}^2 \right) + \nabla \widetilde{h} - \nabla \widetilde{S}}{C_m}. \qquad (1.185)$$

We can now replace the ω_θ term in equation (1.181) to get a Poisson equation solely in terms that are part of our solution system:

$$\nabla^2 \psi = \frac{1}{r} \frac{\partial \psi}{\partial r} - r \left(\boldsymbol{C}_m \times \nabla \rho \right) \hat{e}_\theta + \rho r \frac{-\frac{1}{2} \left(\frac{1}{2\pi r} \right)^2 \nabla \left(\widetilde{\Gamma}^2 \right) + \nabla \widetilde{h} - \nabla \widetilde{S}}{C_m}. \qquad (1.186)$$

We also now take advantage of assumption 1.12 to eliminate the density dilation term, leaving us with

$$\nabla^2 \psi = \frac{1}{r} \frac{\partial \psi}{\partial r} + \frac{\rho r}{C_m} \left(-\frac{1}{2} \left(\frac{1}{2\pi r} \right)^2 \nabla \left(\widetilde{\Gamma}^2 \right) + \nabla \widetilde{h} - \nabla \widetilde{S} \right). \qquad (1.187)$$

We may also express this Poisson equation as

$$\nabla^2 \psi = Q_0 + Q_1 \tag{1.188}$$

where

$$Q_0 = \frac{\psi_r}{r} \tag{1.189}$$

$$Q_1 = \frac{\rho r}{C_m^2}\left[-\frac{1}{2}\left(\frac{1}{2\pi r}\right)^2 C_m \times \nabla\left(\widetilde{\Gamma^2}\right) \right.$$
$$\left. + C_m \times \nabla\widetilde{h} - C_m \times \nabla\widetilde{S}\right]\hat{e}_\theta \tag{1.190}$$

The Q_0 term is a result of the axisymmetry of the problem. The three terms of the source term, Q_1, are first, the transverse circulation gradient, second, the transverse work gradient, and last, the transverse loss gradient.

Elliptic Wake Grid

We are now ready to generate the solution grid, parametrically defined from our global coordinates through Poisson equations:[ag]

$$\xi(z,r) \equiv \nabla^2\xi = \xi_{zz} + \xi_{rr} = P \tag{1.191}$$

$$\eta(z,r) \equiv \nabla^2\eta = \eta_{zz} + \eta_{rr} = Q. \tag{1.192}$$

where η = constant along streamlines (thus η coordinates correspond to the physical location of streamlines) and ξ is constant along radial lines as seen in figure 1.23. With η corresponding to streamlines, it makes sense to set equation (1.192) equal to equation (1.188), such that $\psi = \eta$ and $Q = Q_0 + Q_1$. Since the ξ values are arbitrary, we may as well set $P = 0$ which allows ξ to be arbitrarily chosen. Note that we don't have the information available for source term, Q_1, before solving, so for initialization we simply set it to zero. Later, after the non-linear solve, we may choose to update the grid and re-solve.
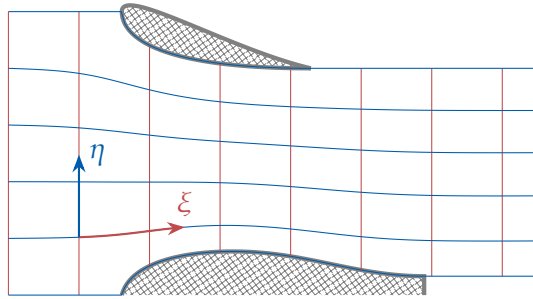

Figure 1.23: Elliptic grid coordinate system showing lines of constant η (blue) coinciding with streamlines, and lines of constant ξ (red) are constant relative to change in radius when the z-coordinates of the upper and lower boundaries are aligned.

In order to solve for the specific (ξ, η) coordinates, we need to invert the dependent and independent variables in equations (1.191) and (1.192). In order to do so, we use the following derivative transformations:

$$f_z = \frac{r_\eta f_\xi - r_\xi f_\eta}{J} \tag{1.193}$$

$$f_r = \frac{-z_\eta f_\xi + z_\xi f_\eta}{J} \tag{1.194}$$

where $J = z_\xi r_\eta - z_\eta r_\xi$.

The details of the inversion are included in section 1.E. After the inversion, we are left with expressions for z and r with respect to ξ and η.

$$\alpha z_{\xi\xi} - 2\beta z_{\xi\eta} + \gamma z_{\eta\eta} = \frac{J}{r} z_\eta z_\xi \tag{1.195}$$

$$\alpha r_{\xi\xi} - 2\beta r_{\xi\eta} + \gamma r_{\eta\eta} = \frac{J}{r} z_\eta r_\xi \tag{1.196}$$

or equivalently in terms of α, β, γ only:

$$\boxed{\begin{aligned}
\alpha z_{\xi\xi} - 2\beta z_{\xi\eta} + \frac{\gamma}{r}\left(r z_\eta\right)_\eta - \frac{\beta}{r} r_\xi z_\eta = 0 \\
\alpha r_{\xi\xi} - 2\beta r_{\xi\eta} + \frac{\gamma}{r}\left(r r_\eta\right)_\eta - \frac{\beta}{r} r_\xi r_\eta = 0
\end{aligned}} \tag{1.197}$$

where

$$\alpha = z_\eta^2 + r_\eta^2 \tag{1.198}$$

$$\beta = z_\xi z_\eta + r_\xi r_\eta \tag{1.199}$$

$$\gamma = z_\xi^2 + r_\xi^2 \tag{1.200}$$

$$J = z_\xi r_\eta - z_\eta r_\xi \tag{1.201}$$

We can obtain expressions for the velocity in terms of z and r if we take the differential identities of the transformations

$$\begin{bmatrix} z_\xi & z_\eta \\ r_\xi & r_\eta \end{bmatrix} \begin{pmatrix} d\xi \\ d\eta \end{pmatrix} = \begin{pmatrix} dz \\ dr \end{pmatrix} \tag{1.202}$$

$$\begin{bmatrix} \xi_z & \xi_r \\ \eta_z & \eta_r \end{bmatrix} \begin{pmatrix} dz \\ dr \end{pmatrix} = \begin{pmatrix} d\xi \\ d\eta \end{pmatrix} \tag{1.203}$$

and invert one, say equation (1.202),

$$\begin{pmatrix} d\xi \\ d\eta \end{pmatrix} = \frac{1}{J} \begin{bmatrix} r_\eta & -z_\eta \\ -r_\xi & z_\xi \end{bmatrix} \begin{pmatrix} dz \\ dr \end{pmatrix} \tag{1.204}$$

then set them equal to each other

$$\begin{bmatrix} \xi_z & \xi_r \\ \eta_z & \eta_r \end{bmatrix} \begin{pmatrix} dz \\ dr \end{pmatrix} = \frac{1}{J} \begin{bmatrix} r_\eta & -z_\eta \\ -r_\xi & z_\xi \end{bmatrix} \begin{pmatrix} dz \\ dr \end{pmatrix} \tag{1.205}$$

we see that

$$\xi_z = \frac{r_\eta}{J} \tag{1.206}$$

$$\xi_r = \frac{-z_\eta}{J} \tag{1.207}$$

$$\eta_z = \frac{-r_\xi}{J} \tag{1.208}$$

$$\eta_r = \frac{z_\xi}{J}. \tag{1.209}$$

Thus the velocities can be computed from equation (1.178) as

$$C_z = \frac{1}{\rho r} \frac{d\psi}{dr} = \frac{\eta_r}{\rho r} = \frac{z_\xi}{\rho r J} \tag{1.210}$$

$$C_r = \frac{-1}{\rho r} \frac{d\psi}{dx} = \frac{-\eta_z}{\rho r} = \frac{z_\xi}{\rho r J}. \tag{1.211}$$

We can now solve for the z and r grid node positions by assigning ξ and η values to each grid line, and solving equation (1.197) using the boundary conditions of fixed geometry (z, r positions) on solid walls and the inlet plane[ah], and fixed velocity magnitude ($C_z^2 + C_r^2$) on streamlines and the outlet plane[ai].

[ah] This is a Dirichlet boundary condition.

One final consideration is the end of the wake. By Helmholtz' theorems, we cannot just have the vortex filaments of the wake (smeared or otherwise) simply end. On the rotor blades, we have lines of circulation [(reference one of the figures)] from which the wake filaments are shed (as would be expected from a lifting line method). We have not, however, defined those shed wake filaments to be semi-infinite, but rather to be discretized into smeared vortex panels. Therefore we need to either extend them to infinity, or "close the loop;" we choose the latter. At the end of each wake element, we add a panel similar to the trailing edge panels for the centerbody, which extends from the last wake node along the streamline to the axis of rotation. In contrast to the centerbody trailing edge panel, we only apply the vorticity portion of the wake panel strength based on the last wake node along the streamline.

[ai] This is a Neumann boundary condition.

Solution Approach:
re-write

1.3.5   Verification and Validation of Isolated Rotor+Wake Aerodynamics

Verification of Induced Velocities

To verify that the rotor and wake models are behaving as expected, we look at the induced velocities (axial and swirl) at locations ranging from upstream of the rotor to downstream of the rotor. We compare to blade element momentum theory (BEMT) using the CCBlade.jl Julia package. The rotor we use for comparison is the APC 10x5 propeller; geometry for which is provided in the CCBlade documentation and in the UIUC database. Figure 1.24 shows the near- and far-field values from BEMT compared to the DuctAPE values across the range of locations sampled. We see that the general trends match well: the upstream velocities are at or near zero, and the far field velocities are approximately double the velocities at the rotor plane. Note that the swirl velocity as modeled in DuctAPE is zero upstream of the rotor, and the far-field value at any point aft of the rotor as described by equations (1.124) and (1.125).
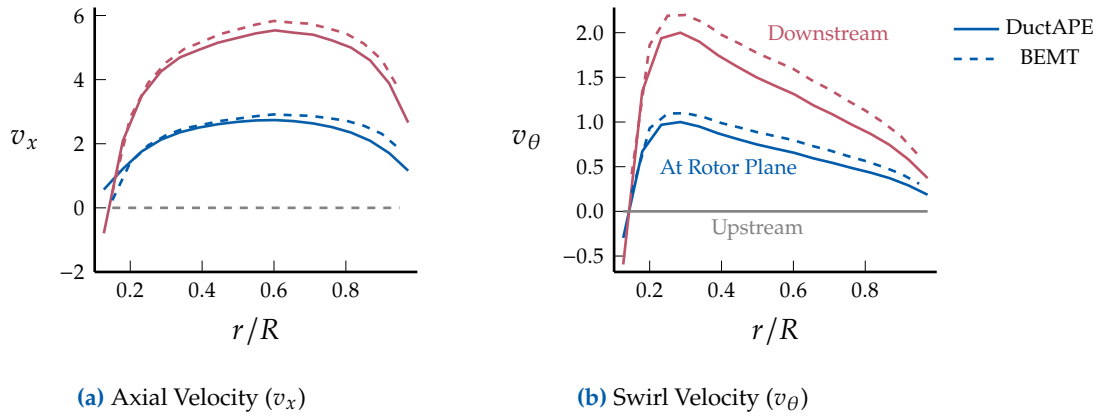

(a) Axial Velocity (v_x)   **(b)** Swirl Velocity (v_θ)

Figure 1.24: Comparison of induced velocities from BEMT near and far field with induced velocities from DuctAPE sample at a range from one diameter upstream (gray) to the rotor plane (blue) and from the rotor plane to one diameter downstream (red).

Validation of Thrust and Power Coefficients

For one validation case, we compare the thrust and power coefficients as well as efficiency with experimental data provided by UIUC for the APC 10x5. We also compare to the BEMT outputs for further context. As can be seen in figure 1.25, DuctAPE matches well with BEMT, and both are within expectations when compared to experimental data.

1.4   Post-Processing

After we have solved the non-linear system for unknown body, rotor, and wake strengths, we need to perform some post-processing in order to assess useful outputs such as thrust, torque, power, efficiency, blade loading, etc. This section covers the methodology for calculating desired outputs.
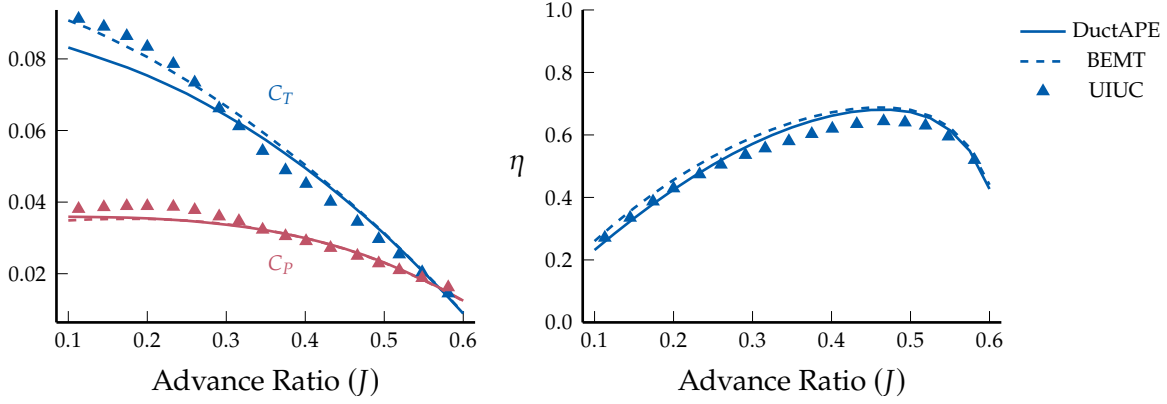
(a) Comparison of rotor power (C_P) and thrust (C_T) coefficients.

(b) Comparison of rotor efficiency (η).

Figure 1.25: A comparison of rotor performance metrics across a range of advance ratios (J) shows good agreement between DuctAPE, BEMT, and experimental data.

1.4.1 Body Thrust

The body thrust is the sum of forces on the bodies and may augment the total system thrust and therefore efficiency. Due to assumption 1.1, the net radial pressure forces on the body cancel; we also assume there are no tangential forces induced due to the bodies. We therefore sum the forces due to pressure in the axial direction to obtain thrust due to the bodies.

$$T_{\text{bod}} = \frac{1}{2}\rho_\infty V_{\text{ref}}^2 f_z \tag{1.212}$$

where the non-dimensional force coefficient, f_z, is the integral of the pressure force coefficient in the axial direction about the body surfaces:

$$f_z = \sum_{i=1}^{N_b} 2\pi \int_{S_i} r(s_i)(c_{p_{\text{out}}} - c_{p_{\text{in}}})(s_i)\hat{n}_z(s_i)\mathrm{d}s_i. \tag{1.213}$$

In the case of a blunt trailing edge, the trailing edge gap panel is also included in the integral for the total axial force coefficient, though the pressure coefficient values used in that case are simply the average of the adjoining panels in the duct case, and the last panel in the center body case. Since the trailing edge gap panels are in general pointing in the positive axial direction, this provides a rough approximation of profile drag due to the blunt trailing edges.

 Note that in equation (1.213) we integrate the difference in surface pressure between the outer and inner sides of the body surface. This is due to the fact that there is a non-zero induced velocity on the inner side of the body boundaries as mentioned in section 1.2.3. To obtain the thrust due to a pressure difference, then, we require to net pressure induced on the body surfaces rather than just the externally induced

surface pressure. Internally, there is no additional effects on the surface pressure by the rotor and wake. Externally however, there is a jump in pressure aft of the rotor(s) inside the duct.

Aft of the rotor plane(s), the pressure coefficient changes due to the enthalpy and entropy jumps across the rotor plane as well as the addition of swirl velocity. Remembering equation (1.157) we see that the steady state pressure coefficient changes due to the disk jumps as

$$
\begin{aligned}
\Delta c_{p_{hs}} &= \frac{\widetilde{p}_t}{\frac{1}{2}\rho V_{\text{ref}}^2} \\
&= \frac{\rho\left(\widetilde{h} - \widetilde{S}\right)}{\frac{1}{2}\rho V_{\text{ref}}^2} \\
&= \frac{\widetilde{h} - \widetilde{S}}{\frac{1}{2}V_{\text{ref}}^2}
\end{aligned}
\tag{1.214}
$$

The pressure is also altered by the addition of swirl velocity due to the rotor. We treat this in the same manner as we do for the nominal, steady pressure coefficient based on the surface velocity. For the nominal case, we only look at the velocity in the axial and radial directions, obtaining the velocity tangent to the body surfaces. The pressure coefficient, is given by

$$
c_p = \frac{p - p_\infty}{\frac{1}{2}\rho V_{\text{ref}}^2}
\tag{1.215}
$$

By assumption 1.3, we can apply Bernoulli's equation

$$
p_\infty + \frac{1}{2}\rho V_\infty^2 = p + \frac{1}{2}\rho V_{\text{tan}}^2
\tag{1.216}
$$

$$
p - p_\infty = \frac{1}{2}\rho V_\infty^2 - \frac{1}{2}\rho V_{\text{tan}}^2
\tag{1.217}
$$

where V_{tan} is the velocity tangent to the body surface, and substitute into the numerator and cancel to obtain

$$
c_p = \frac{V_\infty^2 - V_{\text{tan}}^2}{V_{\text{ref}}^2}
\tag{1.218}
$$

Aft of the rotor, inside the duct, and on the outer side of the body surfaces V_{tan} contains a swirl component that is not present upstream of the rotor. Since the $V_{\theta_\infty} = 0$, the change in pressure coefficient aft of the rotor due to the addition of swirl velocity is simply

$$
\Delta c_{p_\theta} = -\frac{V_\theta^2}{V_{\text{ref}}^2}
\tag{1.219}
$$

All together the outer surface pressure coefficient rise aft of a rotor is then:

$$\Delta c_p = \Delta c_{p_{hs}} + \Delta c_{p_\theta}$$

$$= \frac{2(\widetilde{h} - \widetilde{S}) - V_\theta^2}{V_{\text{ref}}^2}. \tag{1.220}$$

1.4.2 Rotor Performance

Blade Loading

Rotor performance calculation begins with determining the blade element aerodynamic loads. To obtain the loads in the axial and tangential direction, we start with the lift and drag coefficients for the blade elements, calculated as explained in section 1.3.2. The lift and drag coefficients are then rotated into the axial and tangential directions using the inflow angle, β_1:

$$c_z = c_\ell \cos(\beta_1) - c_d \sin(\beta_1) \tag{1.221}$$

$$c_\theta = c_\ell \sin(\beta_1) + c_d \cos(\beta_1), \tag{1.222}$$

where c_z is the force coefficient in the axial direction, and c_θ is the force coefficient in the tangential direction. We then multiply by the chord length to scale the force and dimensionalize to obtain the forces per unit length:[aj]

[aj] It is these forces that are used in an aerostructural analysis and optimization setting.

$$f_n = \frac{1}{2}\rho_\infty W^2 c c_z \tag{1.223}$$

$$f_t = \frac{1}{2}\rho_\infty W^2 c c_\theta. \tag{1.224}$$

We can then integrate these forces per unit length across the blade and multiply by the number of blades to obtain the full rotor thrust, T_{rot}, and torque, Q, on the rotor.

$$T_{\text{rot}} = B \int_{R_{\text{hub}}}^{R_{\text{tip}}} f_n \, dr \tag{1.225}$$

$$Q = B \int_{R_{\text{hub}}}^{R_{\text{tip}}} f_t r \, dr \tag{1.226}$$

Power is related to torque by the rotation rate, Ω, and is therefore immediately found as well:

$$P = Q\Omega. \tag{1.227}$$

It is common to express the rotor thrust, torque and power as non-dimensional coefficients. We use the propeller convention here. The thrust coefficient, C_T, is

$$C_T = \frac{T}{\rho_\infty n^2 D^4}, \tag{1.228}$$

where $n = \Omega/2\pi$ is the rotation rate in revolutions per second and $D = 2R_{\text{tip}}$ is the rotor tip diameter. The torque coefficient, C_Q, is

$$C_Q = \frac{Q}{\rho_\infty n^2 D^5},\tag{1.229}$$

and the power coefficient, C_P, is

$$C_P = C_Q\Omega\tag{1.230}$$

Efficiency

The rotor efficiency is the ratio of the thrust to power multiplied by the freestream velocity.

$$\eta_{\text{rot}} = \frac{T_{\text{rot}}}{P}V_\infty.\tag{1.231}$$

To obtain the total system efficiency, we simply add the body thrust to the rotor thrust.

$$\eta_{\text{tot}} = \frac{T_{\text{tot}}}{P}V_\infty.\tag{1.232}$$

where

$$T_{\text{tot}} = T_{\text{rot}} + T_{\text{bod}}\tag{1.233}$$

The ideal efficiency is useful for comparing the actual efficiency with the theoretical potential and is defined as

$$\eta_{\text{ideal}} = \frac{2}{1 + \left[\dfrac{1+T_{\text{tot}}}{\frac{1}{2}\rho_\infty V_\infty^2 \pi R_{\text{ref}}^2}\right]^{1/2}}.\tag{1.234}$$

1.5   Coupling the Rotor-Wake and Body Aerodynamics

Coupling the body and rotor-wake aerodynamics is, for the most part, a straightforward process, with only a few particular concerns. Essentially, the coupling takes place through mutually induced velocities. Specifically, the solid bodies, rotor(s), and wake(s), all induce velocities one themselves and each other. Accounting for these induced velocities is nearly the totality of the coupling methodology.

For the solid bodies, we subtract the induced velocities normal to the panels to the right hand side of the linear system, just as we do for the freestream velocities. In addition, at the wake-body interfaces, or in other words, for the wake elements shed from the rotor hub and tip (assuming the rotor tip "touches" the duct wall), the wake panels lie directly on the boundary being solved by the linear system. This requires the use of the separation of singularity integration when applying the induced velocity of the wake panels onto the body panels on which they lie. In order to make this consistent, the geometry is defined from the outset to have the body and wake panel nodes and control points be

coincident in order that the separation of singularity method in which we assume the position of the singular portion, functions properly. In addition, since the wake panels lie on the boundary being solved, they will also induce a jump in tangential velocity across the boundary which must be accounted for the post-processing step to calculate the body surface velocity, pressure, and thereby thrust/drag. Since the rotor tip and hub wakes interact with the body surfaces, additional consideration is also required for considering the strengths to define along the wake elements inside the duct. In reality, this is a complex interaction that we cannot properly capture given the inviscid methodologies of DuctAPE. As an approximation, we apply a linear interpolation from the body trailing edge, which gets the full rotor wake strength at that point, to the intersection of the rotor plane and wall, which we set to zero just ahead of the rotor. [look into what happens experimentally/in reality/in cfd. is the wake vorticity suppressed by the body and then pops back up outside the duct?]

For the rotor(s) we simply the induced axial and radial velocities from the bodies and wakes to the relative axial and radial velocities used in determining the inflow angles and magnitudes across the blades. Similarly for the wake, we combine all the induced velocities together to obtain the average meridional velocities required to compute the wake node strengths.

Chapter 1 Appendices

1.A   Detailed derivation of vortex ring induced velocity

As mentioned at the end of section 1.2.4, in this section we go through the somewhat tedious algebra required to take the partial derivatives of the vector potential in order to obtain the induced velocity from a vortex ring. We begin with the terms remaining in section 1.2.4:

$$v_r = -\frac{\partial \psi_\theta}{\partial z}, \tag{1.235}$$

$$v_z = \frac{1}{r}\frac{\partial (r\psi_\theta)}{\partial r}. \tag{1.236}$$

Now we need to take these partial derivatives to arrive at our final expressions of induced velocity. Because our current vector potential expressions are in terms of m and normalized values, we will require the application of the chain rule. Therefore it will be important to have the expressions for the various partial derivatives along the way. The derivative of the elliptic integral of the first kind with respect to m is

$$\frac{\partial \mathcal{K}(m)}{\partial m} = \frac{\mathcal{E}(m)}{2m(1-m)} - \frac{\mathcal{K}(m)}{2m}. \tag{1.237}$$

The derivative of the elliptic integral of the second kind is

$$\frac{\partial \mathcal{E}(m)}{\partial m} = \frac{\mathcal{E}(m)}{2m} - \frac{\mathcal{K}(m)}{2m}. \tag{1.238}$$

The partial of m with respect to ξ is

$$\frac{\partial m}{\partial \xi} = -\frac{8\rho\xi}{\left((\rho+1)^2 + \xi^2\right)^2}. \tag{1.239}$$

The partial of ξ with respect to z is

$$\frac{\partial \xi}{\partial z} = \frac{1}{r_o}. \tag{1.240}$$

The partial of m with respect to ρ is

$$\frac{\partial m}{\partial \rho} = \frac{4\left(-\rho^2 + \xi^2 + 1\right)}{\left((\rho+1)^2 + \xi^2\right)^2}. \tag{1.241}$$

The partial of ρ with respect to r is

$$\frac{\partial \rho}{\partial r} = \frac{1}{r_o}. \tag{1.242}$$

Though simple to write symbolically, the overall derivatives become very cumbersome. To keep things manageable, let us separate out the expression for ψ_θ into the constant (C), numerator ($\mathcal{N}$), and denominator ($\mathcal{D}$) portions, respectively:

$$C = -\frac{\Gamma}{\pi}$$

$$\mathcal{N} = \frac{2}{m}\mathcal{E}(m) - \frac{2}{m}\mathcal{K}(m) + \mathcal{K}(m) \qquad (1.243)$$

$$\mathcal{D} = \left[(\rho+1)^2 + \xi^2\right]^{1/2}.$$

The partial of the numerator with respect to z is

$$\frac{\partial \mathcal{N}}{\partial z} = -\frac{\partial m}{\partial \xi}\frac{\partial \xi}{\partial z}\left[\frac{\mathcal{K}(m) + \mathcal{E}(m)}{m^2}\right.$$
$$-\frac{3\mathcal{K}(m)(m-1) + \mathcal{E}(m)}{m^2(m-1)} \qquad (1.244)$$
$$\left.+\frac{\mathcal{K}(m)(m-1) + \mathcal{E}(m)}{2m(m-1)}\right].$$

The partial of the denominator with respect to z is

$$\frac{\partial \mathcal{D}}{\partial z} = \frac{\partial \xi}{\partial z}\frac{\xi}{\mathcal{D}} = \frac{\xi}{r_o \mathcal{D}}. \qquad (1.245)$$

The partial of the numerator with respect to r is

$$\frac{\partial \mathcal{N}}{\partial r} = \frac{\partial m}{\partial \rho}\frac{\partial \rho}{\partial r}\left[-\frac{3\mathcal{E}(m) + (m-5)\mathcal{K}(m)}{2m(m-1)}\right.$$
$$\left.+\frac{2\mathcal{E}(m) - 2\mathcal{K}(m)}{m^2(m-1)}\right] \qquad (1.246)$$

The partial of the denominator with respect to r is

$$\frac{\partial \mathcal{D}}{\partial r} = \frac{\partial \rho}{\partial r}\frac{\rho+1}{\mathcal{D}} = \frac{\rho+1}{r_o \mathcal{D}}. \qquad (1.247)$$

Putting things together for v_r with the quotient rule gives

$$v_r = -\frac{\partial \psi_\theta}{\partial z} = -C\frac{\frac{\partial \mathcal{N}}{\partial z}\mathcal{D} - \mathcal{N}\frac{\partial \mathcal{D}}{\partial z}}{\mathcal{D}^2}. \qquad (1.248)$$

Putting things together for v_z we start with the quotient rule, then apply the product rule to arrive at

$$v_z = \frac{1}{r}\frac{\partial (r\psi_\theta)}{\partial r}$$
$$= \frac{C}{r}\frac{\frac{\partial (\mathcal{N}r)}{\partial r}\mathcal{D} - (\mathcal{N}r)\frac{\partial \mathcal{D}}{\partial r}}{\mathcal{D}^2} \qquad (1.249)$$
$$= C\frac{\left(\mathcal{N} + r\frac{\partial \mathcal{N}}{\partial r}\right)\mathcal{D} - (\mathcal{N}r)\frac{\partial \mathcal{D}}{\partial r}}{r\mathcal{D}^2}.$$

Radially Induced Velocity Component

Now let's see what we can do about simplifying these expressions. We'll start with equation (1.248). To get started, we'll split up the fraction, and expand out the partial of $\mathcal{D}$,

$$v_r = -C \left[\underbrace{\frac{\frac{\partial N}{\partial z}}{\mathcal{D}}}_{\text{Term 1}} - \underbrace{\frac{N\xi}{r_o D^3}}_{\text{Term 2}} \right] \tag{1.250}$$

We are going to look at each term in the brackets of equation (1.250) separately first, then bring them together. We'll start with Term 2. Expanding gives

$$\frac{N\xi}{r_o D^3} = \frac{\xi}{r_o D^3} \left[\frac{2}{m}\mathcal{E}(m) + \left(1 - \frac{2}{m}\right)\mathcal{K}(m) \right] \tag{1.251}$$

Let us address the m's in the denominators by realizing that a comparison of equations (1.79) and (1.243) indicates that

$$\mathcal{D}^2 = \frac{4\rho}{m}. \tag{1.252}$$

Making this replacement in equation (1.251) gives

$$\begin{aligned} \frac{N\xi}{r_o D^3} &= \frac{\xi \cancel{m}}{4\rho r_o D} \left[\frac{2}{\cancel{m}}\mathcal{E}(m) + \left(\cancel{1}^{\frac{m}{m}} - \frac{2}{\cancel{m}}\right)\mathcal{K}(m) \right] \\ &= \frac{\xi/\rho}{4 r_o D} \left[2\mathcal{E}(m) + (m-2)\mathcal{K}(m) \right] \end{aligned} \tag{1.253}$$

Now let's look at Term 1 from equation (1.248). Expanding out gives

$$\begin{aligned} \frac{\frac{\partial N}{\partial z}}{\mathcal{D}} = \frac{8\rho\xi}{r_o D\left((\rho+1)^2+\xi^2\right)^2} &\left[\frac{\mathcal{K}(m)+\mathcal{E}(m)}{m^2} \right. \\ &- \frac{3\mathcal{K}(m)(m-1)+\mathcal{E}(m)}{m^2(m-1)} \\ &\left. + \frac{\mathcal{K}(m)(m-1)+\mathcal{E}(m)}{2m(m-1)} \right]. \end{aligned} \tag{1.254}$$

We can see right away that part of the fraction outside of the brackets closely resembles the parameter m^2, all we're missing is 2ρ in the numerator, so we'll multiply and divide by 2ρ.

$$\begin{aligned} \frac{\frac{\partial N}{\partial z}}{\mathcal{D}} = \frac{(2\rho)8\rho\xi}{2\rho r_o D\left((\rho+1)^2+\xi^2\right)^2} &\left[\frac{\mathcal{K}(m)+\mathcal{E}(m)}{m^2} \right. \\ &- \frac{3\mathcal{K}(m)(m-1)+\mathcal{E}(m)}{m^2(m-1)} \\ &\left. + \frac{\mathcal{K}(m)(m-1)+\mathcal{E}(m)}{2m(m-1)} \right]. \end{aligned} \tag{1.255}$$

which allows us to remove some of the m^2 denominators inside the brackets

$$\frac{\frac{\partial N}{\partial z}}{\mathcal{D}} = \frac{\xi \cancel{m^2}}{2\rho r_o D}\left[\frac{\mathcal{K}(m) + \mathcal{E}(m)}{\cancel{m^2}}\right.$$
$$- \frac{3\mathcal{K}(m)(m-1) + \mathcal{E}(m)}{\cancel{m^2}(m-1)}$$
$$\left.+ \frac{m(\mathcal{K}(m)(m-1) + \mathcal{E}(m))}{2\cancel{m}(m-1)}\right]. \tag{1.256}$$

$$\frac{\frac{\partial N}{\partial z}}{\mathcal{D}} = \frac{\xi/\rho}{2r_o D}\left[\mathcal{K}(m) + \mathcal{E}(m)\right.$$
$$- \frac{3\mathcal{K}(m)(m-1) + \mathcal{E}(m)}{m-1}$$
$$\left.+ \frac{m(\mathcal{K}(m)(m-1) + \mathcal{E}(m))}{2(m-1)}\right]. \tag{1.257}$$

Splitting up the fractions inside the brackets will let us simplify further.

$$\frac{\frac{\partial N}{\partial z}}{\mathcal{D}} = \frac{\xi/\rho}{2r_o D}\left[\mathcal{K}(m) + \mathcal{E}(m)\right.$$
$$- \frac{3\mathcal{K}(m)\cancel{(m-1)}}{\cancel{m-1}} - \frac{\mathcal{E}(m)}{m-1}$$
$$\left.+ \frac{m\mathcal{K}(m)\cancel{(m-1)}}{2\cancel{(m-1)}} + \frac{m\mathcal{E}(m)}{2(m-1)}\right]. \tag{1.258}$$

$$\frac{\frac{\partial N}{\partial z}}{\mathcal{D}} = \frac{\xi/\rho}{2r_o D}\left[\mathcal{K}(m) + \mathcal{E}(m) - 3\mathcal{K}(m) - \frac{1}{m-1}\mathcal{E}(m)\right.$$
$$\left.+ \frac{m}{2}\mathcal{K}(m) + \frac{m}{2(m-1)}\mathcal{E}(m)\right]. \tag{1.259}$$

Grouping like terms

$$\frac{\frac{\partial N}{\partial z}}{\mathcal{D}} = \frac{\xi/\rho}{2r_o D}\left[\left(1 - \frac{1}{m-1} + \frac{m}{2(m-1)}\right)\mathcal{E}(m)\right.$$
$$\left.+ \left(\frac{m}{2} - 2\right)\mathcal{K}(m)\right]. \tag{1.260}$$

Simplifying the gathered terms for $\mathcal{E}(m)$

$$\frac{\frac{\partial N}{\partial z}}{\mathcal{D}} = \frac{\xi/\rho}{2r_o D}\left[\left(\frac{2(m-1) - 2 + m}{2(m-1)}\right)\mathcal{E}(m)\right.$$
$$\left.- \left(\frac{m}{2} - 2\right)\mathcal{K}(m)\right]. \tag{1.261}$$

$$\frac{\frac{\partial N}{\partial z}}{\mathcal{D}} = \frac{\xi/\rho}{2r_o D}\left[\left(\frac{3m-4}{2(m-1)}\right)\mathcal{E}(m)\right.$$
$$\left. - \left(\frac{m}{2}-2\right)\mathcal{K}(m)\right].$$

(1.262)

Multiplying and dividing by 2

$$\frac{\frac{\partial N}{\partial z}}{\mathcal{D}} = \frac{\xi/\rho}{4r_o D}\left[\left(\frac{3m-4}{m-1}\right)\mathcal{E}(m) - (m-4)\mathcal{K}(m)\right].$$

(1.263)

Noting that the fractions outside of the brackets are now the same for both of the simplified expressions for Term 1 (see equation (1.263)) and Term 2 (see equation (1.253), we'll substitute the expression for Term 2 in equation (1.253) and the expression for Term 1 in equation (1.263) back in to equation (1.250).

$$\frac{\frac{\partial N}{\partial z}\mathcal{D} - N\frac{\partial \mathcal{D}}{\partial z}}{\mathcal{D}^2} = \frac{\xi/\rho}{4r_o D}\left[\left(\frac{3m-4}{m-1}\right)\mathcal{E}(m) - (m-4)\mathcal{K}(m)\right]$$
$$- \frac{\xi/\rho}{4r_o D}\left[2\mathcal{E}(m) + (m-2)\,\mathcal{K}(m)\right].$$

(1.264)

Let's first look at just the difference of the $\mathcal{K}(m)$ terms:

$$((m-1)-(m-2))K = (m-4-m+2)\mathcal{K}(m) = -2\mathcal{K}(m)$$

(1.265)

Now just looking at the $\mathcal{E}(m)$ terms:

$$\left(\frac{3m-4}{m-1}-2\right)\mathcal{E}(m)$$
$$\left(\frac{3m-4-2(m-1)}{m-1}\right)\mathcal{E}(m) \quad \text{(common denominators)}$$
$$\left(\frac{3m-4-2m+2}{m-1}\right)\mathcal{E}(m) \quad \text{(expand)}$$
$$\left(\frac{m-2}{m-1}\right)\mathcal{E}(m) \quad \text{(simplify)}$$

(1.266)

Applying the definition of m in equation (1.79)

$$\left(\frac{\frac{4\rho}{\mathcal{D}^2} - 2}{\frac{4\rho}{\mathcal{D}^2} - 1}\right)\mathcal{E}(m)$$

$$\left(\frac{\frac{4\rho - 2\mathcal{D}^2}{\mathcal{D}^2}}{\frac{4\rho - \mathcal{D}^2}{\mathcal{D}^2}}\right)\mathcal{E}(m) \quad \text{(common denominators)} \tag{1.267}$$

$$\left(\frac{4\rho - 2\mathcal{D}^2}{4\rho - \mathcal{D}^2}\right)\mathcal{E}(m) \qquad \text{(divide)}$$

$$2\left(\frac{2\rho - \mathcal{D}^2}{4\rho - \mathcal{D}^2}\right)\mathcal{E}(m) \qquad \text{(pull out a 2)}$$

Expanding out the $\mathcal{D}$ terms

$$2\left(\frac{2\rho - ((\rho + 1)^2 + \xi^2)}{4\rho - ((\rho + 1)^2 + \xi^2)}\right)\mathcal{E}(m)$$

$$2\left(\frac{2\rho - \rho^2 - 2\rho - 1 - \xi^2}{4\rho - \rho^2 - 2\rho - 1 - \xi^2}\right)\mathcal{E}(m) \qquad \text{(expand and cancel)}$$

$$2\left(\frac{-\rho^2 - 1 - \xi^2}{2\rho - \rho^2 - 1 - \xi^2}\right)\mathcal{E}(m)$$

$$-2\left(\frac{-\rho^2 - 1 - \xi^2}{(\rho - 1)^2 + \xi^2}\right)\mathcal{E}(m) \quad \text{(multiply by -1 and simplify)}$$

$$-2\left(\frac{-\rho^2 - 1 - \xi^2 + 2\rho - 2\rho}{(\rho - 1)^2 + \xi^2}\right)\mathcal{E}(m) \qquad \text{(add and subtract } 2\rho)$$

$$2\left(\frac{(\rho - 1)^2 + \xi^2 + 2\rho}{(\rho - 1)^2 + \xi^2}\right)\mathcal{E}(m) \qquad \text{(consolidate numerator)}$$

$$2\left(\frac{(\rho - 1)^2 + \xi^2}{(\rho - 1)^2 + \xi^2} + \frac{2\rho}{(\rho - 1)^2 + \xi^2}\right)\mathcal{E}(m) \qquad \text{(split fraction and cancel)}$$

$$2\left(1 + \frac{2\rho}{\xi^2 + (\rho - 1)^2}\right)\mathcal{E}(m)$$

$$\tag{1.268}$$

Now putting the $\mathcal{K}(m)$ terms from equation (1.265) and the $\mathcal{E}(m)$ terms from equation (1.268) together in the difference, remembering the fraction out front of both Term 1 and Term 2:

$$v_r = -C\left[\frac{\xi/\rho}{4\mathcal{D}r_o}\left(-2\mathcal{K}(m) + 2\left[1 + \frac{2\rho}{\xi^2 + (\rho - 1)^2}\right]\mathcal{E}(m)\right)\right] \tag{1.269}$$

And finally expanding out C and $\mathcal{D}$ as well as some minor cleanup and rearranging we have the expression presented in equation (1.88b):

$$v_r = -\frac{\Gamma}{2\pi r_o} \frac{\xi/\rho}{[\xi^2 + (\rho+1)^2]^{1/2}} \left(\mathcal{K}(m) - \left[1 + \frac{2\rho}{\xi^2 + (\rho-1)^2} \right] \mathcal{E}(m) \right)$$

(1.270)

Axially Induced Velocity Component

Next let's simplify equation (1.249)

$$v_z = C \left[\underbrace{\frac{\mathcal{N}\mathcal{D}}{r\mathcal{D}^2}}_{\text{Term 1}} + \underbrace{\frac{r\frac{\partial \mathcal{N}}{\partial r}\mathcal{D}}{r\mathcal{D}^2}}_{\text{Term 2}} - \underbrace{\frac{(\mathcal{N}r)\frac{\partial \mathcal{D}}{\partial r}}{r\mathcal{D}^2}}_{\text{Term 3}} \right].$$

(1.271)

We'll first expand the partials. Term 1 has no partials to expand:

$$\text{Term 1} = \frac{\mathcal{N}\mathcal{D}}{r\mathcal{D}^2}.$$

(1.272)

Term 2 has several sets of partials to expand:

$$\text{Term 2} = \frac{r\mathcal{D}}{r\mathcal{D}^2} \frac{\partial m}{\partial \rho} \frac{\partial \rho}{\partial r} \left[-\frac{3\mathcal{E}(m) + (m-5)\mathcal{K}(m)}{2m(m-1)} \right. $$
$$\left. + \frac{2\mathcal{E}(m) - 2\mathcal{K}(m)}{m^2(m-1)} \right],$$

(1.273)

$$\text{Term 2} = \frac{r\mathcal{D}}{r\mathcal{D}^2} \frac{4(-\rho^2 + \xi^2 + 1)}{\mathcal{D}^4} \frac{1}{r_o} \left[-\frac{3\mathcal{E}(m) + (m-5)\mathcal{K}(m)}{2m(m-1)} \right.$$
$$\left. + \frac{2\mathcal{E}(m) - 2\mathcal{K}(m)}{m^2(m-1)} \right].$$

(1.274)

Term 3 also has a couple sets of partials to expand:

$$\text{Term 3} = -\frac{\mathcal{N}r}{r\mathcal{D}^2} \frac{\partial \rho}{\partial r} \frac{\rho+1}{\mathcal{D}},$$

(1.275)

$$\text{Term 3} = -\frac{\mathcal{N}r}{r\mathcal{D}^2} \frac{1}{r_o} \frac{\rho+1}{\mathcal{D}}.$$

(1.276)

Next let's expand out the $\mathcal{N}$'s. For Term 1

$$\text{Term 1} = \frac{\mathcal{D}}{r\mathcal{D}^2} \left[\frac{2}{m}\mathcal{E}(m) + \frac{m-2}{m}\mathcal{K}(m) \right].$$

(1.277)

Term 2 is already expanded, but let us gather the $\mathcal{E}(m)$ and $\mathcal{K}(m)$ terms.

$$\text{Term 2} = \frac{r\mathcal{D}}{r\mathcal{D}^2} \frac{4(-\rho^2 + \xi^2 + 1)}{\mathcal{D}^4} \frac{1}{r_o} \left[-\frac{3m - 4}{2m^2(m-1)} \mathcal{E}(m) \right.$$
$$\left. -\frac{(m-4)(m-1)}{2m^2(m-1)} \mathcal{K}(m) \right]. \tag{1.278}$$

For Term 3:

$$\text{Term 3} = -\frac{r}{r\mathcal{D}^2} \frac{1}{r_o} \frac{\rho+1}{\mathcal{D}} \left[\frac{2}{m} \mathcal{E}(m) + \frac{m-2}{m} \mathcal{K}(m) \right]. \tag{1.279}$$

In order to add the terms together, we require a common denominator. Let us gather the multipliers of each of the terms to see what we're working with and decide what common denominator to choose.

$$\text{Term 1 Multiplier} = \frac{\mathcal{D}}{r\mathcal{D}^2 m}; \tag{1.280}$$

$$\text{Term 2 Multiplier} = \frac{4r\mathcal{D}(-\rho^2 + \xi^2 + 1)}{2rr_o\mathcal{D}^6 m^2(m-1)}; \tag{1.281}$$

$$\text{Term 3 Multiplier} = \frac{r(\rho+1)}{rr_o\mathcal{D}^3 m}. \tag{1.282}$$

We may expect our final expression to look similar to the expression for v_r, so we may want to make sure to keep a $r_o D$ in the denominator as we go forward. Therefore we'll start by multiplying Term 1 by r_o/r_o:

$$\text{Term 1 Multiplier} = \frac{\mathcal{D}r_o}{rr_o\mathcal{D}^2 m}; \tag{1.283}$$

$$\text{Term 2 Multiplier} = \frac{4r\mathcal{D}(-\rho^2 + \xi^2 + 1)}{2rr_o\mathcal{D}^6 m^2(m-1)}; \tag{1.284}$$

$$\text{Term 3 Multiplier} = \frac{r(\rho+1)}{rr_o\mathcal{D}^3 m}. \tag{1.285}$$

Term 2 seems to have some extraneous values, so let's divide out the 2 and one of the $\mathcal{D}$'s,

$$\text{Term 1 Multiplier} = \frac{\mathcal{D}r_o}{rr_o\mathcal{D}^2 m}; \tag{1.286}$$

$$\text{Term 2 Multiplier} = \frac{2r(-\rho^2 + \xi^2 + 1)}{rr_o\mathcal{D}^5 m^2(m-1)}; \tag{1.287}$$

$$\text{Term 3 Multiplier} = \frac{r(\rho+1)}{rr_o\mathcal{D}^3 m}. \tag{1.288}$$

Now we just need to multiply the top and bottom of Term 1 by $\mathcal{D}^3 m(m-1)$ and the top and bottom of Term 3 by $\mathcal{D}^2 m(m-1)$ to get a common denominator between the terms.

$$\text{Term 1 Multiplier} = \frac{r_o \mathcal{D}^4 m(m-1)}{rr_o \mathcal{D}^5 m^2 (m-1)}; \tag{1.289}$$

$$\text{Term 2 Multiplier} = \frac{2r(-\rho^2 + \xi^2 + 1)}{rr_o \mathcal{D}^5 m^2 (m-1)}; \tag{1.290}$$

$$\text{Term 3 Multiplier} = \frac{r(\rho + 1)\mathcal{D}^2 m(m-1)}{rr_o \mathcal{D}^5 m^2 (m-1)}. \tag{1.291}$$

With a common denominator in place, we can start to add the various terms together. Let us try to begin with the $\mathcal{K}(m)$ terms:

$$
\frac{\mathcal{K}(m)}{rr_o \mathcal{D}^5 m^2 (m-1)} \bigg[r_o \mathcal{D}^4 m(m-1)(m-2) \qquad \text{(from Term 1)}
$$
$$
- 2r(-\rho^2 + \xi^2 + 1)(m-4)(m-1) \quad \text{(from Term 2)}
$$
$$
- r(\rho+1)\mathcal{D}^2 m(m-1)(m-2) \bigg]. \qquad \text{(from Term 3)}
$$
$$\tag{1.292}$$

We see immediately that we can cancel out the $(m-1)$ from all the terms.

$$
\frac{\mathcal{K}(m)}{rr_o \mathcal{D}^5 m^2} \bigg[r_o \mathcal{D}^4 m(m-2) \qquad \text{(from Term 1)}
$$
$$
- 2r(-\rho^2 + \xi^2 + 1)(m-4) \quad \text{(from Term 2)} \tag{1.293}
$$
$$
- r(\rho+1)\mathcal{D}^2 m(m-2) \bigg]. \qquad \text{(from Term 3)}
$$

Unfortunately, that appears to be the only obvious cancellation to make right away. Perhaps expanding things out more will help. Let us expand the m's out next, remembering that $m = 4\rho/\mathcal{D}^2$.

$$
\frac{\mathcal{K}(m)\mathcal{D}^4}{rr_o \mathcal{D}^5 16\rho^2} \bigg[r_o \mathcal{D}^4 \frac{4\rho}{\mathcal{D}^2} \left(\frac{4\rho}{\mathcal{D}^2} - 2 \right) \qquad \text{(from Term 1)}
$$
$$
- 2r(-\rho^2 + \xi^2 + 1) \left(\frac{4\rho}{\mathcal{D}^2} - 4 \right) \quad \text{(from Term 2)} \tag{1.294}
$$
$$
- r(\rho+1)\mathcal{D}^2 \frac{4\rho}{\mathcal{D}^2} \left(\frac{4\rho}{\mathcal{D}^2} - 2 \right) \bigg]; \quad \text{(from Term 3)}
$$

then canceling out the obvious items and cleaning up:

$$
\frac{\mathcal{K}(m)}{4\rho^2 rr_o \mathcal{D}} \bigg[\rho r_o \mathcal{D}^2 \left(\frac{4\rho}{\mathcal{D}^2} - 2 \right) \qquad \text{(from Term 1)}
$$
$$
- 2r(-\rho^2 + \xi^2 + 1) \left(\frac{\rho}{\mathcal{D}^2} - 1 \right) \quad \text{(from Term 2)} \tag{1.295}
$$
$$
- \rho r(\rho+1) \left(\frac{4\rho}{\mathcal{D}^2} - 2 \right) \bigg].
$$

We see that $r_o \rho = r$, which gives us a mutual r that we can cancel out of all the terms.

$$
\begin{aligned}
\frac{\mathcal{K}(m)}{4\rho^2 r_o \mathcal{D}} &\left[\mathcal{D}^2 \left(\frac{4\rho}{\mathcal{D}^2} - 2 \right) \right. && \text{(from Term 1)} \\
&- 2(-\rho^2 + \xi^2 + 1) \left(\frac{\rho}{\mathcal{D}^2} - 1 \right) && \text{(from Term 2)} \\
&\left. - \rho(\rho + 1) \left(\frac{4\rho}{\mathcal{D}^2} - 2 \right) \right]. && \text{(from Term 3)}
\end{aligned}
\tag{1.296}
$$

We also see that we can cancel out an additional 2 from everything.

$$
\begin{aligned}
\frac{\mathcal{K}(m)}{2\mathcal{D} r_o \rho^2} &\left[\mathcal{D}^2 \left(\frac{2\rho}{\mathcal{D}^2} - 1 \right) \right. && \text{(from Term 1)} \\
&- (-\rho^2 + \xi^2 + 1) \left(\frac{\rho}{\mathcal{D}^2} - 1 \right) && \text{(from Term 2)} \\
&\left. - \rho(\rho + 1) \left(\frac{2\rho}{\mathcal{D}^2} - 1 \right) \right]. && \text{(from Term 3)}
\end{aligned}
\tag{1.297}
$$

We've found ourselves with some more uncommon denominators, so let's expand and gather terms.

$$
\begin{aligned}
\frac{\mathcal{K}(m)}{2\mathcal{D} r_o \rho^2} &\left[2\rho - \mathcal{D}^2 \right. && \text{(from Term 1)} \\
&- \frac{-\rho^3 + \rho\xi^2 + \rho}{\mathcal{D}^2} - \rho^2 + \xi^2 + 1 && \text{(from Term 2)} \\
&\left. - \frac{2\rho^3 + 2\rho^2}{\mathcal{D}^2} + \rho^2 + \rho \right]; && \text{(from Term 3)}
\end{aligned}
\tag{1.298}
$$

$$
\begin{aligned}
\frac{\mathcal{K}(m)}{2\mathcal{D} r_o \rho^2} &\left[2\rho - \mathcal{D}^2 - \cancel{\rho^2} + \xi^2 + 1 + \cancel{\rho^2} + \rho \right. \\
&\left. - \frac{-\rho^3 + \rho\xi^2 + \rho}{\mathcal{D}^2} - \frac{2\rho^3 + 2\rho^2}{\mathcal{D}^2} \right].
\end{aligned}
\tag{1.299}
$$

Expanding out the $\mathcal{D}$ in the numerator:

$$
\begin{aligned}
\frac{\mathcal{K}(m)}{2\mathcal{D} r_o \rho^2} &\left[\cancel{3}\rho + \cancel{\xi^2} + \cancel{1} - (\rho^2 + \cancel{2\rho} + \cancel{1} + \cancel{\xi^2}) \right. \\
&\left. - \frac{-\rho^3 + \rho\xi^2 + \rho}{\mathcal{D}^2} - \frac{2\rho^3 + 2\rho^2}{\mathcal{D}^2} \right].
\end{aligned}
\tag{1.300}
$$

Now let's get a common denominator again, pulling the ρ^2 inside the brackets.

$$
\frac{\mathcal{K}(m)}{2\mathcal{D} r_o} \left[\frac{\rho\mathcal{D}^2 - \rho^2\mathcal{D}^2 + \cancel{\rho^3} - \rho\xi^2 - \rho - \cancel{2}\rho^3 - 2\rho^2}{\mathcal{D}^2 \rho^2} \right].
\tag{1.301}
$$

We can immediately cancel out a ρ:

$$\frac{\mathcal{K}(m)}{2\mathcal{D}r_o}\left[\frac{\mathcal{D}^2 - (\rho^2 + 2\rho + 1 + \xi^2) - \rho\mathcal{D}^2}{\mathcal{D}^2\rho}\right]. \tag{1.302}$$

We also see that $\mathcal{D}^2 = \rho^2 + 2\rho + 1 + \xi^2$, which cancels in the numerator.

$$\frac{\mathcal{K}(m)}{2\mathcal{D}r_o}\left[\frac{-\rho\mathcal{D}^2}{\rho\mathcal{D}^2}\right]. \tag{1.303}$$

We are finally left with

$$-\frac{\mathcal{K}(m)}{2\mathcal{D}r_o}. \tag{1.304}$$

Now let's look at the $\mathcal{E}(m)$ terms start back with the term multipliers with common denominators: equations (1.289) to (1.291).

$$\frac{\mathcal{E}(m)}{rr_o\mathcal{D}^5m^2(m-1)}\Big[2r_o\mathcal{D}^4m(m-1) \qquad \text{(from Term 1)}$$
$$- 2r(-\rho^2 + \xi^2 + 1)(3m - 4) \quad \text{(from Term 2)} \tag{1.305}$$
$$- 2r(\rho + 1)\mathcal{D}^2m(m-1)\Big]. \qquad \text{(from Term 3)}$$

Unlike the $\mathcal{K}(m)$ terms, it doesn't appear as though anything will cancel out immediately. Let's take a similar approach as before and expand out the m terms.

$$\frac{\mathcal{E}(m)}{rr_o\mathcal{D}^5m^2(m-1)}\Big[2r_o\mathcal{D}^4\left(\frac{4\rho}{\mathcal{D}^2}\right)\left(\frac{4\rho}{\mathcal{D}^2}\right) - 1) \qquad \text{(from Term 1)}$$
$$- 2r(-\rho^2 + \xi^2 + 1)\left(3\left(\frac{4\rho}{\mathcal{D}^2}\right) - 4\right) \quad \text{(from Term 2)}$$
$$- 2r(\rho + 1)\mathcal{D}^2\left(\frac{4\rho}{\mathcal{D}^2}\right)\left(\frac{4\rho}{\mathcal{D}^2}\right) - 1)\Big]. \quad \text{(from Term 3)}$$
$$\tag{1.306}$$

Again noting that $r_o\rho = r$, we can cancel out an r.

$$\frac{\mathcal{E}(m)}{r_o\mathcal{D}^5m^2(m-1)}\Big[2\mathcal{D}^4\left(\frac{4}{\mathcal{D}^2}\right)\left(\frac{4\rho}{\mathcal{D}^2}\right) - 1) \qquad \text{(from Term 1)}$$
$$- 2(-\rho^2 + \xi^2 + 1)\left(3\left(\frac{4\rho}{\mathcal{D}^2}\right) - 4\right) \quad \text{(from Term 2)}$$
$$- 2(\rho + 1)\mathcal{D}^2\left(\frac{4\rho}{\mathcal{D}^2}\right)\left(\frac{4\rho}{\mathcal{D}^2}\right) - 1)\Big]. \quad \text{(from Term 3)}$$
$$\tag{1.307}$$

We may also want to expand the m^2 on the outside—

$$\frac{1}{r_o\mathcal{D}^5m^2(m-1)} = \frac{\mathcal{D}^4}{r_o\mathcal{D}^5 16\rho^2(m-1)} \tag{1.308}$$

—which leaves us with

$$\frac{\mathcal{E}(m)}{r_o\mathcal{D}16\rho^2(m-1)}\left[2\mathcal{D}^4\left(\frac{4}{\mathcal{D}^2}\right)\left(\frac{4\rho}{\mathcal{D}^2}\right)-1)\right.\qquad\text{(from Term 1)}$$

$$-2(-\rho^2+\xi^2+1)\left(3\left(\frac{4\rho}{\mathcal{D}^2}\right)-4\right)\quad\text{(from Term 2)}$$

$$\left.-2(\rho+1)\mathcal{D}^2\left(\frac{4\rho}{\mathcal{D}^2}\right)\left(\frac{4\rho}{\mathcal{D}^2}\right)-1)\right].\quad\text{(from Term 3)}$$

$$(1.309)$$

We can now take an 8 out of everything:

$$\frac{\mathcal{E}(m)}{2\mathcal{D}r_o\rho^2(m-1)}\left[\mathcal{D}^4\left(\frac{1}{\mathcal{D}^2}\right)\left(\frac{4\rho}{\mathcal{D}^2}\right)-1)\right.\qquad\text{(from Term 1)}$$

$$-(-\rho^2+\xi^2+1)\left(3\left(\frac{\rho}{\mathcal{D}^2}\right)-1\right)\quad\text{(from Term 2)}$$

$$\left.-(\rho+1)\mathcal{D}^2\left(\frac{\rho}{\mathcal{D}^2}\right)\left(\frac{4\rho}{\mathcal{D}^2}\right)-1)\right].\quad\text{(from Term 3)}$$

$$(1.310)$$

Cleaning up a bit:

$$\frac{\mathcal{E}(m)}{2\mathcal{D}r_o\rho^2(m-1)}\left[\mathcal{D}^2\left(\frac{4\rho}{\mathcal{D}^2}\right)-1)\right.\qquad\text{(from Term 1)}$$

$$-(-\rho^2+\xi^2+1)\left(3\left(\frac{\rho}{\mathcal{D}^2}\right)-1\right)\quad\text{(from Term 2)}\quad(1.311)$$

$$\left.-(\rho+1)\rho\left(\frac{4\rho}{\mathcal{D}^2}\right)-1)\right].\qquad\text{(from Term 3)}$$

Let's next expand out the multiplications.

$$\frac{\mathcal{E}(m)}{2\mathcal{D}r_o\rho^2(m-1)}\left[4\rho-\mathcal{D}^2\right.\qquad\text{(from Term 1)}$$

$$-\frac{-3\rho^3+3\rho\xi^2+3\rho}{\mathcal{D}^2}-\rho^2+\xi^2+1\quad\text{(from Term 2)}$$

$$\left.-\frac{4\rho^3+4\rho^2}{\mathcal{D}^2}+\rho^2+\rho\right].\qquad\text{(from Term 3)}$$

$$(1.312)$$

Gathering terms:

$$\frac{\mathcal{E}(m)}{2\mathcal{D}r_o\rho^2(m-1)}\left[5\rho+\xi+1-\mathcal{D}^2\quad-\frac{-3\rho^3+3\rho\xi^2+3\rho}{\mathcal{D}^2}-\frac{4\rho^3+4\rho^2}{\mathcal{D}^2}\right].$$

$$(1.313)$$

Expanding the $\mathcal{D}$ in the numerator:

$$\frac{\mathcal{E}(m)}{2\mathcal{D}r_o\rho^2(m-1)}\left[\cancel{3}^{3}\rho + \cancel{\xi} + \cancel{1} - (\rho^2 + 2\cancel{\rho} + \cancel{1} + \cancel{\xi}) \quad -\frac{-3\cancel{\rho}^{3} + 3\rho\xi^2 + 3\rho + \cancel{4}\rho^3 + 4\rho^2}{\mathcal{D}^2}\right].$$

(1.314)

We can take a ρ out of everything now as well.

$$\frac{\mathcal{E}(m)}{2\mathcal{D}r_o\rho(m-1)}\left[3 - \rho \quad -\frac{3\xi^2 + 3 + \rho^2 + 4\rho}{\mathcal{D}^2}\right].$$

(1.315)

Let's move the 3 into the fraction and expand the $\mathcal{D}$ that will appear in the numerator.

$$\frac{\mathcal{E}(m)}{2\mathcal{D}r_o\rho(m-1)}\left[-\rho - \frac{-\cancel{3}^{2}\rho^2 - \cancel{6}^{2}\rho - \cancel{3} - 3\cancel{\xi} + 3\xi^2 + \cancel{3} + \rho^2 + 4\cancel{\rho}}{\mathcal{D}^2}\right].$$

(1.316)

After cleaning up the various cancelations, we can take another ρ out of everything.

$$\frac{\mathcal{E}(m)}{2\mathcal{D}r_o(m-1)}\left[-1 + \frac{2(\rho + 1)}{\mathcal{D}^2}\right].$$

(1.317)

Now let's move the $(m-1)$ into the inside and expand out the m and $\mathcal{D}$ terms.

$$\frac{\mathcal{E}(m)}{2\mathcal{D}r_o}\left[\frac{-1}{\frac{4\rho}{(\rho+1)^2+\xi^2} - 1} + \frac{2(\rho + 1)}{\left(\frac{4\rho}{(\rho+1)^2+\xi^2} - 1\right)\left((\rho + 1)^2 + \xi^2\right)}\right].$$

(1.318)

Combining fractions:

$$\frac{\mathcal{E}(m)}{2\mathcal{D}r_o}\left[\frac{2\rho + 2 - (\rho + 1)^2 - \xi^2}{\left(\frac{4\rho}{(\rho+1)^2+\xi^2} - 1\right)\left((\rho + 1)^2 + \xi^2\right)}\right].$$

(1.319)

Expanding the numerator:

$$\frac{\mathcal{E}(m)}{2\mathcal{D}r_o}\left[\frac{2\cancel{\rho} + \cancel{2}^{1} - \rho^2 - 2\cancel{\rho} - \cancel{1} - \xi^2}{\left(\frac{4\rho}{(\rho+1)^2+\xi^2} - 1\right)\left((\rho + 1)^2 + \xi^2\right)}\right];$$

(1.320)

$$\frac{\mathcal{E}(m)}{2\mathcal{D}r_o}\left[\frac{1 - \rho^2 - \xi^2}{\left(\frac{4\rho}{(\rho+1)^2+\xi^2} - 1\right)\left((\rho + 1)^2 + \xi^2\right)}\right].$$

(1.321)

Getting a common denominator in the denominator:

$$\frac{\mathcal{E}(m)}{2\mathcal{D}r_o}\left[\frac{1-\rho^2-\xi^2}{4\rho-(\rho+1)^2-\xi^2}\right]. \tag{1.322}$$

Expanding then simplifying the denominator:

$$\frac{\mathcal{E}(m)}{2\mathcal{D}r_o}\left[\frac{1-\rho^2-\xi^2}{\cancel{4}\rho-\rho^2-\cancel{2\rho}-1-\xi^2}\right]; \tag{1.323}$$

$$\frac{\mathcal{E}(m)}{2\mathcal{D}r_o}\left[\frac{\rho^2-1+\xi^2}{(\rho-1)^2+\xi^2}\right]. \tag{1.324}$$

Adding and subtracting $2\rho+1$ to the numerator:

$$\frac{\mathcal{E}(m)}{2\mathcal{D}r_o}\left[\frac{\rho^2-2\rho+1+\xi^2+2\rho-2}{(\rho-1)^2+\xi^2}\right]. \tag{1.325}$$

Simplifying:

$$\frac{\mathcal{E}(m)}{2\mathcal{D}r_o}\left[\frac{(\rho-1)^2+\xi^2+2(\rho-1)}{(\rho-1)^2+\xi^2}\right]. \tag{1.326}$$

Splitting the fraction:

$$\frac{\mathcal{E}(m)}{2\mathcal{D}r_o}\left[\frac{\cancel{(\rho-1)^2+\xi^2}}{\cancel{(\rho-1)^2+\xi^2}}+\frac{2(\rho-1)}{(\rho-1)^2+\xi^2}\right]. \tag{1.327}$$

Finally, we are left with

$$\frac{\mathcal{E}(m)}{2\mathcal{D}r_o}\left[1+\frac{2(\rho-1)}{(\rho-1)^2+\xi^2}\right]. \tag{1.328}$$

Now combining our $\mathcal{K}(m)$ and $\mathcal{E}(m)$ terms from equation (1.304) and equation (1.328), respectively, we arrive at

$$v_z = C\frac{1}{2\mathcal{D}r_o}\left[-\mathcal{K}(m)+\left(1+\frac{2(\rho-1)}{(\rho-1)^2+\xi^2}\right)\mathcal{E}(m)\right]. \tag{1.329}$$

Expanding out C and $\mathcal{D}$ gives us our final expression as presented in equation (1.88a):

$$v_z = \frac{\Gamma}{2\pi r_o}\frac{1}{\left[\xi^2+(\rho+1)^2\right]^{1/2}}\left[\mathcal{K}(m)-\left(1+\frac{2(\rho-1)}{\xi^2+(\rho-1)^2}\right)\mathcal{E}(m)\right]. \tag{1.330}$$

1.B Detailed Derivation of Singular Portions of the Panel Surface Integral and Their Analytic Solutions

1.B.1 Unit Axial Velocity Induced by a Vortex Ring

We start with the expression for the axial induced velocity from equation (1.88).

$$v_z = \frac{1}{2\pi r_o} \frac{1}{D_1} \left[\mathcal{K}(m) - \left(1 + \frac{2(\rho - 1)}{D_2} \right) \mathcal{E}(m) \right] \tag{1.88a}$$

where $\mathcal{K}(m)$ and $\mathcal{E}(m)$ are complete elliptic integrals of the first and second kind, respectively, and

$$m = \left(\frac{4\rho}{\xi^2 + (\rho + 1)^2} \right)$$
$$\xi = \frac{z - z_o}{r_o}$$
$$\rho = \frac{r}{r_o}$$
$$D_1 = \left[\xi^2 + (\rho + 1)^2 \right]^{1/2}$$
$$D_2 = \xi^2 + (\rho - 1)^2.$$

Expaning everything out we can begin to see where the singular portions of the integral over the panel lie:

$$
v_z^\gamma = \int_{(z_1,r_1)}^{(z_2,r_2)} \left[\frac{\int_0^1 \frac{1}{\left[1 - \left(\frac{4\frac{r}{r_o}}{\left(\frac{z-z_o}{r_o}\right)^2 + \left(\frac{r}{r_o}+1\right)^2} \right) \sin^2\theta \right]^{1/2}} d\theta}{2\pi r_o \left[\left(\frac{z-z_o}{r_o}\right)^2 + \left(\frac{r}{r_o}+1\right)^2 \right]^{1/2}} \right.
$$

$$
- \frac{\int_0^{\pi/2} \left[1 - \left(\frac{4\frac{r}{r_o}}{\left(\frac{z-z_o}{r_o}\right)^2 + \left(\frac{r}{r_o}+1\right)^2} \right) \sin^2\theta \right]^{1/2} d\theta}{2\pi r_o \left[\left(\frac{z-z_o}{r_o}\right)^2 + \left(\frac{r}{r_o}+1\right)^2 \right]^{1/2}}
$$

$$
\left. - \frac{\int_0^{\pi/2} \left[1 - \left(\frac{4\frac{r}{r_o}}{\left(\frac{z-z_o}{r_o}\right)^2 + \left(\frac{r}{r_o}+1\right)^2} \right) \sin^2\theta \right]^{1/2} d\theta}{2\pi r_o \left[\left(\frac{z-z_o}{r_o}\right)^2 + \left(\frac{r}{r_o}+1\right)^2 \right]^{1/2}} \left(\frac{2\left(\frac{r}{r_o}-1\right)}{\left(\frac{z-z_o}{r_o}\right)^2 + \left(\frac{r}{r_o}-1\right)^2} \right) \right] ds. \tag{1.331}
$$

Let's plug in $z_o = z$ and $r_o = r$ and simplify to show more explicitly where the singularities in the integrand lie

$$\frac{\displaystyle\int_0^{\pi/2} \frac{1}{\left[1-\left(\frac{4}{(0)^2+(1+1)^2}\right)\sin^2\theta\right]^{1/2}}d\theta}{2\pi r_o \left[(0)^2+(1+1)^2\right]^{1/2}} \quad \text{(Term 1)}$$

$$-\frac{\displaystyle\int_0^{\pi/2}\left[1-\left(\frac{4}{(0)^2+(1+1)^2}\right)\sin^2\theta\right]^{1/2}d\theta}{2\pi r_o \left[(0)^2+(1+1)^2\right]^{1/2}} \quad \text{(Term 2)}$$

$$-\frac{\displaystyle\int_0^{\pi/2}\left[1-\left(\frac{4}{(0)^2+(1+1)^2}\right)\sin^2\theta\right]^{1/2}d\theta}{2\pi r_o \left[(0)^2+(1+1)^2\right]^{1/2}}\left(\frac{2(1-1)}{(0)^2+(1-1)^2}\right). \quad \text{(Term 3)}$$

$$(1.332)$$

We first note that the elliptic integral of the second kind (in Terms 1 and 3) goes to 1, so we can simplify to

$$\underbrace{\frac{\displaystyle\int_0^{\pi/2}\frac{1}{[1-\sin^2\theta]^{1/2}}d\theta}{4\pi r_o}}_{\text{Term 1}} - \underbrace{\frac{1}{4\pi r_o}}_{\text{Term 2}} - \underbrace{\frac{1}{4\pi r_o}\left(\frac{0}{0}\right)}_{\text{Term 3}}. \quad (1.333)$$

We immediately see that Term 2 is not singular, and therefore we can ignore it going forward. Term 3 on the other hand, is singular. Going back to the full expression for Term 3, we have:

$$\frac{-1}{2\pi r_o\left[\left(\frac{z-z_o}{r_o}\right)^2+\left(\frac{r}{r_o}+1\right)^2\right]^{1/2}}\left(\frac{2\left(\frac{r-r_o}{r_o}\right)}{\left(\frac{z-z_o}{r_o}\right)^2+\left(\frac{r-r_o}{r_o}\right)^2}\right). \quad (1.334)$$

At the singular point, the outer denominator here isn't singular, so we can simplify it to 2 when $z = z_o$ and $r = r_o$;

$$\frac{-1}{4\pi r_o}\left(\frac{2\left(\frac{r-r_o}{r_o}\right)}{\left(\frac{z-z_o}{r_o}\right)^2+\left(\frac{r-r_o}{r_o}\right)^2}\right). \quad (1.335)$$

We can simplify further by noting that both a 2 and r_o^2 cancel.

$$\frac{r_o-r}{2\pi\left[(z-z_o)^2+(r-r_o)^2\right]} \quad (1.336)$$

We will leave Term 3 for now, and go back and address Term 1. For the first term, we need to address the non-convergence of the elliptic integral of the first kind. The asymptotic behavior of the complete elliptic integral of the first kind ($\mathcal{K}(m)$) as m approaches 1—where

$$m = \frac{4\frac{r}{r_o}}{\left(\frac{z-z_o}{r_o}\right)^2+\left(\frac{r}{r_o}+1\right)^2}$$

—is well known to be

$$\mathcal{K}(m) \approx \ln \frac{4}{\sqrt{1 - \frac{4\frac{r}{r_o}}{\left(\frac{z-z_0}{r_o}\right)^2 + \left(\frac{r}{r_o}+1\right)^2}}}. \tag{1.337}$$

So the whole singular Term 1 can be approximated as

$$\frac{1}{4\pi r_o} \ln \frac{4}{\sqrt{1 - \frac{4\frac{r}{r_o}}{\left(\frac{z-z_0}{r_o}\right)^2 + \left(\frac{r}{r_o}+1\right)^2}}}. \tag{1.338}$$

We can use logarithm rules to pull out the square root and the 4 for now

$$\frac{1}{4\pi r_o} \left[\ln(4) - 0.5 \ln \left(1 - \frac{4\frac{r}{r_o}}{\left(\frac{z-z_0}{r_o}\right)^2 + \left(\frac{r}{r_o}+1\right)^2} \right) \right]. \tag{1.339}$$

Simplifying inside the second logarithm term

$$1 - \frac{4\frac{r}{r_o}}{\left(\frac{z-z_0}{r_o}\right)^2 + \left(\frac{r}{r_o}+1\right)^2}$$

$$= \frac{\left(\frac{z-z_0}{r_o}\right)^2 + \left(\frac{r}{r_o}+1\right)^2 - 4\frac{r}{r_o}}{\left(\frac{z-z_0}{r_o}\right)^2 + \left(\frac{r}{r_o}+1\right)^2} \qquad \text{getting a common denominator}$$

$$= \frac{\left(\frac{z-z_0}{r_o}\right)^2 + \left(\frac{r}{r_o}\right)^2 + 2\frac{r}{r_o} + 1 - 4\frac{r}{r_o}}{\left(\frac{z-z_0}{r_o}\right)^2 + \left(\frac{r}{r_o}+1\right)^2} \qquad \text{expanding}$$

$$= \frac{\left(\frac{z-z_0}{r_o}\right)^2 + \left(\frac{r}{r_o}\right)^2 - 2\frac{r}{r_o} + 1}{\left(\frac{z-z_0}{r_o}\right)^2 + \left(\frac{r}{r_o}+1\right)^2} \qquad \text{simplifying}$$

$$= \frac{\left(\frac{z-z_0}{r_o}\right)^2 + \left(\frac{r}{r_o}-1\right)^2}{\left(\frac{z-z_0}{r_o}\right)^2 + \left(\frac{r}{r_o}+1\right)^2}$$

$$= \frac{(z-z_0)^2 + (r-r_0)^2}{(z-z_0)^2 + (r+r_0)^2}. \qquad \text{canceling common denominators}$$

$$\tag{1.340}$$

Plugging this into the full expression gives us

$$\frac{1}{4\pi r_o} \left[\ln(4) - 0.5 \ln \left(\frac{(z-z_0)^2 + (r-r_0)^2}{(z-z_0)^2 + (r+r_0)^2} \right) \right]. \tag{1.341}$$

Let's now bring the 4 back inside the logarithm (noting the negative out front, so it goes into the denominator now), and resolving the non-singular denominator at $z_o = z$ and $r_o = r$,

$$\frac{1}{4\pi r}\left[-0.5\ln\left(\frac{[(z-z_o)^2+(r-r_o)^2]}{16\left(0^2+(2r)^2\right)}\right)\right]$$

$$= -\frac{1}{8\pi r}\left[\ln\left(\frac{(z-z_o)^2+(r-r_o)^2}{64r^2}\right)\right]. \tag{1.342}$$

Now we have both of the singular pieces (Terms 1 and 3) that we need to subtract from the vortex ring induced axial velocity in our subtraction of singularity method. Together they are:

$$\frac{r_o-r}{2\pi\left[(z-z_o)^2+(r-r_o)^2\right]} - \frac{1}{8\pi r}\left[\ln\left(\frac{(z-z_o)^2+(r-r_o)^2}{64r^2}\right)\right].$$

$$\tag{1.343}$$

1.B.2 Unit Radial Velocity Induced by a Vortex Ring

For the radial component of velocity induced by a vortex ring, we again start with our expression from equation (1.88)

$$v_r = -\frac{1}{2\pi r_o}\frac{\xi/\rho}{D_1}\left[\mathcal{K}(m) - \left(1 + \frac{2\rho}{D_2}\right)\mathcal{E}(m)\right], \tag{1.88b}$$

where again, $\mathcal{K}(m)$ and $\mathcal{E}(m)$ are complete elliptic integrals of the first and second kind, respectively, and

$$m = \left(\frac{4\rho}{\xi^2+(\rho+1)^2}\right)$$

$$\xi = \frac{z-z_o}{r_o}$$

$$\rho = \frac{r}{r_o}$$

$$D_1 = \left[\xi^2+(\rho+1)^2\right]^{1/2}$$

$$D_2 = \xi^2+(\rho-1)^2.$$

Expanding things out as before:

$$v_r^\gamma = \int_{(z_1,r_1)}^{(z_2,r_2)} \left[\left(\frac{z-z_o}{r_o}\right) \frac{\int_0^{\pi/2} \frac{1}{\left[1-\left(\frac{4\frac{r}{r_o}}{\left(\frac{z-z_o}{r_o}\right)^2+\left(\frac{r}{r_o}+1\right)^2}\right)\sin^2\theta\right]^{1/2}}d\theta}{2\pi r_o\left(\frac{r}{r_o}\right)\left[\left(\frac{z-z_o}{r_o}\right)^2+\left(\frac{r}{r_o}+1\right)^2\right]^{1/2}} \right.$$

$$-\left(\frac{z-z_o}{r_o}\right) \frac{\int_0^{\pi/2}\left[1-\left(\frac{4\frac{r}{r_o}}{\left(\frac{z-z_o}{r_o}\right)^2+\left(\frac{r}{r_o}+1\right)^2}\right)\sin^2\theta\right]^{1/2}d\theta}{2\pi r_o\left(\frac{r}{r_o}\right)\left[\left(\frac{z-z_o}{r_o}\right)^2+\left(\frac{r}{r_o}+1\right)^2\right]^{1/2}}$$

$$\left. -\left(\frac{z-z_o}{r_o}\right) \frac{\int_0^{\pi/2}\left[1-\left(\frac{4\frac{r}{r_o}}{\left(\frac{z-z_o}{r_o}\right)^2+\left(\frac{r}{r_o}+1\right)^2}\right)\sin^2\theta\right]^{1/2}d\theta}{2\pi r_o\left(\frac{r}{r_o}\right)\left[\left(\frac{z-z_o}{r_o}\right)^2+\left(\frac{r}{r_o}+1\right)^2\right]^{1/2}}\left(\frac{2\left(\frac{r}{r_o}\right)}{\left(\frac{z-z_o}{r_o}\right)^2+\left(\frac{r-r_o}{r_o}\right)^2}\right)\right] ds.$$

$$(1.344)$$

Again plugging in $z = z_o$ and $r = r_o$ to clearly see the singularities

$$\left(\frac{0}{r_o}\right) \frac{\int_0^{\pi/2}\frac{1}{\left[1-\left(\frac{4}{\left(\frac{0}{r_o}\right)^2+(1+1)^2}\right)\sin^2\theta\right]^{1/2}}d\theta}{2\pi r_o(1)\left[\left(\frac{0}{r_o}\right)^2+(1+1)^2\right]^{1/2}} \qquad \text{Term 1}$$

$$-\left(\frac{0}{r_o}\right) \frac{\int_0^{\pi/2}\left[1-\left(\frac{4}{\left(\frac{0}{r_o}\right)^2+(1+1)^2}\right)\sin^2\theta\right]^{1/2}d\theta}{2\pi r_o(1)\left[\left(\frac{0}{r_o}\right)^2+(1+1)^2\right]^{1/2}} \qquad \text{Term 2}$$

$$-\left(\frac{0}{r_o}\right) \frac{\int_0^{\pi/2}\left[1-\left(\frac{4}{\left(\frac{0}{r_o}\right)^2+(1+1)^2}\right)\sin^2\theta\right]^{1/2}d\theta}{2\pi r_o(1)\left[\left(\frac{0}{r_o}\right)^2+(1+1)^2\right]^{1/2}}\left(\frac{2(1)}{\left(\frac{0}{r_o}\right)^2+\left(\frac{0}{r_o}\right)^2}\right). \quad \text{Term 3}$$

$$(1.345)$$

As before, we'll start with the second term and third terms. Again, the elliptic integral of the second kind will go to 1, meaning Term 2 is non-singular. For Term 3, we go back to the original expression and have

$$\left(\frac{z - z_o}{r_o}\right) \frac{1}{2\pi r_o \left(\frac{r}{r_o}\right)\left[\left(\frac{z-z_o}{r_o}\right)^2 + \left(\frac{r}{r_o} + 1\right)^2\right]^{1/2}} \left(\frac{2\left(\frac{r}{r_o}\right)}{\left(\frac{z-z_o}{r_o}\right)^2 + \left(\frac{r-r_o}{r_o}\right)^2}\right) \quad (1.346)$$

Here a r/r_o will cancel along with a r_o^2; futhermore, the non-singular outer denominator again goes to 2 (which also cancels), so we are left with

$$\frac{z_o - z}{2\pi \left[(z - z_o)^2 + (r - r_o)^2\right]} \quad (1.347)$$

For Term 1, we have from the original expression

$$\left(\frac{z - z_o}{r_o}\right) \frac{\mathcal{K}(m)}{2\pi r_o \left(\frac{r}{r_o}\right)\left[\left(\frac{z-z_o}{r_o}\right)^2 + \left(\frac{r}{r_o} + 1\right)^2\right]^{1/2}}. \quad (1.348)$$

Simplifying the denominator leaves

$$\frac{z - z_o}{4\pi r_o^2}\mathcal{K}(m). \quad (1.349)$$

Applying the asymptotic approximation for $\mathcal{K}(m)$,

$$\frac{z - z_o}{4\pi r_o^2} \ln \frac{4}{\sqrt{1 - \dfrac{4\frac{r}{r_o}}{\left(\frac{z-z_o}{r_o}\right)^2 + \left(\frac{r}{r_o} + 1\right)^2}}}. \quad (1.350)$$

Note that as $z \to z_o$ and $r \to r_o$ the r terms actually don't induce any singularity, simplifying out these terms (setting $r = r_o$) leaves

$$\frac{z - z_o}{4\pi r_o^2} \ln \frac{4}{\sqrt{1 - \dfrac{4}{\left(\frac{z-z_o}{r_o}\right)^2 + 4}}}. \quad (1.351)$$

Getting a common denominator in the radicand gives

$$\frac{z - z_o}{4\pi r_o^2} \ln \frac{4}{\sqrt{\dfrac{\left(\frac{z-z_o}{r_o}\right)^2}{\left(\frac{z-z_o}{r_o}\right)^2 + 4}}}. \quad (1.352)$$

Again applying logarithm rules to pull out the radical and 4, then noting that the log(4) is non-singular we ignore it going forward, we have

$$\frac{z - z_o}{8\pi r_o^2} \ln \frac{\left(\frac{z-z_o}{r_o}\right)^2}{\left(\frac{z-z_o}{r_o}\right)^2 + 4}. \quad (1.353)$$

Applying logarithm rules again we see

$$\frac{z - z_o}{8\pi r_o^2} \left(\ln \left(\frac{z - z_o}{r_o} \right)^2 - \ln \left[\left(\frac{z - z_o}{r_o} \right)^2 + 4 \right] \right). \tag{1.354}$$

At this point (if not already) we can see that this term is analogous to a sum of expressions taking the form $x \ln(x)$ which is not, in fact, singular. Therefore Term 1 is not singular and we can ignore it. Thus the singular expression which we need to subtract from the radially induced velocity due a vortex ring is simply that from Term 3 (equation (1.347)):

$$\boxed{\frac{z - z_o}{2\pi \left[(z - z_o)^2 + (r - r_o)^2 \right]}} \tag{1.347}$$

1.B.3 Analytic Solutions of Singular Portions of Integrals to Add Back in

Now that we have all the singular parts that are subtracted, we need to take the integrals analytically. We will integrate along the panel lengths, noting that the panel length, $\Delta s = |p_2 - p_1|$. Therefore, all of the non-logarithmic terms will cancel in the integral since the distances from the end points to the midpoint is equal, but with opposite sign, from the endpoints. This just leaves the logarithmic terms which we integrate as follows:[ak]

[ak] Note that in the integration step, $s_i - \overline{p} = \pm \Delta s$ depending on which side of the panel the subtraction is taking place.

$$\frac{-1}{8\pi r} \iint \left[\ln \left(\frac{(z - z_o)^2 + (r - r_o)^2}{64r^2} \right) \right] \mathrm{d}z_o \mathrm{d}r_o \tag{1.355}$$

$$= \frac{-1}{8\pi r} \int_{p_1}^{p_2} \left[\ln \left(\frac{|\overline{p} - s|^2}{64r^2} \right) \right] \mathrm{d}s \qquad \text{get in terms of single variable} \tag{1.356}$$

$$= \frac{-1}{4\pi r} \int_{p_1}^{p_2} \left[\ln \left(\frac{|\overline{p} - s|}{8r} \right) \right] \mathrm{d}s \qquad \text{pull the power of 2 out of the log} \tag{1.357}$$

$$= \frac{-1}{4\pi r} \left(\Delta s \ln \frac{\Delta s}{16r} - \Delta s \right) \qquad \text{integrate} \tag{1.358}$$

$$= \frac{1}{4\pi r} \left(\Delta s \ln \frac{16r}{\Delta s} + \Delta s \right) \qquad \text{cancel a negative} \tag{1.359}$$

$$= \frac{\Delta s}{4\pi r} \left(1 + \ln \frac{16r}{\Delta s} \right). \qquad \text{gather terms} \tag{1.360}$$

1.B.4 Unit Axial Velocity Induced by a Source Ring

Add: add in the source ring derivations at some point

1.C Airfoil Polar Corrections for Ducted Rotors

When airfoil/cascade aerodynamic data is unavailable for each of the rotor blade sections, it may be possible to use airfoil section data for

subsonic flow regimes (and perhaps even mildly super sonic regimes) without terrible inaccuracy if we apply some corrections to the airfoil polar. Though the accuracy of solutions does break down quickly for high subsonic, transonic, and supersonic cases. If supersonic airfoil or cascade data is an absolute necessity (e.g. for fully super sonic data), then the following corrections should not be used, and proper section polars should be generated through appropriate means. The following subsections cover the airfoil data corrections and adjustments available in DuctAPE as well as addition adjustments made to the implementation of each as required for suitability in gradient-based optimization. Specifically, we discuss the nominal correction methodology and then go over implementation details required for removing any discontinuities[al] present in the nominal formulation.

[al] As we do not necessarily know a priori where in the design space an optimizer will search, we need to ensure that the correction models are continuous over the entire design space when using gradient-based optimization.

1.C.1 Stall Cutoffs

Before any actual corrections are applied, we need to make an important adjustment to the nominal airfoil data. Especially if the airfoil data provided includes information in the post stall regime, we see that it is possible to obtain the same lift coefficient at two different angles of attack. This feature of the airfoil data can make it difficult for the DuctAPE solver to converge, since a blade element method is the foundation of the rotor and wake models. To remove the possibility of multiple solutions for the lift, we effectively cut off the airfoil data post stall and assign our own, slightly positive lift slope above the maximum lift coefficient and below the minimum lift coefficient. We keep the nominal data between the minimum and maximum lift coefficients and smoothly blend that data into the prescribed lift slopes for the rest of the possible range of angles of attack. We apply a similar procedure to the drag data, but use the cutoff angles of attack from the lift curve. Figure 1.C.1 shows an example of our stall cutoff adjustment to lift and drag data.

1.C.2 Solidity and Stagger Corrections

Isolated airfoil data needs to be corrected to account for cascade, or multi-plane interference, effects since the airfoils along a rotor blade section are not actually isolated. This is especially true for higher solidities, where blades are relatively close together. We apply corrections based on a simple model published by Wallis[12–14], which assumes smooth transition between isolated airfoil and cascade data as solidity increases, as well as circular camber line airfoil geometries.

12 Wallis, "A Rationalised Approach to Blade Element Design, Axial Flow Fans," 1968.

13 Wallis, "The F-Series Aerofoils, for Fan Blade Sections," 1977.

14 Wallis, *Axial Flow Fans and Ducts*, 1983.
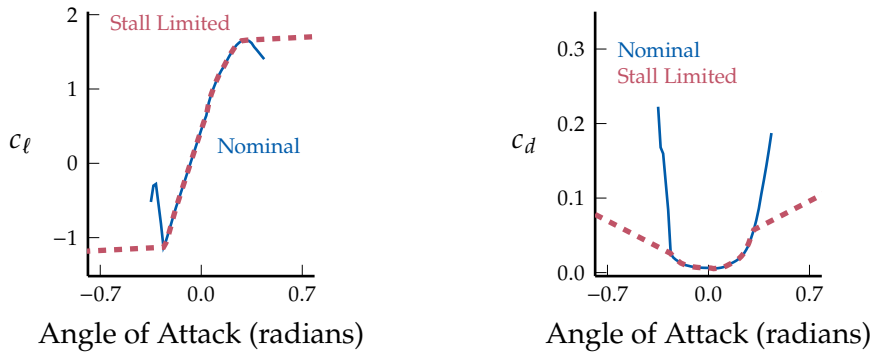
(a) Lift data is overwritten and extended outside the minimum and maximum lift coefficient values.

(b) We cutoff Drag data at the same angles of attack as the lift data.

Figure 1.C.1: We cut off airfoil data outside the range of minimum and maximum lift coefficient and replace/extend the data using a prescribed lift curve slope in order to avoid numerical difficulties associated with multiple angles of attack resulting in equal lift coefficients.

The corrections depend both on solidity and stagger, though stagger only begin to effect the correction after 20 degrees. These corrections are somewhat limited as they assume the airfoil camber is well matched to the operating conditions such that the deviation angle isn't overly large, but they should be sufficient for our purposes. Wallis gives his corrections in the form of a line plot, to which quadratic fits are made. Specifically, we use the quadratic fits provided in the DFDC source code. The model is also applied only for stagger angles less than 90 degrees, and stagger effects are held constant after that. Furthermore, the total correction factor is set to a maximum of 1, since, as stated by Wallis, "there are no documented examples of factors exceeding unity," and the tendency of theoretical models predict values above 1 appears to be due to not capturing increased deviation angles completely.

For implementation, since the solidity and stagger corrections only apply for stagger angles between 20 and 90 degrees, and we also set a maximum adjustment factor of 1, we limit stagger angles below 20 degrees to 20 degrees, and above 90 degrees to 90 degrees. We apply these limits using a sigmoid blending function between the limited ranges and the nominal range. For the limit of the overall adjustment factor, we subtract the difference of the unlimited adjustment factor and the factor limit of 1 from the unlimited factor. To keep the end product smooth, we actually apply another sigmoid blending function to the difference to be subtracted and zero, centered just before the point of limitation to mitigate overshoot by the blending function. Figure 1.C.3 shows the limited correction curves with respect to changes in solidity and stagger. We also see in figure 1.C.3 that our applications of smooth blending functions have minimal effect on the calculated correction values.
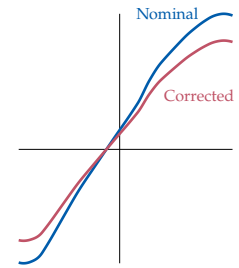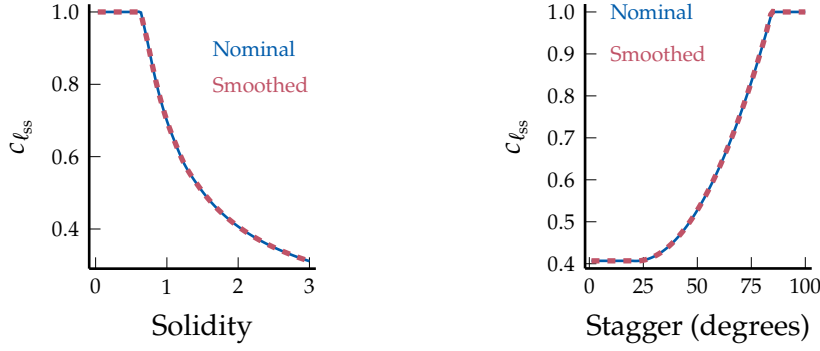

Figure 1.C.2: Example curves demonstrating the changes to the lift coefficient vs angle of attack for the nominal polar when corrections for a solidity of 1.0 at a stagger angle of $\pi/4$ are applied.

(a) Corrected value vs solidity for a stagger angle of $\pi/4$.

(b) Corrected value vs stagger angle for a solidity of $\sigma = 2$

Figure 1.C.3: Nominal (with cutoffs) and smoothed solidity and stagger corrections for a nominal lift coefficient of 1.

1.C.3 Compressibility Lift Corrections

For subsonic compressibility corrections, we apply the well-used Pradtl-Glauert correction, which is based off of compressible potential flow and thin airfoil theories[15]. The Pradtl-Glauert correction states that for the nominal lift coefficient (which in our case is already corrected for solidty and stagger effects), $c_{\ell_{ss}}$, one can apply a correction factor of $\beta = \left[1 - M^2\right]^{-1/2}$ to correct for compressibility affects of lift on the airfoil for Mach numbers, M, up to about 0.7.

$$c_{\ell_{pg}} = \frac{c_{\ell_{ss}}}{[1 - M^2]^{1/2}} \tag{1.361}$$

where the Mach number is defined as

$$M = \frac{W}{V_s} \tag{1.362}$$

where W is the local inflow velocity magnitude and V_s is the local speed of sound (which we assume to be the freestream speed of sound). Figure 1.C.4 shows an example application of the Pradtl-Glauert correction applied to an arbitrary set of airfoil data for a Mach number of 0.5.

For implementation in a gradient-based optimization setting, we note that equation (1.361) is only valid for Mach numbers less than 1. At $M = 1$ we get infinity, and for $M > 1$ the output is not a real number. In order to remedy these issues, we first set a limit on the Mach numbers that can be input, say $M = 0.999$, we then apply a quintic polynomial blend between equation (1.361) and the output for the limit of $M = 0.999$ centered at $M = 0.975$ with an interpolation range of 0.02 on either side of the center point. This provides a smooth transition to the cutoff value as well as avoids the possibility of equation (1.361) being evaluated at or above $M = 1$. Although, as may be seen in figure 1.C.5, this adjustments causes a slight deviation from the nominal correction for high subsonic

[15] Glauert *et al.*, "The effect of compressibility on the lift of an aerofoil," 1928.
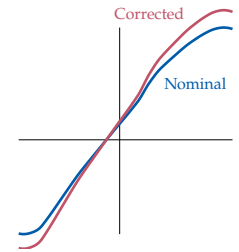

Figure 1.C.4: Example curves demonstrating the changes to the lift coefficient vs angle of attack for the nominal polar when the Prandtl-Glauert correction applied.
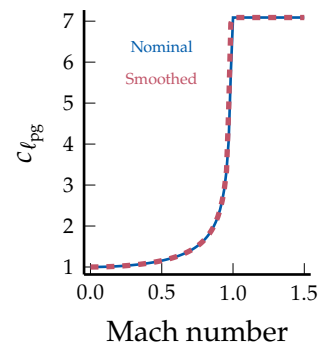

Figure 1.C.5: Nominal (with cutoff Mach number) and smoothed versions of the Prandtl-Glauert correction compared for a nominal lift coefficient of 1.

Mach numbers, the deviations are small and in ranges that we do not expect to operate frequently.

1.C.4   Reynolds Number Drag Adjustments

If we have airfoil data at one Reynolds number, but we need to know how the airfoil behaves at a slightly different Reynolds number, we can apply an adjustment to the drag coefficient based on similarity between flat plate skin friction drag. The limitation here is that we assume that the flow regimes between the Reynolds numbers are similar, in that they have similar laminar vs turbulent behavior, so that we can cancel out unknown constants due to airfoil shape and flow regime to arrive at

$$c_{d_{Re}} = c_{d_o} \left(\frac{Re_o}{Re} \right)^p ; \tag{1.363}$$

where Re is the local Reynolds number, Re_o is the Reynolds number at which the data was generated, and the exponent terms are defined, for example, as $p = 0.5$ for fully laminar flow and $p = 0.2$ for fully turbulent flow. Figure 1.C.6 shows an example of the Reynolds number drag adjustment for an arbitrary drag curve applied for use at a Reynolds number 2.5 times larger than the nominal case. Note that we do not have to apply a similar correction to the lift coefficient, because within the constraint of similar flow regimes (that is, relatively small changes in Reynolds number), the lift does not actually change significantly. Also note that in practice, it may be better to simply utilize an interpolation between data at various Reynolds numbers, especially if the laminar vs turbulent regime is not fully characterized a priori.
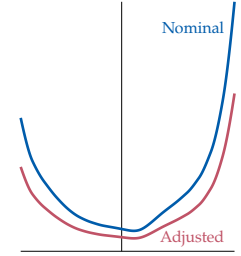

Figure 1.C.6: Example curves demonstrating the changes to the drag coefficient vs angle of attack for the nominal polar when the Reynolds number adjustment is applied for a slightly higher Reynolds number.

1.C.5   Transonic Effects on Lift and Drag Coefficients

Above a critical Mach number, often around 0.7, the Pradtl-Glauert correction begins to break down due to transonic effects over the airfoil. If shock waves are present on the airfoil, we can expect a decrease in lift as early separation can occur. For these high subsonic and transonic cases, we apply limiters to the maximum and minimum lift coefficients. We choose to employ the method used in XROTOR[am] and DFDC[an]. The lift curve limiter correction used in these codes takes the form:

$$c_{\ell_{corr}} = c_{\ell_{pg}} - (1 - f_{stall}) c_{\ell_{lim}}, \tag{1.364}$$

where

$$f_{stall} = \frac{\left. \frac{dc_\ell}{d\alpha} \right|_{stall}}{\frac{dc_\ell}{d\alpha}}, \tag{1.365}$$

and

$$c_{\ell_{lim}} = \Delta c_{\ell_{stall}} \ln \left[\frac{1 + exp\left(\frac{c_{\ell_{pg}} - c'_{\ell_{max}}}{\Delta c_{\ell_{stall}}} \right)}{1 + exp\left(\frac{c'_{\ell_{min}} - c_{\ell_{pg}}}{\Delta c_{\ell_{stall}}} \right)} \right] ; \tag{1.366}$$

[am] https://web.mit.edu/drela/Public/web/xrotor/
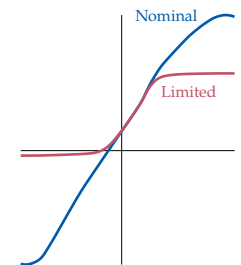
[an] https://web.mit.edu/drela/Public/web/dfdc/

Figure 1.C.7: Example curves demonstrating the changes to the lift coefficient vs angle of attack for the nominal polar when the critical mach limiter is applied.

where $\frac{dc_\ell}{d\alpha}\big|_{\text{stall}}$ is the lift curve slope to apply in the post stall region as part of this limiting correction, and $\frac{dc_\ell}{d\alpha}$ is the nominal lift curve slope. The $\Delta c_{\ell_{\text{stall}}}$ term is the change in c_ℓ between incipient and total stall. The $c'_{\ell_{\text{max}}}$ and $c'_{\ell_{\text{min}}}$ values are the minimum and maximum of the nominal $c_{\ell_{\text{max}_o}}$ and $c_{\ell_{\text{min}_o}}$ and the following expressions, respectively:

$$c'_{\ell_{\text{max}}} = min\left[c_\ell\big|_{c_{d_{\text{min}}}} + 4\left(M_{\text{crit}} - M + \Delta M_{\text{stall}}\right), \ c_{\ell_{\text{max}_o}} \right] \quad (1.367a)$$

$$c'_{\ell_{\text{min}}} = max\left[c_\ell\big|_{c_{d_{\text{min}}}} - 4\left(M_{\text{crit}} - M + \Delta M_{\text{stall}}\right), \ c_{\ell_{\text{min}_o}} \right], \quad (1.367b)$$

where M_{crit} is the critical Mach number, $c_\ell\big|_{c_{dmin}}$ is the lift coefficient at the minimum drag angle of attack, and

$$\Delta M_{\text{stall}} = \left(\frac{0.1}{10}\right)^{1/3} \quad (1.368)$$

is comprised of chosen factors that yield reasonable results.[ao] Figure 1.C.7 shows an example transonic limit adjustment for an arbitrary lift curve given a critical Mach number of 0.7 and an operational Mach number of 0.8.

[ao] These numbers are hard coded into XROTOR and DFDC.

Along with the limiters placed on the lift curve due to transonic effects for Mach numbers above the critical Mach number for the airfoil, there are accompanying increases in the drag coefficients. Again, we turn to the corrections provided in the XROTOR and DFDC codes, which add compressibility drag based on the limited lift coefficients described previously. The added compressibility drag takes the form

$$c_{d_c} = c_{d_{Re}} + 10\left(M - M_{\text{crit}}(c_\ell)\right)^3, \quad (1.369)$$

where the critical Mach adjusted for the limited lift coefficient takes the form

$$M_{\text{crit}}(c_\ell) = M_{\text{crit}} - \frac{\left| c_{\ell_{\text{lim}}} - c_\ell\big|_{c_{d_{\text{min}}}} \right|}{4} - \Delta M_{\text{crit}}, \quad (1.370)$$

where

$$\Delta M_{\text{crit}} = \left(\frac{0.002}{10}\right)^{1/3} \quad (1.371)$$

comes from the difference in Mach corresponding to a rise in c_d of 0.002 at M_{crit}, which is chosen to match empirical experience.[ap] Similarly, as before, the other constants are chosen to yield reasonable results. Figure 1.C.8 shows an example comparison between a nominal drag curve and one for which the transonic compressibility augmentations have been applied for a Mach number 0.1 above M_{crit}.

For smooth implementation there are several min/max operations in the lift limiter function, these have been smoothed with sigmoid blending
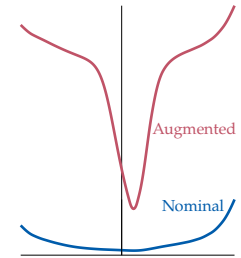

Figure 1.C.8: Example curves demonstrating the changes to the drag coefficient vs angle of attack for the nominal polar when the transonic compressibility corrections are added for a Mach number of 0.1 above M_{crit}.

[ap] Again, these values are hard coded into XROTOR and DFDC.

functions, and very little change is introduced from the nominal function as seen in figure 1.C.9. In addition, the nominal drag limiter function only adds drag after the critical Mach number is reached. We smoothed this transition, which is perhaps less physical, but the differences are minimal as seen in figure 1.C.9. Furthermore, we used a smoothed absolute value with relatively tight smoothing range. In this case, there is a slight over-prediction of the corrected drag for values at and just above the critical mach number, which actually counters the under prediction introduced by smoothing across the critical mach.
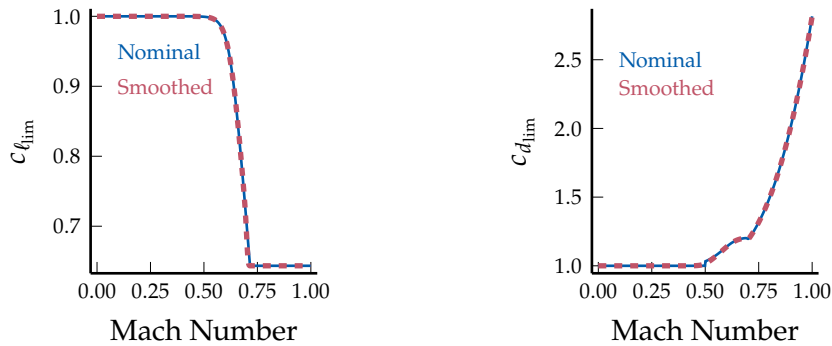

Figure 1.C.9: Nominal and smoothed transonic lift and drag coefficient limits across a range of Mach numbers for a Nominal lift coefficient of unity.

1.C.6 Combined Implementation

In DuctAPE, these corrections are applied as follows. First, it is assumed that the user inputs airfoil data that is already pre-processed with the stall limits applied. Ideally, the airfoil data also inherently has Reynolds number dependencies (data at various Reynolds numbers) already as well. Then during computation, the corrections are applied on-the-fly, beginning with the solidity/stagger correction. The Prandtl-Glauert compressibility correction is applied next, followed by the Reynolds number drag correction if data at multiple Reynolds numbers was not provided. Finally, the transonic effect lift limiter and drag addition corrections are applied.

1.D Comparison of Corrected Airfoil Polars to Experimental Cascade Data

To see how the corrections actually fare (especially the solidity and stagger corrections), we compare to experimental data produced by NACA for their NACA 65-410 airfoil. The NACA 65-series compressor blade airfoils are base on a basic thickness form and mean line. The basic thickness form comes from the 65_2-016 airfoil which is first scaled down to 10% thickness and then the y-coordinates are increased by 0.0015 times the chord-wise coordinate to slightly thicken the trailing edge. There are also directly derived values for the coordinates; they

are slightly different than the scaled values used in the study. The basic mean line comes from the NACA 6-series method to obtain a design lift coefficient of 1.0, and then scaled based on the desired lift coefficient. For example the 65-410 mean camber line takes the basic mean camber line and scales it by 0.4, while the 65-(12)10 mean camber line is the basic mean camber line scaled by a factor of 1.2. Tests were run for at solidities from 0.5 to 1.5 and inflow angles of 30° to 70°, although not every combination was tested. Tests at solidities of 1.0 and above were performed at a Reynolds number of 2.45e5; for solidities less than 1.0 tests were performed at a Reynolds number of 2e5. The experimental data for lift and drag coefficients in the NACA report is given for each tested combination of inflow angle and solidity across a range of angles of attack, generally ranging from negative to positive stall. Note that the lift and drag forces were not measured directly, but rather calculated from pressure and velocity measurements. In order to apply our airfoil corrections we calculate the stagger angles, γ, from the provided inflow angles, β_1, and angles of attack, α, as

$$\gamma = \beta_1 - \alpha \qquad (1.372)$$

Figure 1.D.1: NACA 65-410 compressor series airfoil geometry (using the scaled ordinates).

As can be seen in figure 1.D.2, the method of corrected airfoil data does not do especially well at matching actual cascade data. In general, the lift curve slopes of the cascades are much shallower than that of the isolated and corrected XFOIL outputs. In addition, the drag "bucket" of the isolated airfoil is much narrower than for the cascades. We note that we did not apply drag corrections in an attempt to capture cascade effects. Such corrections would increase the drag due to blockage from solidity and increase the discrepancies we already see in figure 1.D.2.
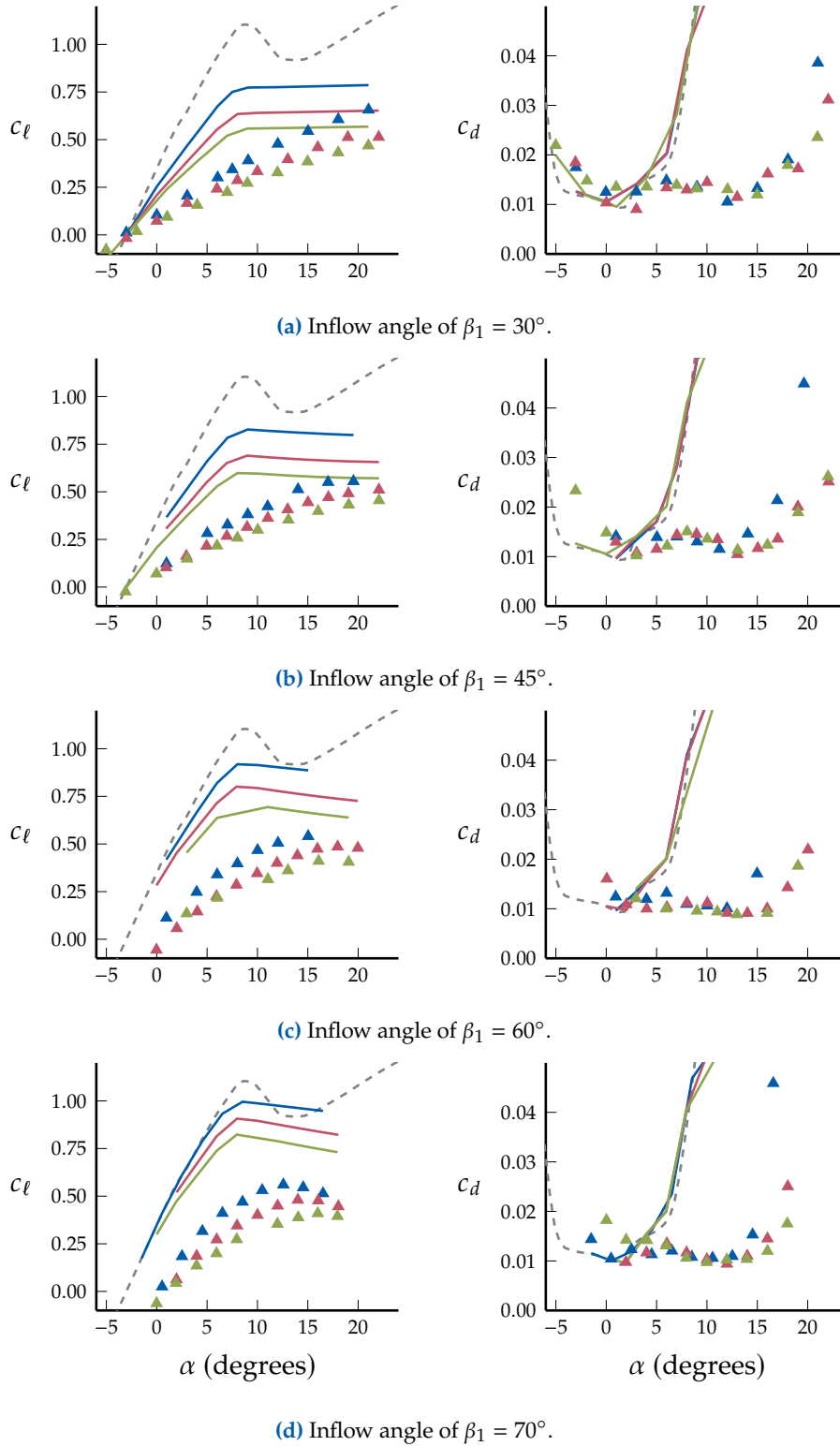
(a) Inflow angle of $\beta_1 = 30°$.

(b) Inflow angle of $\beta_1 = 45°$.

(c) Inflow angle of $\beta_1 = 60°$.

(d) Inflow angle of $\beta_1 = 70°$.

Figure 1.D.2: Comparison of NACA experimental data (▲ markers) and XFOIL airfoil outputs with applied corrections (lines) for angles of attack vs lift (c_ℓ) and drag (c_d) coefficients at various inflow angles (β_1) and solidities. Blue indicates solidity = 1.0, red indicates solidity = 1.25, and green indicates solidity = 1.5; Grey dashed lines indicate the uncorrected, smoothed XFOIL outputs.

1.E Transformation of Poisson Equations

In order to interchange the dependent and independent variables of

$$\xi(z,r) \equiv \xi_{zz} + \xi_{rr} = 0 \tag{1.373a}$$

$$\eta(z,r) \equiv \eta_{zz} + \eta_{rr} = \frac{\psi_r}{r}, \tag{1.373b}$$

where $\eta = \psi =$ constant along streamlines (thus η coordinates correspond to the physical location of streamlines) and ξ is constant along radial lines and can be arbitrarily chosen, we apply the derivative transformations:

$$f_z = \frac{r_\eta f_\xi - r_\xi f_\eta}{J} \tag{1.374a}$$

$$f_r = \frac{-z_\eta f_\xi + z_\xi f_\eta}{J}, \tag{1.374b}$$

where $J = z_\xi r_\eta - z_\eta r_\xi$.

Let's look first at the ξ_{zz} term. We will begin by applying equation (1.374a):

$$\xi_z = \frac{r_\eta \xi_\xi - r_\xi \xi_\eta}{J} \tag{1.375}$$

$$\xi_{zz} = \frac{r_\eta \left(\frac{r_\eta \xi_\xi - r_\xi \xi_\eta}{J}\right)_\xi - r_\xi \left(\frac{r_\eta \xi_\xi - r_\xi \xi_\eta}{J}\right)_\eta}{J}. \tag{1.376}$$

Recognizing that $\xi_\xi = 1$, and $\xi_\eta = 0$ (by orthogonality), we can simplify.

$$\xi_{zz} = \frac{r_\eta \left(\frac{r_\eta}{J}\right)_\xi - r_\xi \left(\frac{r_\eta}{J}\right)_\eta}{J}.$$

Applying the quotient rule:

$$\xi_{zz} = \frac{r_\eta \left(\frac{r_{\eta\xi}J - r_\eta J_\xi}{J^2}\right) - r_\xi \left(\frac{r_{\eta\eta}J - r_\eta J_\eta}{J^2}\right)}{J}$$

$$= \frac{r_\eta \left(r_{\eta\xi}J - r_\eta J_\xi\right) - r_\xi \left(r_{\eta\eta}J - r_\eta J_\eta\right)}{J^3}.$$

Expanding:

$$\xi_{zz} = \frac{r_\eta r_{\eta\xi}J - r_\eta^2 J_\xi - r_\xi r_{\eta\eta}J + r_\xi r_\eta J_\eta}{J^3}. \tag{1.377}$$

We'll leave ξ_{zz} here for now and follow the same procedure for ξ_{rr}— beginning by applying equation (1.374b):

$$\xi_r = \frac{-z_\eta \xi_\xi + z_\xi \xi_\eta}{J} \tag{1.378}$$

$$\xi_{rr} = \frac{-z_\eta \left(\frac{-z_\eta \xi_\xi + z_\xi \xi_\eta}{J}\right)_\xi + z_\xi \left(\frac{-z_\eta \xi_\xi + z_\xi \xi_\eta}{J}\right)_\eta}{J}. \tag{1.379}$$

Again recognizing that $\xi_\xi = 1$, and $\xi_\eta = 0$ (by orthogonality), we can simplify:

$$\xi_{rr} = \frac{-z_\eta \left(\frac{-z_\eta}{J}\right)_\xi + z_\xi \left(\frac{-z_\eta}{J}\right)_\eta}{J}. \tag{1.380}$$

Applying the quotient rule:

$$\xi_{rr} = \frac{-z_\eta \left(\frac{-z_{\eta\xi}J + z_\eta J_\xi}{J^2}\right) + z_\xi \left(\frac{-z_{\eta\eta}J + z_\eta J_\eta}{J^2}\right)}{J}. \tag{1.381}$$

Expanding:

$$\xi_{rr} = \frac{z_\eta z_{\eta\xi}J - z_\eta^2 J_\xi - z_\xi z_{\eta\eta}J + z_\xi z_\eta J_\eta}{J^3}. \tag{1.382}$$

Now that we have both ξ_{zz} and ξ_{rr}, let us perform similar transformations for η_{zz} and η_{rr}. Let us begin with equation (1.374a):

$$\eta_z = \frac{r_\eta \eta_\xi - r_\xi \eta_\eta}{J} \tag{1.383}$$

$$\eta_{zz} = \frac{r_\eta \left(\frac{r_\eta \eta_\xi - r_\xi \eta_\eta}{J}\right)_\xi - r_\xi \left(\frac{r_\eta \eta_\xi - r_\xi \eta_\eta}{J}\right)_\eta}{J}. \tag{1.384}$$

Here, $\eta_\xi = 0$ (by orthogonality), and $\eta_\eta = 1$. So we simplify as follows

$$\eta_{zz} = \frac{r_\eta \left(\frac{-r_\xi}{J}\right)_\xi - r_\xi \left(\frac{-r_\xi}{J}\right)_\eta}{J}. \tag{1.385}$$

Applying the quotient rule:

$$\eta_{zz} = \frac{r_\eta \left(\frac{-r_{\xi\xi}J + r_\xi J_\xi}{J^2}\right) - r_\xi \left(\frac{-r_{\xi\eta}J + r_\xi J_\eta}{J^2}\right)}{J}. \tag{1.386}$$

Expanding:

$$\eta_{zz} = \frac{-r_\eta r_{\xi\xi}J + r_\eta r_\xi J_\xi + r_\xi r_{\xi\eta}J - r_\xi^2 J_\eta}{J^3}. \tag{1.387}$$

As we saw above, the expression for η_{rr} will be nearly identical to that for η_{zz}

$$\eta_r = \frac{-z_\eta \eta_\xi + z_\xi \eta_\eta}{J} \tag{1.388}$$

$$\eta_{rr} = \frac{-z_\eta \left(\frac{-z_\eta \eta_\xi + z_\xi \eta_\eta}{J}\right)_\xi + z_\xi \left(\frac{-z_\eta \eta_\xi + z_\xi \eta_\eta}{J}\right)_\eta}{J}. \tag{1.389}$$

Again recognizing that $\eta_\xi = 0$, and $\eta_\eta = 1$, we simplify:

$$\eta_{rr} = \frac{-z_\eta \left(\frac{z_\xi}{J}\right)_\xi + z_\xi \left(\frac{z_\xi}{J}\right)_\eta}{J}. \tag{1.390}$$

Applying the quotient rule:

$$\eta_{rr} = \frac{-z_\eta \left(\frac{z_{\xi\xi}J - z_\xi J_\xi}{J^2}\right) + z_\xi \left(\frac{z_{\xi\eta}J - z_\xi J_\eta}{J^2}\right)}{J}. \tag{1.391}$$

Expanding:

$$\eta_{rr} = \frac{-z_\eta z_{\xi\xi}J + z_\eta z_\xi J_\xi + z_\xi z_{\xi\eta}J - z_\xi^2 J_\eta}{J^3}. \tag{1.392}$$

Before putting everything together, we also need to transform the right hand side of equation (1.373b) using equation (1.374b) as we have done, noting in this case that we only have a single, rather than a double, derivative.

$$\frac{1}{r}\psi_r = \frac{-z_\eta \psi_\xi + z_\xi \psi_\eta}{rJ}. \tag{1.393}$$

Remembering that we have chosen $\psi = \eta$, and making similar simplifications with the derivitives we have thus far ($\eta_\eta = 1$, $\eta_\xi = 0$), we are left with

$$\frac{1}{r}\psi_r = \frac{z_\xi}{rJ}. \tag{1.394}$$

Let's now bring it all together in the Poisson equations to see where we are, multiplying everything by J^3 to remove all the fractions. For convenience and clarity, we'll also note that $(\cdot)_{\xi\eta} = (\cdot)_{\eta\xi}$ and put every instance in the $\xi\eta$ order.

$$\left[r_\eta r_{\xi\eta}J - r_\eta^2 J_\xi - r_\xi r_{\eta\eta}J + r_\xi r_\eta J_\eta\right] + \left[z_\eta z_{\xi\eta}J - z_\eta^2 J_\xi - z_\xi z_{\eta\eta}J + z_\xi z_\eta J_\eta\right] = 0 \tag{1.395a}$$

$$\left[-r_\eta r_{\xi\xi}J + r_\eta r_\xi J_\xi + r_\xi r_{\xi\eta}J - r_\xi^2 J_\eta\right] + \left[-z_\eta z_{\xi\xi}J + z_\eta z_\xi J_\xi + z_\xi z_{\xi\eta}J - z_\xi^2 J_\eta\right] = \frac{z_\xi J^2}{r}. \tag{1.395b}$$

In order to get the final $z(\xi, \eta)$ and $r(\xi, \eta)$ relations, we'll first need to do some more expanding, specifically of the jacobian (and its derivatives, applying the product rule):

$$J = z_\xi r_\eta - z_\eta r_\xi \tag{1.396a}$$

$$J_\xi = z_{\xi\xi} r_\eta + z_\xi r_{\xi\eta} - z_{\xi\eta} r_\xi - z_\eta r_{\xi\xi} \tag{1.396b}$$

$$J_\eta = z_{\xi\eta} r_\eta + z_\xi r_{\eta\eta} - z_{\eta\eta} r_\xi - z_\eta r_{\xi\eta}. \tag{1.396c}$$

Now we just need to expand everything out. Let's start with the transformation of the ξ_{zz} term (first term on the left hand side of equation (1.395a)). As we expand things out, we'll also rearrange terms to facilitate easier comparison.

$$
\begin{aligned}
\xi_{zz} =& r_\eta r_{\xi\eta}(z_\xi r_\eta - z_\eta r_\xi) \\
& - r_\eta^2(z_{\xi\xi} r_\eta + z_\xi r_{\xi\eta} - z_{\xi\eta} r_\xi - z_\eta r_{\xi\xi}) \\
& - r_\xi r_{\eta\eta}(z_\xi r_\eta - z_\eta r_\xi) \\
& + r_\xi r_\eta(z_{\xi\eta} r_\eta + z_\xi r_{\eta\eta} - z_{\eta\eta} r_\xi - z_\eta r_{\xi\eta}) \\
=& z_\xi \cancel{r_{\xi\eta} r_\eta^2} - z_\eta r_\xi r_{\xi\eta} r_\eta \\
& - z_{\xi\xi} r_\eta^3 - z_\xi \cancel{r_{\xi\eta} r_\eta^2} + z_{\xi\eta} r_\xi r_\eta^2 + z_\eta r_{\xi\xi} r_\eta^2 \\
& - \underline{z_\xi r_\xi r_{\eta\eta} r_\eta} + z_\eta r_\xi^2 r_{\eta\eta} \\
& + z_{\xi\eta} r_\xi r_\eta^2 + \underline{z_\xi r_\xi r_{\eta\eta} r_\eta} - z_{\eta\eta} r_\xi^2 r_\eta - z_\eta r_\xi r_{\xi\eta} r_\eta \\
=& - z_{\xi\xi} r_\eta^3 - z_{\eta\eta} r_\xi^2 r_\eta \\
& - 2z_\eta r_\xi r_{\xi\eta} r_\eta + 2z_{\xi\eta} r_\xi r_\eta^2 \\
& + z_\eta r_{\xi\xi} r_\eta^2 + z_\eta r_\xi^2 r_{\eta\eta}.
\end{aligned}
\tag{1.397}
$$

Now ξ_{rr} (second term in equation (1.395a)):

$$
\begin{aligned}
\xi_{rr} =& z_\eta z_{\xi\eta}(z_\xi r_\eta - z_\eta r_\xi) \\
& - z_\eta^2(z_{\xi\xi} r_\eta + z_\xi r_{\xi\eta} - z_{\xi\eta} r_\xi - z_\eta r_{\xi\xi}) \\
& - z_\xi z_{\eta\eta}(z_\xi r_\eta - z_\eta r_\xi) \\
& + z_\xi z_\eta(z_{\xi\eta} r_\eta + z_\xi r_{\eta\eta} - z_{\eta\eta} r_\xi - z_\eta r_{\xi\eta}) \\
=& z_\xi z_{\xi\eta} z_\eta r_\eta - \cancel{z_{\xi\eta} z_\eta^2 r_\xi} \\
& - z_{\xi\xi} z_\eta^2 r_\eta - z_\xi z_\eta^2 r_{\xi\eta} + \cancel{z_{\xi\eta} z_\eta^2 r_\xi} + z_\eta^3 r_{\xi\xi} \\
& - z_\xi^2 z_{\eta\eta} r_\eta + \underline{z_\xi z_{\eta\eta} z_\eta r_\xi} \\
& + z_\xi z_{\xi\eta} z_\eta r_\eta + z_\xi^2 z_\eta r_{\eta\eta} - \underline{z_\xi z_{\eta\eta} z_\eta r_\xi} - z_\xi z_\eta^2 r_{\xi\eta} \\
=& - z_{\xi\xi} z_\eta^2 r_\eta - z_\xi^2 z_{\eta\eta} r_\eta \\
& + 2z_\xi z_{\xi\eta} z_\eta r_\eta - 2z_\xi z_\eta^2 r_{\xi\eta} \\
& + z_\eta^3 r_{\xi\xi} + z_\xi^2 z_\eta r_{\eta\eta}.
\end{aligned}
\tag{1.398}
$$

Next η_{zz} (first term in equation (1.395b)):

$$
\begin{aligned}
\eta_{zz} = &- r_\eta r_{\xi\xi}(z_\xi r_\eta - z_\eta r_\xi) \\
&+ r_\eta r_\xi(z_{\xi\xi}r_\eta + z_\xi r_{\xi\eta} - z_{\xi\eta}r_\xi - z_\eta r_{\xi\xi}) \\
&+ r_\xi r_{\xi\eta}(z_\xi r_\eta - z_\eta r_\xi) \\
&- r_\xi^2(z_{\xi\eta}r_\eta + z_\xi r_{\eta\eta} - z_{\eta\eta}r_\xi - z_\eta r_{\xi\eta}) \\
= &- z_\xi r_{\xi\xi}r_\eta^2 + \cancel{z_\eta r_{\xi\xi}r_\xi r_\eta} \\
&+ z_{\xi\xi}r_\xi r_\eta^2 + z_\xi r_\xi r_{\xi\eta}r_\eta - z_{\xi\eta}r_\xi^2 r_\eta - \cancel{z_\eta r_{\xi\xi}r_\xi r_\eta} \\
&+ z_\xi r_\xi r_{\xi\eta}r_\eta - \cancel{z_\eta r_\xi^2 r_{\xi\eta}} \\
&- z_{\xi\eta}r_\xi^2 r_\eta - z_\xi r_\xi^2 r_{\eta\eta} + z_{\eta\eta}r_\xi^3 + \cancel{z_\eta r_\xi^2 r_{\xi\eta}} \\
= & z_{\xi\xi}r_\xi r_\eta^2 + z_{\eta\eta}r_\xi^3 \\
&+ 2z_\xi r_\xi r_{\xi\eta}r_\eta - 2z_{\xi\eta}r_\xi^2 r_\eta \\
&- z_\xi r_{\xi\xi}r_\eta^2 - z_\xi r_\xi^2 r_{\eta\eta}.
\end{aligned}
\tag{1.399}
$$

Then η_{rr} (second term in equation (1.395b)):

$$
\begin{aligned}
\eta_{rr} = &- z_\eta z_{\xi\xi}(z_\xi r_\eta - z_\eta r_\xi) \\
&+ z_\eta z_\xi(z_{\xi\xi}r_\eta + z_\xi r_{\xi\eta} - z_{\xi\eta}r_\xi - z_\eta r_{\xi\xi}) \\
&+ z_\xi z_{\xi\eta}(z_\xi r_\eta - z_\eta r_\xi) \\
&- z_\xi^2(z_{\xi\eta}r_\eta + z_\xi r_{\eta\eta} - z_{\eta\eta}r_\xi - z_\eta r_{\xi\eta}) \\
= &- \cancel{z_{\xi\xi}z_\xi z_\eta r_\eta} + z_{\xi\xi}z_\eta^2 r_\xi \\
&+ \cancel{z_{\xi\xi}z_\xi z_\eta r_\eta} + z_\xi^2 z_\eta r_{\xi\eta} - z_\xi z_{\xi\eta}z_\eta r_\xi - z_\xi z_\eta^2 r_{\xi\xi} \\
&+ \cancel{z_\xi^2 z_{\xi\eta}r_\eta} - z_\xi z_{\xi\eta}z_\eta r_\xi \\
&- \cancel{z_\xi^2 z_{\xi\eta}r_\eta} - z_\xi^3 r_{\eta\eta} + z_\xi^2 z_{\eta\eta}r_\xi + z_\xi^2 z_\eta r_{\xi\eta} \\
= & z_{\xi\xi}z_\eta^2 r_\xi + z_\xi^2 z_{\eta\eta}r_\xi \\
&+ 2z_\xi^2 z_\eta r_{\xi\eta} - 2z_\xi z_{\xi\eta}z_\eta r_\xi \\
&- z_\xi z_\eta^2 r_{\xi\xi} - z_\xi^3 r_{\eta\eta}.
\end{aligned}
\tag{1.400}
$$

Finally, we'll partially expand the right hand side term of equation (1.395b):

$$
\frac{z_\xi J^2}{r} = \frac{J}{r}z_\xi(z_\xi r_\eta - z_\eta r_\xi).
\tag{1.401}
$$

Let's first look at the case where both parametric expressions are Laplace equations, that is to say, if the right hand side of equation (1.373b) was zero. We can put our expanded expressions back together, gathering like terms.

$$\xi_{zz} + \xi_{rr} = -z_{\xi\xi}(z_\eta^2 + r_\eta^2)r_\eta$$
$$-z_{\eta\eta}(z_\xi^2 + r_\xi^2)r_\eta$$
$$+2z_{\xi\eta}(z_\xi z_\eta + r_\xi r_\eta)r_\eta$$
$$-2r_{\xi\eta}(z_\xi z_\eta + r_\xi r_\eta)z_\eta$$
$$+r_{\xi\xi}(z_\eta^2 + r_\eta^2)z_\eta$$
$$+r_{\eta\eta}(z_\xi^2 + r_\xi^2)z_\eta$$

(1.402a)

$$\eta_{zz} + \eta_{rr} = z_{\xi\xi}(z_\eta^2 + r_\eta^2)r_\xi$$
$$+z_{\eta\eta}(z_\xi^2 + r_\xi^2)r_\xi$$
$$-2z_{\xi\eta}(z_\xi z_\eta + r_\xi r_\eta)r_\xi$$
$$+2r_{\xi\eta}(z_\xi z_\eta + r_\xi r_\eta)z_\xi$$
$$-r_{\xi\xi}(z_\eta^2 + r_\eta^2)z_\xi$$
$$-r_{\eta\eta}(z_\xi^2 + r_\xi^2)z_\xi.$$

(1.402b)

What we actually need from the above equations is $z(\xi, \eta)$ and $r(\xi, \eta)$, so we'll equate the two expressions and put the z terms together, and the r terms together.

$$0 = z_{\xi\xi}(z_\eta^2 + r_\eta^2)(r_\xi - r_\eta)$$
$$-2z_{\xi\eta}(z_\xi z_\eta + r_\xi r_\eta)(r_\xi - r_\eta)$$
$$+z_{\eta\eta}(z_\xi^2 + r_\xi^2)(r_\xi - r_\eta)$$

(1.403a)

$$0 = r_{\xi\xi}(z_\eta^2 + r_\eta^2)(z_\xi - z_\eta)$$
$$-2r_{\xi\eta}(z_\xi z_\eta + r_\xi r_\eta)(z_\xi - z_\eta)$$
$$+r_{\eta\eta}(z_\xi^2 + r_\xi^2)(z_\xi - z_\eta).$$

(1.403b)

Since both of the expressions equal zero, we can divide out the common terms and we are left with

$$z(\xi, \eta) \equiv \alpha z_{\xi\xi} - 2\beta z_{\xi\eta} + \gamma z_{\eta\eta} = 0 \tag{1.404a}$$
$$r(\xi, \eta) \equiv \alpha r_{\xi\xi} - 2\beta r_{\xi\eta} + \gamma r_{\eta\eta} = 0. \tag{1.404b}$$

where

$$\alpha = z_\eta^2 + r_\eta^2 \tag{1.405a}$$
$$\beta = z_\xi z_\eta + r_\xi r_\eta \tag{1.405b}$$
$$\gamma = z_\xi^2 + r_\xi^2. \tag{1.405c}$$

Now in the case where the right hand side of equation (1.373b) is not zero, we need to apply some more considerations rather than simply

equating things and dividing out terms. Putting things together with the full Poisson equations we have

$$
\begin{aligned}
\xi_{zz} + \xi_{rr} = & - z_{\xi\xi}(z_\eta^2 + r_\eta^2)r_\eta \\
& - z_{\eta\eta}(z_\xi^2 + r_\xi^2)r_\eta \\
& + 2z_{\xi\eta}(z_\xi z_\eta + r_\xi r_\eta)r_\eta \\
& - 2r_{\xi\eta}(z_\xi z_\eta + r_\xi r_\eta)z_\eta \\
& + r_{\xi\xi}(z_\eta^2 + r_\eta^2)z_\eta \\
& + r_{\eta\eta}(z_\xi^2 + r_\xi^2)z_\eta
\end{aligned}
\tag{1.406a}
$$

$$
\begin{aligned}
\eta_{zz} + \eta_{rr} - \frac{\eta_r}{r} = & z_{\xi\xi}(z_\eta^2 + r_\eta^2)r_\xi \\
& + z_{\eta\eta}(z_\xi^2 + r_\xi^2)r_\xi \\
& - 2z_{\xi\eta}(z_\xi z_\eta + r_\xi r_\eta)r_\xi \\
& + 2r_{\xi\eta}(z_\xi z_\eta + r_\xi r_\eta)z_\xi \\
& - r_{\xi\xi}(z_\eta^2 + r_\eta^2)z_\xi \\
& - r_{\eta\eta}(z_\xi^2 + r_\xi^2)z_\xi \\
& - \frac{J}{r}z_\xi(r_\eta)z_\xi \\
& + \frac{J}{r}z_\xi(z_\eta)r_\xi.
\end{aligned}
\tag{1.406b}
$$

To help combine things, we'll add and subtract the same expression from equation (1.407).

$$
\begin{aligned}
\xi_{zz} + \xi_{rr} = & - z_{\xi\xi}(z_\eta^2 + r_\eta^2)r_\eta \\
& - z_{\eta\eta}(z_\xi^2 + r_\xi^2)r_\eta \\
& + 2z_{\xi\eta}(z_\xi z_\eta + r_\xi r_\eta)r_\eta \\
& - 2r_{\xi\eta}(z_\xi z_\eta + r_\xi r_\eta)z_\eta \\
& + r_{\xi\xi}(z_\eta^2 + r_\eta^2)z_\eta \\
& + r_{\eta\eta}(z_\xi^2 + r_\xi^2)z_\eta \\
& + \frac{J}{r}z_\xi r_\eta z_\eta \\
& - \frac{J}{r}z_\xi r_\eta z_\eta.
\end{aligned}
\tag{1.407}
$$

Now adding equation (1.407) to equation (1.406b) gives

$$
\begin{aligned}
0 =\ & z_{\xi\xi}(z_\eta^2 + r_\eta^2)(r_\xi - r_\eta) \\
& - 2z_{\xi\eta}(z_\xi z_\eta + r_\xi r_\eta)(r_\xi - r_\eta) \\
& + z_{\eta\eta}(z_\xi^2 + r_\xi^2)(r_\xi - r_\eta) \\
& - \frac{J}{r} z_\xi(z_\eta)(r_\xi - r_\eta) \\
& - r_{\xi\xi}(z_\eta^2 + r_\eta^2)(z_\xi - z_\eta) \\
& + 2r_{\xi\eta}(z_\xi z_\eta + r_\xi r_\eta)(z_\xi - z_\eta) \\
& - r_{\eta\eta}(z_\xi^2 + r_\xi^2)(z_\xi - z_\eta) \\
& + \frac{J}{r} z_\xi(r_\eta)(z_\xi - z_\eta).
\end{aligned}
\tag{1.408}
$$

Separating out expressions for z and r gives

$$
\begin{aligned}
0 =\ & z_{\xi\xi}(z_\eta^2 + r_\eta^2)(r_\xi - r_\eta) \\
& - 2z_{\xi\eta}(z_\xi z_\eta + r_\xi r_\eta)(r_\xi - r_\eta) \\
& + z_{\eta\eta}(z_\xi^2 + r_\xi^2)(r_\xi - r_\eta) \\
& - \frac{J}{r} z_\xi(z_\eta)(r_\xi - r_\eta)
\end{aligned}
\tag{1.409a}
$$

$$
\begin{aligned}
0 =\ & - r_{\xi\xi}(z_\eta^2 + r_\eta^2)(z_\xi - z_\eta) \\
& + 2r_{\xi\eta}(z_\xi z_\eta + r_\xi r_\eta)(z_\xi - z_\eta) \\
& - r_{\eta\eta}(z_\xi^2 + r_\xi^2)(z_\xi - z_\eta) \\
& + \frac{J}{r} z_\xi(r_\eta)(z_\xi - z_\eta).
\end{aligned}
\tag{1.409b}
$$

Dividing out common terms leaves

$$
\begin{aligned}
0 =\ & z_{\xi\xi}(z_\eta^2 + r_\eta^2) \\
& - 2z_{\xi\eta}(z_\xi z_\eta + r_\xi r_\eta) \\
& + z_{\eta\eta}(z_\xi^2 + r_\xi^2) \\
& - \frac{J}{r} z_\xi(z_\eta)
\end{aligned}
\tag{1.410a}
$$

$$
\begin{aligned}
0 =\ & - r_{\xi\xi}(z_\eta^2 + r_\eta^2) \\
& + 2r_{\xi\eta}(z_\xi z_\eta + r_\xi r_\eta) \\
& - r_{\eta\eta}(z_\xi^2 + r_\xi^2) \\
& + \frac{J}{r} z_\xi(r_\eta).
\end{aligned}
\tag{1.410b}
$$

After final rearranging, we are left with

$$z(\xi,\eta) \equiv \alpha z_{\xi\xi} - 2\beta z_{\xi\eta} + \gamma z_{\eta\eta} = \frac{J}{r} z_\xi z_\eta \quad\quad (1.411a)$$

$$r(\xi,\eta) \equiv \alpha r_{\xi\xi} - 2\beta r_{\xi\eta} + \gamma r_{\eta\eta} = \frac{J}{r} z_\xi r_\eta, \quad\quad (1.411b)$$

where again (repeated for convenience),

$$\alpha = z_\eta^2 + r_\eta^2 \quad\quad (1.412a)$$

$$\beta = z_\xi z_\eta + r_\xi r_\eta \quad\quad (1.412b)$$

$$\gamma = z_\xi^2 + r_\xi^2 \qu\quad (1.412c)$$

$$J = z_\xi r_\eta - z_\eta r_\xi. \quad\quad (1.412d)$$

References

1   Fredholm, I., "Sur une classe d'équations fonctionnelles," *Acta Mathematica*, vol. 27, no. none, 1903, pp. 365–390. DOI: 10.1007/bf02421317   cited on p. 3

2   Lewis, R. I., *Vortex Element Methods for Fluid Dynamic Analysis of Engineering Systems*, ser. Cambridge engine technology series 1. Cambridge ; New York: Cambridge University Press, 1991.   cited on pp. 5, 27

3   Martensen, E., "Die Berechnung der Druckverteilung an dicken Gitterprofilen mit Hilfe von Fredholmschen Integralgleichungen zweiter Art," *Archive for Rational Mechanics and Analysis*, vol. 3, 1959, pp. 235–270.   cited on pp. 5, 17

4   Courant, R. and Hilbert, D., *Methods of Mathematical Physics*. Interscience Publishers, 1962, vol. 2.   cited on p. 5

5   Katz, J. and Plotkin, A., *Low speed aerodynamics*, 2nd ed. Cambridge, UK: Cambridge University Press Cambridge, UK, 2001.   cited on p. 8

6   Bezanson, J., Edelman, A., Karpinski, S., and Shah, V. B., "Julia: A fresh approach to numerical computing," *SIAM Review*, vol. 59, no. 1, 2017, pp. 65–98. DOI: 10.1137/141000671   cited on p. 8

7   Drela, M., "XFOIL: An Analysis and Design System for Low Reynolds Number Airfoils," *Low Reynolds Number Aerodynamics*, Mueller, T. J., Ed., Berlin, Heidelberg: Springer Berlin Heidelberg, 1989, pp. 1–12.   cited on p. 14

8   Fidkowski, K. J., "A Coupled Inviscid–Viscous Airfoil Analysis Solver, Revisited," en, *AIAA Journal*, vol. 60, no. 5, May 2022, pp. 2961–2971. DOI: 10.2514/1.j061341   cited on p. 14

9   Ryall, D. L. and Collins, I. F., "Design and Test of a Series of Annular Aerofoils," Reports and Memoranda 3492, Ministry of Technology Aeronautical Research Council, March 1967.   cited on p. 26

10   McDonald, R. A. and Gloudemans, J. R., "Open Vehicle Sketch Pad: An Open Source Parametric Geometry and Analysis Tool for Conceptual Aircraft Design," *AIAA SCITECH Forum 2022*, AIAA, January 2022.   cited on p. 27

11   Thompson, J. F., Thames, F. C., and Mastin, C., "Automatic numerical generation of body-fitted curvilinear coordinate system for field containing any number of arbitrary two-dimensional bodies," en, *Journal of Computational Physics*, vol. 15, no. 3, July 1974, pp. 299–319. DOI: 10.1016/0021-9991(74)90114-4   cited on p. 48

12   Wallis, R. A., "A Rationalised Approach to Blade Element Design, Axial Flow Fans," *Proceedings of the third Australasian Conference on Hydraulics and Fluid Mechanics*, The Institution of Engineers, Australia, Sydney, New South Wales, Australia, November 1968, pp. 23–29.   cited on p. 82

13   Wallis, R. A., "The F-Series Aerofoils, for Fan Blade Sections," *Mechanical Engineering Transactions*, vol. 2, no. 1, 1977, pp. 12–20.   cited on p. 82

14   Wallis, R., *Axial Flow Fans and Ducts*. Wiley, 1983.   cited on p. 82

cited on p. 84

15 Glauert, H. and Taylor, G. I., "The effect of compressibility on the lift of
    an aerofoil," *Proceedings of the Royal Society of London. Series A, Containing
    Papers of a Mathematical and Physical Character*, vol. 118, no. 779, 1928,
    pp. 113–119. DOI: 10.1098/rspa.1928.0039